STUDIES ON THE ALCOHOL OXIDASE FROM *PICHIA PASTORIS* FOR DEVELOPING NANOCOMPOSITE BASED ALCOHOL BIOSENSORS

A Thesis

Submitted by

SOMASEKHAR REDDY CD

For the award of the degree

of

Doctor of Philosophy

DEPARTMENT OF BIOSCIENCES AND BIOENGINEERING

INDIAN INSTITUTE OF TECHNOLOGY GUWAHATI

GUWAHATI-781039, ASSAM, INDIA

JAN 2015

Dedicated to my most precious possession-
My family

INDIAN INSTITUTE OF TECHNOLOGY GUWAHATI
Department of Biosciences and Bioengineering
Guwahati – 781039

STATEMENT

I do hereby declare that the matter embodied in this thesis is the result of investigations carried out by me in the Department of Biosciences and Bioengineering, Indian Institute of Technology Guwahati, Assam, India, under the guidance of Prof. Pranab Goswami.

In keeping with the general practice of reporting scientific observations, due acknowledgements have been made wherever the work described is based on the findings of other investigators.

January, 2015 **Somasekhar Reddy CD**

INDIAN INSTITUTE OF TECHNOLOGY GUWAHATI
Department of Biosciences and Bioengineering
Guwahati – 781039, Assam, INDIA

Dr. Pranab Goswami
Professor

Tel: +91-(0)361 2582202
Fax: +91-(0)361 2582249/2690762
Email: pgoswami@iitg.ernet.in

Date: 27.01.2015

CERTIFICATE

It is certified that the work described in this thesis, entitled "**Studies on the Alcohol Oxidase from *Pichia pastoris* for Developing Nanocomposite based Alcohol Biosensor**", done by **Mr. Somasekhar reddy CD (Roll No. 09610611)** for the award of degree of Doctor of Philosophy is an authentic record of the results obtained from the research work carried out under my supervision in the Department of Biosciences and Bioengineering, Indian Institute of Technology Guwahati, India.

The results embodied in this thesis have not been submitted to any other University or Institute for the award of any degree.

January, 2015

Prof. Pranab Goswami
(Research supervisor)

ACKNOWLEDGMENTS

I take this opportunity with much pleasure to express my sincere gratitude to all those who have supported me through the course of my journey towards producing this thesis. First of all, I am thankful to Indian Institute of Technology Guwahati for giving me the opportunity to carry out Ph.D in this esteemed Institute and providing me the financial support. I am deeply indebted to my supervisor, Prof. Pranab Goswami for his enthusiastic guidance during my P.hD from its conception to its completion and most importantly, for the conviction he has shown in my abilities.

I am thankful to my doctoral committee members, Dr. Aiyagari Ramesh, Dr. Utpal Bora and Dr. Sunil K Khijwania for their constructive criticism and helpful suggestions during my various progress seminars. I am gratified to Prof. Pranab Goswami, Dr, Biplab Bose, Dr. S. S. Ghosh, Dr. A. Ramesh and Dr. L. Sahoo for providing excellent lab facilities. I am also greatful to other faculty members, office staff and my colleagues from Department of Biosciences and Bioengineering for their inestimable support and help.

I would like to thank Central Instruments Facility, IIT Guwahati for providing the access to various instruments without which this study would not be feasible.

I especially appreciate my former colleagues Dr. Preety Vatsyayan and Dr. Urmila Saxena for their inspired support at the time of my acclimatization in the lab and guidance in learning various experimental techniques. I would like to mention my special thanks to my amazing fellow lab members, Santosh, Seraj, Mitun, Ankana, Babina, Priyamvada, Madhuri, Mrinal, Naveen, Phurpa, Farhan, Priyanki, Sharbani and Abdul who have shared their struggles so intimately and trusted my assistance in their various endeavors.

The beauty of Assam, beauty of IITG campus never let me feel bored. Memories of this place and time spent together with friends (especially our numerous tea breaks) will always be remembered by me later in my life. I am also thankful to my friends Dr. Aadi Moolam Ramesh, Dr. Nani babu, Anil, Sai Krishna Santosh, Dr. Amit, Dr. Gaurav Saxena, Dr. Asim Bikas Das, Dr. Prakash Saudagar, Thiyagarajan, Shanmuga reddy, Surya prakash, Dr. Lakshman, Kiran, Dr. Poju Loying, Munendhar, Tripati, Ashish Kumar Yadav, Mishra with whom I share tons of fond memories.

Most of all, I would like to dedicate this work to my appa and amma whose love, teaching and unconditional support have brought me this far. I thank my sisters and brothers in law, for all the long and refreshing conversations we had over the phone and their support, from which I always benefitted.

Somasekhar Reddy CD
January 2015

Abstract

The present investigation is focused on fabricating amperometric alcohol biosensors with high sensitivity, selectivity and wide dynamic range using the alcohol oxidase (AOx) from *Pichia pastoris* as the biorecognition element. Preliminary characterization of the AOx was carried out in terms of molecular weight, kinetic parameters, secondary structure, optimum working parameters and size, necessary for exploration of the enzyme in fabricating alcohol biosensor. The molecular weight of the AOx was found to be 575 kDa and the secondary structure showed a stable α- helical conformation. We adopted a novel approach of amplifying the biocatalytic activity of the AOx by stably entrapping ferrocene, which is a known chemical activator of the enzyme, within its protein matrix using a microwave (MW) based technique and then immobilized the enzyme with amplified activity on the electrode surface using biocompatible nanocomposite matrices for finally developing the alcohol biosensors. A reversible effect of microwave (2.45 GHz and 900 W) mediated denaturation of the protein at low exposure time of 10 s at pH 7.5 was demonstrated. The unfolding events occurred during the denaturation did not transverse through any intermediate states and no subunits of the protein were detached during the process. The refolding of the protein achieved at 4 °C for 24 h had regenerated the native enzyme. This reversible refolding approach excludes any chemical reagent and therefore established as a simple technique for protein unfolding-folding studies. The ferrocene entrapped AOx (FcAOx) showed improved kinetic parameters with increase in catalytic efficiency (K_{cat}/K_m) of 116 %. The conjugate showed increase in sedimentation co-efficient ('s':19.4 s) and molecular mass ('Mw':582 kDa) in comparison to the native enzyme ('s': 18.7 s, 'Mw': 575 kDa). The ferrocene molecules were stably entrapped in the AOx protein matrix in a molar ratio of ~3:1 through electrostatic interaction with the Trp residues involved in the catalytic activity of the enzyme as demonstrated by advanced analytical techniques. A bioelectrode was fabricated by

immobilizing FcAOx and sol–gel chitosan film coated horseradish peroxidase (HRP) on a multi-walled carbon nanotube (MWCNT) modified glassy carbon electrode (GCE) through layer-by-layer technique. The bioelectrode reactions involved the formation of H_2O_2 by FcAOx biocatalysis of substrate alcohol followed by HRP-catalyzed reduction of the liberated H_2O_2 through MWCNT supported direct electron transfer mechanism. The amperometric biosensor exhibited a linear response to alcohol in the range of 5.0×10^{-6} to 30×10^{-4} mol L^{-1} with a detection limit of 2.3×10^{-6} mol L^{-1}, and a sensitivity of 150 µA mM^{-1} cm^{-2}. The biosensor response was steady for 28 successive measurements completed in a period of 5 h and retained ~90 % of the original response even after four weeks when stored at 4 °C. The biosensor was successfully applied for the determination of alcohol in commercial samples and its performance was validated by comparing with the data obtained by GC analyses of the samples. The fabricated biosensor also efficiently excluded interference from electroactive species present in samples such as ascorbic acid, uric acid, lactic acid, glucose and urea. Later, we also developed another technique for preparing AOx with amplified activity for bioelectrode fabrication. A stable AOx protein surface stabilized AuNPs was synthesized *in-situ* by exploiting the native chemical drive of the protein molecules under alkaline condition (pH 8.5). The formation of the AOx conjugated AuNPs was confirmed by advanced analytical and spectroscopic techniques. The significant increase in zeta potential (ζ) value of -57 mV for the synthesized AOx-AuNPs conjugate from the AOx (p*I* 4.5) protein (ζ, -30 mV) implied good stability of the *in-situ* synthesized nano-conjugate. The AOx-AuNPs conjugate showed steady stability in alkaline (up to pH 8.5) and NaCl (up to10^{-1} M) solutions. The efficiency (K_{cat}/K_m) of the AuNP conjugated AOx was increased by 18 % from the free enzyme confirming the activating role of the surface stabilized AuNPs for the enzyme. The AuNPs–AOx conjugate was encapsulated with polyaniline (PANI) synthesized by oxidative polymerization of aniline using H_2O_2 generated

in-situ from the AOx catalyzed oxidation of alcohol. The PANI encapsulated AuNPs–AOx assembly was stabilized on a GCE by chitosan–nafion mixture and then utilized the fabricated bioelectrode for detection of alcohol amperometrically using H_2O_2 as redox indicator at + 0.6 V. The constructed biosensor showed high stability (5 % less in 4 weeks), wide linear detection range of 10 µM – 4.7 mM (R^2= 0.9731), high sensitivity of 68.3±0.35 µA mM^{-1} and low detection limit of 7±0.027 µM for ethanol. The fabricated bioelectrode was successfully used for the selective determination of alcohol in beverage samples.

CONTENTS

List of figures

List of tables

List of schemes

List of acronyms

AOx	Alcohol oxidase
AA	Ascorbic acid
ABTS	2, 2'-azino-bis [3-ethylbenzothiazoline-6-sulfonic acid]
ADH	Alcohol dehydrogenase
ADP	Adenine dinucleotide phosphate
AFM	Atomic force microscopy
Ag	Silver
AgCl	Silver chloride
APDMOS	(3-aoryloxypropyl) dimethoxymethylsilane
Au	Gold
AuNPs	Gold nanoparticles
BSA	Bovine serum albumin
CA	Citric acid
CBB	Coomassie brilliant blue
CD	Circular dichroism
CHIT	Chitosan
CNF	Carbon nano fibres
CNTs	Carbon nanotubes
CPs	Conducting polymers
CSA	(±)-10-camphorsulfonicacid
CV	Cyclic voltammetry
DET	Direct electron transfer
df	Dilution factor
DL	Detection limit
DMFc	1, 1' dimethylferrocene
DMSO	Dimethyl sulphoxide
DPV	Differential pulse voltammetry
EDC	N-ethyl-N'-(3-dimethylaminopropyl) carbodimide
EDP	Electrodeposition paints
EIS	Electrochemical impedance spectroscopy
EtOH	Ethanol

FAD	Flavin adenine dinucleotide
$FADH_2$	Flavin adenine dinucleotide (reduced)
FcAOx	Ferrocene entrapped alcohol oxidase
FESEM	Field emission scanning electron microscopy
FPLC	Fast protein liquid chromatography
FTIR	Fourier transform infrared spectroscopy
GCE	Glassy carbon electrode
GdnHcl	Guanidinium hydrochloride
Glu	Glucose
GMC	Glucose-methanol-choline
H_2O_2	Hydrogen peroxide
HRP	Horse radish peroxidase
ITO	Indium tin oxide
K_2HPO_4	Di potassium hydrogen phosphate
kDa	Kilo Dalton
KH_2PO_4	Potassium dihydrogen phosphate
KPBS	Potassium Phosphate buffer solution
LA	Lactic acid
LED	Light emitting diode
MB	Meladolas blue
MW	Microwave radiation
Mw	Molecular weight
MWCNT	Multiwalled carbon nanotubes
MWCO	Molecular weigth cutoff
NAD^+	Nicotinamide adenine dinucleotide
NADH	Nicotinamide adenine dinucleotide (reduced)
NBS	N-hydroxysuccinimide
Nf	Nafion
NHS	N-hydroxysuccinimide
NBS	N-hydroxysuccinimide
Nf	Nafion
NHS	N-hydroxysuccinimide
NPs	Nanoparticles

O_2	Oxygen
OD	Optical density
Os	Osmium
PANI	Polyaniline
PCS	Poly(carbamoyl)sulfonate
PEDOP	Poly(3,4-ethylenedioxypyrrole)
PEDOT	Poly(3,4-etylenedioxythiophene)
PEG	Polyethylene glycol
PEGDGE	Poly(ethylene glycol) diglycidyl ether
PEI	Polyethyleneimine
pHEMA	Poly(hydroxymethyl methacrylate
pI	Iso electric point
PPy	Polypyrrole
PVC	polyvinylferrocenium
PVI-dme-Os	Os(4,4' dimethylbipyridine)2Cl
RSD	Relative standard deviation
RT	Room temperature
S.E.M.	Standard error mean
SAM	Self assembled monolayer
SD	Standard deviation
SDS	Sodium dodecylsulfate
SDS-PAGE	Sodium dodecyl sulfate polyacrylamide gel electrophoresis
SEC	Size exclusion chromatography
SEDFIT	Software for Spectral Energy Distribution Fitting of Photometric Data
SG	Sol gel
SH	Sulphydryl
SPR	Surface plasmon resonance
TA	Tartaric acid
TBTD	4,7-dithien-2-yl-2,1,3-benzothiadiazole
TEM	Transmission electron microscopy
TEOS	Tetraethylorthosilicate
TMOS	Tetramethoxysilane
TPP	5,10,15,20-tetra-phenyl porphyrin

Trp	Tryptophan
U	Units of enzyme
UA	Uric acid
UV-Vis	UV-Visible
ZnO	Zinc oxide

List of symbols

A	Electrode surface area
$c(s)$	Continuos sedimentation co-efficient
cP	Centipoise
df	Dilution factor
$E^{o'}$	Apparent standard potential
E_p	Peak potential
E_{pa}	Anodic peak potential
E_{pc}	Cathodic peak potential
F	Faraday constant
f/f_0	Frictional co-efficient
GHz	Gigahertz
I_{pa}	Anodic peak current
I_{pc}	Cathodic peak current
K_{cat}	Turnover number
$K_{ca}t/K_m$	Catalytic efficiency
k_m	Michaelis-Menten constant
k_s	Electron transfer constant
R	Thermodynamic rate constant
R^2	Regression coefficient
Ret	Electron transfer resistance
s	Sedimentatoin co-efficient
$t_{1/2}$	Half life
W	Watt
Z	Impedance
α	Charge transfer coefficient
ΔE_p	Potential Peak separation
ε	Extinction coefficient
ζ	Zeta potential
ν	Potential scan rate
MΩ	Megaohm
Γ	Surface concentration of ionic species

Introduction

Introduction

The detection and quantification of alcohols with high sensitivity, selectivity and accuracy is required in clinical and forensic analysis. The measurement of blood alcohol concentration is seen as the most convincing evidence to judge drunk driving and hence, very important for forensic medicine and lawsuit. Accurate quantification of ethanol content in sample is also crucial in the design assessment and improvement of fermentation process, and to control the quality of food and alcoholic beverages such as beer, wine, liquor and spirits. Additionally, the determination of ethanol is important in agricultural and environmental analysis, e.g. for the assessment of ethanol at a spill site or in ground waters. Therefore, the need for rapid, reliable and reproducible measurement of alcohol in biological fluids, food, beverage and environmental samples has been continuously stimulating interest in the field of analytical science. So far many analytical methods have been developed for the determination of alcohols which comprises mostly chemical and physical methods, such as redox titrations, colorimetric methods, specific gravity, refractive index measurements, spectroscopic and chromatographic techniques such as, gas chromatography and high performance liquid chromatography. Although some of these methods are precise and reliable, they are complex, time consuming and require previous separation processes (distillation, pervaporation), expensive instrumentation and trained operators. Such disadvantages could be overcome by the use of biosensors using specific biorecognition element for detection of alcohol in

samples. A biosensor is commonly described as an analytical device incorporating a biological or biologically derived recognition element, either intimately associated or integrated within a physiochemical transducer. The basic concept of a biosensor's operation can be illustrated with the help of (Scheme A). The biological component recognizes the specific target analyte and the change (physical or chemical) produced by their specific interaction is transduced by a transducer. The transduced background corrected signal is than amplified, processed and converted into a digital format for reading the existence or concentration of the target analyte in the test sample. Biosensor research holds promise for developing stable portable devices for rapid, sensitive, selective, reproducible, and economical detection of analytes of different chemical natures. It has the advantage of being used by semiskilled operators and by patients themselves.

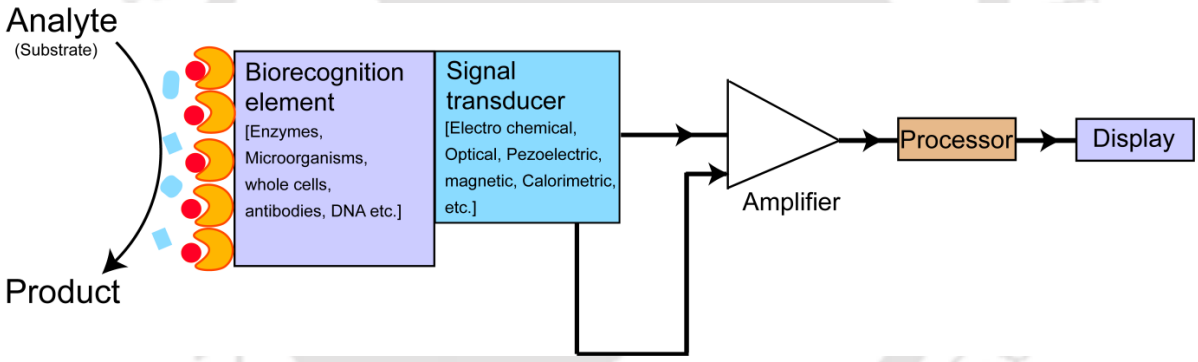

Scheme A Schematic representation on the general configuration of biosensor

The biorecognition elements studied so far for developing alcohol biosensors are limited mostly to microbial whole cells and redox enzymes. The progress on the cell-based alcohol sensors, which commonly employ polarographic technique, is yet to gain momentum due to several reasons, among which the long response time and technical difficulty in maintaining the sensor assembly during the assay are prominent. The enzyme, alcohol dehydrogenase (ADH) (Alcohol: NAD^+ oxidoreductase; EC 1.1.1.1) has been intensively

investigated for developing various alcohol biosensors (Azevedo et al. 2005). In nature, the ADH enzyme (Mw ~80 kDa) serves to breakdown alcohols. In yeasts and several bacteria, ADH also catalyzes the opposite reaction as a part of metabolism in the fermentation process (Scheme B **a**). The enzyme usually exhibits high selectivity towards ethanol. However, the need of supplementing the cofactor to the reaction media makes the ADH based alcohol biosensing expensive (Svensson et al. 2005; Razumiene et al. 2001). Although there is a continuous effort to regenerate the co-factor in the reaction system to sustain the catalytic activity of ADH, efficient co-factor regenerating system for biosensor application of ADH is yet to develop properly. Moreover, the cofactor needs to be placed closer to the enzyme without being irreversibly trapped or leached from the electrode surface during the operation, thus complicating the fabrication design of the biosensor. Moreover, direct electrochemical regeneration of the co-factor occurs only at a high overvoltage, where gradual passivation (fouling) of the electrode surface may take place. To mitigate the problem electron transfer mediator with low oxidation potential has been investigated which however, succumb to many drawbacks among which leaching of the mediator to the electrolyte solution and associated dipping of the biosensor's operational stability is pertinent (Vijayakumar et al. 1996).

We focused our attention on the relatively less studied group of alcohol oxidizing enzyme namely, alcohol oxidase (AOx) (alcohol: oxygen oxidoreductases, EC 1.1.3.13) as biorecognition element for developing alcohol biosensor. The AOx (Mw ~600 kDa) belonging to the group of glucose-methanol-choline family, is an oligomeric enzyme consisting of eight identical subunits arranged in a quasi-cubic arrangement, each containing a strongly bound cofactor, flavin adenine dinucleotide (FAD) (Ozimek et al. 2005). It is mostly produced by methylotrophic yeasts. The concept of using AOx in biosensor has emerged since recent past owing to its many distinct properties identified as advantageous

such as, irreversible catalytic oxidation (Scheme B **b**) and selectivity towards the alcohols, avidly bound flavin co-factor to the redox center of the enzyme, it's easy availability since these enzymes are widely produced by different aerobic microorganisms, making the production of these enzymes possible in large scale (Goswami et al. 2013).

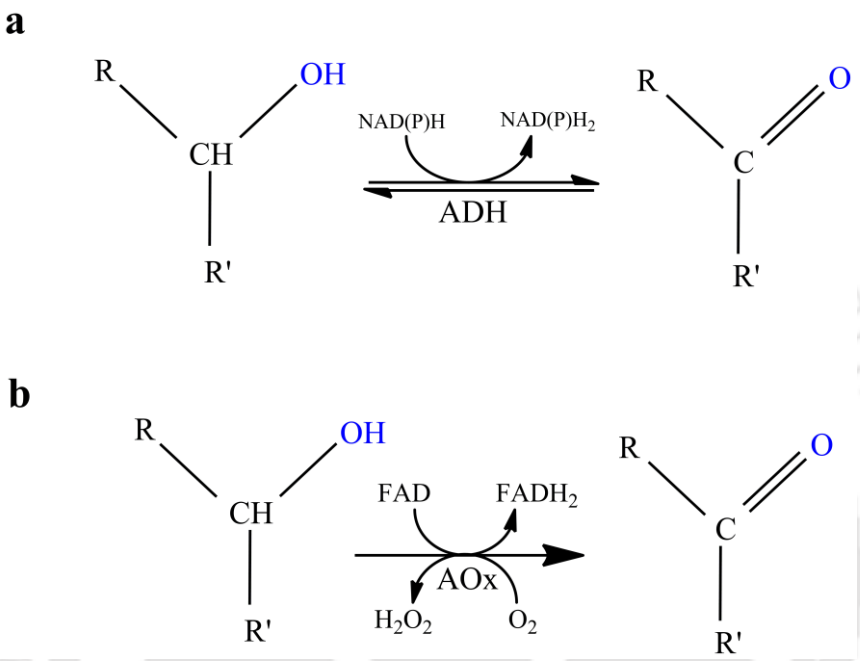

Scheme B a. Alcohol dehydrogenase (ADH) as catalyst and **b.** Alcohol oxidase (AOx) as catalyst, R' = -H or any other alkyl/aryl group.

We proposed to utilize amperometric principle for developing AOx based alcohol biosensor considering its certain innate advantages such as, label free detection, faster response time and low cost of production. However, AOx based electrochemical biosensors described so far are yet to address adequately the drawbacks, such as low sensitivity, poor stability, and narrow dynamic range of operation for their practical utility. The factors responsible for these limitations are attributed to poor signal transduction, degradation or denaturation of enzyme, leaching of mediator and low loading of kinetically active enzymes

on the electrode surface. We would like to address the above challenges with the aid of novel approaches of amplifying the biocatalytic activity of the AOx first and then immobilizing the enzyme with amplified activity on the electrode surface using biocompatible nanocomposite matrices and polymers for finally developing the alcohol biosensors. It was expected that the enzyme with amplified biocatalytic activity would enhance the sensitivity of the sensors while, enhanced enzyme immobilization on the electrode surface being achieved by using nanocomposite matrix would expand the dynamic range for ready detection of alcohol in samples from various sources. Additionally, the biocompatible nanocomposite matrix embedded with suitable polymers expected to stabilize the construct and enhance the operational stability of the biosensors.

In view of the above challenges and projected plan, we proposed to conduct a study on the AOx from *Pichia pastoris* for developing nanocomposite based alcohol biosensors with the following specific objectives: 1. Entrapment of AOx activator molecule (ferrocene) in the protein matrix of the enzyme using novel protein unfolding and refolding techniques. 2. Utilize the AOx with amplified biocatalytic activity for developing amperometric alcohol biosensor in a peroxidase coupled format of direct electron transfer signal transduction principle using multiwalled carbon nanotube (MWCNT) and biocompatible Sol-Gel/Chitosan as enzyme immobilization matrix on the electrode. 3. Application of AOx protein mediated *in-situ* synthesised and stabilized gold nanoparticles as activating and enhanced enzyme loading material for developing amperometric alcohol biosensor. The contents of this thesis entitled "Studies on the alcohol oxidase from *Pichia pastoris* for developing nano-composite based alcohol biosensor" have been divided into five chapters. At the end a brief section entitled "Conclusions and scope for future work" is also included to apprise the readers on the major findings of the current work and the important gaps that need to be bridged to attain the state of art for a commercially viable biosensor product.

Chapter 1: Literature Review

The objective of this chapter is to summarize the current status and progress in the area of alcohol biosensors. The chapter highlights the general principles governing electrochemical alcohol biosensors that specifically utilize immobilized enzymes. Special emphasis has been given on discussing technical importance, performance, benefits and limitations of different types of materials and techniques currently used for alcohol biosensors design and construction.

Chapter 2: Alcohol oxidase from *Pichia pastoris*

In this chapter, preliminary characterization of AOx from *Pichia pastoris* has been described. The analysis of AOx subunit molecular weight, *pI*, secondary structure, and its sedimentation co-efficient were carried out. The optimum physical parameters for enzyme activity were also studied and presented in this chapter.

Chapter 3: Amplification of AOx activity by entrapping activator within protein matrix

In this chapter, an investigation on the physical entrapment of the AOx activator (ferrocene) in the protein matrix of the enzyme was performed by exploiting a novel microwave based partial unfolding technique. The successful entrapment of the activator within the AOx protein and the activity amplification by the entrapment were validated.

Chapter 4: Ferrocene activated alcohol oxidase as biorecognition element for developing alcohol biosensor

The studies in this chapter include the fabrication of an amperometric bioelectrode based on ferrocene entrapped alcohol oxidase (FcAOx) immobilized on biocompatible sol-gel chitosan matrix and horse radish peroxidase (HRP) immobilized within MWCNTs matrix. Detailed electrochemical and morphological characterization of the fabrication process is

presented. Further characterization of the fabricated bioelectrode in terms of sensitivity, detection limit, and stability is discussed. Ultimately the application potential of the bienzyme based bioelectrode for the real sample analysis was also investigated and presented in this chapter.

Chapter 5: Gold nanoparticle activated alcohol oxidase as biorecognition element for developing alcohol biosensor

The chapter describes a simple one step method for the AOx protein mediated synthesis and stabilization of gold nanoparticles (AuNPs). The formation of the AOx conjugated AuNPs was confirmed by advanced analytical and biophysical techniques. An amperometric alcohol biosensor was fabricated by immobilizing the AOx–AuNPs conjugate within Polyaniline (PANI) polymer. The morphological and electrochemical characterization of the fabricated bioelectrode is discussed in detail. The response of the biosensor was checked with alcohol and various response parameters were estimated. The application of the biosensor for real sample analysis is also demonstrated.

Chapter I

Literature review

CHAPTER 1

Literature Review

Rapid and quantitative analysis of ethanol is an important task frequently involved in characterizing or probing samples from various origin such as, food, beverage, cosmetic, environmental, clinical and forensic samples (Patel et al. 2001). In this regard biosensor research has been gaining enormous importance due to its simplicity and analytical power being acquired by exploiting microelectronics for various applications. Among the various recognition elements enzymes have received wide attention for developing biosensors of different analytical applications (D'Orazio 2003).

1.1. Electrochemical alcohol biosensors

Biosensors can be categorized into electrochemical, optical, thermometric, piezoelectric, and magnetic biosensors depending on the transducing mechanism being used (Singh et al. 2012). Alcohol biosensors of different categories have been reported and among them electrochemical transducer based biosensors are prominent because of their label free detection, better sensitivity, faster response time, easy maintenance as well as their low cost (Vijayakumar et al. 1996). The selection of biorecognition element specific to the target analyte is the first and critical step involved in the fabrication of biosensor. Both enzyme and microbial cell based alcohol biosensors have been reported.

1.2. Enzyme based electrochemical alcohol biosensors

A considerable interest has been aroused in the development of different electrochemical alcohol biosensors based on either alcohol oxidase (Guilbault et al. 1983, Morales et al. 1998; Patel et al. 2001, Yildiz and Toppare 2006) or alcohol dehydrogenase (Cai et al. 1997; Park et al. 1999) as biorecognition element. A brief introduction on these enzymes commonly being utilized as biorecognition element for the fabrication of amperometric alcohol biosensors is given below:

1.2.1. Alcohol oxidase

Alcohol oxidase (AOx; Alcohol: O_2 oxidoreductase, EC 1.1.3.13) belonging to the group of glucose-methanol-choline (GMC) family, is an oligomeric enzyme consisting of eight identical sub-units arranged in a quasi-cubic arrangement, each containing a strongly bound cofactor, flavin adenine dinucleotide (FAD) molecule (Ozimek et al. 2005). It is produced by methylotrophic yeasts (e.g. *Hansenula*, *Pichia*, and *Candida*) in subcellular microbodies known as peroxisomes, during growth on methanol (Waterham et al. 1997). AOx is the first enzyme involved in the methanol oxidation pathway of methylotrophic yeasts. Although its physiological role is the oxidation of methanol, it is also able to oxidize other short-chain alcohols, such as ethanol, propanol and butanol. AOx catalyzed oxidation of alcohols yields the corresponding aldehyde or ketone and hydrogen peroxide (H_2O_2) (Janssen et al. 1965). The FAD in the redox centre of AOx is a primary acceptor of hydride from alcohol. Upon oxidation of substrate, the FAD is reduced to $FADH_2$. The reduced FAD then transfers the redox equivalents to dioxygen as the final acceptor. The structure of AOx has a FAD binding domain, a flavin attachment loop and a substrate binding domain. In addition to these domains there are two minor domains, namely a FAD-covering loop and an extended FAD-binding domain. The FAD-binding domain is the most conserved region and consists of

an ADP-binding motif (βαβ) and a characteristic nucleotide-binding site GXGXXG (amino acids 13-18 of AOx) (Ozimek et al. 2005). Two inserts have also been identified in the substrate-binding domain that are probably involved in AOx-octamer formation. The conformation of AOx is irreversibly changed following the dissociation of FAD, which is deeply buried in the protein matrix (Zlateva et al. 2001). Owing to the substrate specificity, irreversible catalytic oxidation of alcohols and the avidly bound co-factor to the redox center of the enzyme, AOx has emerged as a potential biorecognition element for developing alcohol biosensors (Goswami et al. 2013).

1.2.2. Alcohol dehydrogenase

The other redox enzyme, namely, alcohol dehydrogenase has been conventionally studied for amperometric determination of alcohol (Svensson et al. 2005; Tsai et al. 2007). Alcohol dehydrogenases (ADH ; Alcohol: NAD^+ oxidoreductase; EC 1.1.1.1) are widely distributed in animals, plants and lower microorganisms and are, by far, one of the most thoroughly studied enzymes as evident from the literatures reviewed in some of the selected papers (Radianingtyas and Wright 2003; Reid and Fewson 1994; Sofer and Presley 1987). Humans have at least six slightly different ADHs. These proteins exist in multiple forms as a dimer with a subunit mass of approximately 80 kDa and are encoded by at least seven different genes (Hammes-Schiffer et al. 2006). In humans and many other animals, they serve to breakdown alcohols which could otherwise be toxic; in yeast and several bacteria, some ADHs catalyze the opposite reaction as a part of fermentation. ADH catalyzes the reversible oxidation of primary aliphatic and aromatic alcohols other than methanol. In addition to the aforesaid AOx and ADH, enzymes such as horse radish peroxidase (HRP) and catalase were also used in the fabrication of numerous electrochemical alcohol biosensors in conjugation with AOx (Hasunuma et al. 2004; Smutok et al. 2006; Hnaien et al. 2010, Boguslavsky et al.

1995). However, these additional enzymes are used to improve the signal transduction rather than using them for biorecognition of the analytes. Using oxidase/peroxidase bienzyme systems the detection principle switches from an electrochemical oxidation to a reduction process, which occurs at much lower potentials, and thus, improves considerably the sensitivity and selectivity of the device (Castillo et al. 2003). Peroxidases are among the few enzymes able to directly transfer electrons to an electrode at relatively low applied potentials (Csöregi et al. 1993b; Gorton et al. 1992a; Gorton et al. 1999). One of the most promising approaches of AOx/peroxidase bienzyme system, involving electron transfer through immobilized osmium complexes, is 'wiring' the peroxidase by using redox polymers (Smutok et al. 2006). This design offers a hydrophilic environment where enzymes can maintain their native properties and activity. At the same time, a redox hydrogel not only act as an immobilization matrix but also as an electron transfer solution. Redox centers dispersed in the hydrogel assure the transfer of the electrons to/from the enzyme's redox center from/to the electrode by the so-called 'electron hopping' phenomenon (Katakis and Heller 1997).

1.3. Cell and tissue based alcohol biosensors

Most of the enzymes being used in the development of biosensor are expensive for routine analysis of the target analyte. Therefore few reports were focused on microbial cells for developing ethanol biosensors. These biosensors operate at fixed potentials with respect to a reference electrode and involve the detection of the current generated by the oxidation or reduction of species at the surface of the electrode. Table 1.1 summarizes a few of the prominent amperometric microbial biosensors reported in literature. The amperometric microbial biosensor for alcohol determination has been investigated largely for its importance in fermentation industry and clinical applications. Different microorganisms metabolizing ethanol such as *T. brassicae* (Karube et al. 1992), *A. aceti* (Ikeda et al. 1997), *C. vini*

(Mascini et al. 1989), *G. suboxydans* (Kitagawa et al. 1987), *C. tropicalis* (Akyilmaz and Dinckaya 2005), *A. niger* (Subrahmanyam et al. 2001), *S. ellipsoideus* (Rotariu and Bala 2003) and *P. methanolica* (Reshetilo et al. 2001) have been immobilized on oxygen electrode to fabricate ethanol biosensors. While these biosensors posses good sensitivity and stability, they usually have poor selectivity. Thus, there is a great interest to develop selective microbial ethanol biosensor.

An improved selectivity for ethanol determination in presence of glucose was achieved by replacing oxygen with ferricyanide as the electron acceptor for *G. oxydans* immobilized on a glassy carbon electrode by cellulose acetate membrane which also restricted the availability of glucose to the cells by size exclusion (Tkac et al. 2002). A homogenized mushroom (*A. bisporus*) tissue based alcohol bioelectrode was developed by immobilizing the tissue with gelatin and crosslinked agent glutaraldehyde at dissolved oxygen probe (Akyilmaz and Dinckya 2000).

Table 1.1 Amperometry based microbial ethanol biosensors.

Microorganism	Limit of detection	References
G. oxydans or P. methanolica	0.05 mM	Reshetilo et al. 2001
A. aceti (IFO 3284)	<0.2 mM	Ikeda et al. 1997
C. vini	0.02-0.2 mM	Mascini et al. 1989
G. suboxydans	0-25 mg/L	Kitagawa et al. 1987
C. tropicalis	0.5-7.5 mM	Akyilmaz and Dinckaya 2005
A. niger	1-32 ppm	Subrahmanyam et al. 2001
S. ellipsoideus	69 µM	Rotariu and Bala 2003
G. oxydans	0.85 µM	Tkac et al. 2002

1.4. Electron transfer mechanism in bioelectrodes

The stoichiometric consumption of O_2 and production of H_2O_2 upon catalysis of alcohol by AOx as well as the transfer of electrons during the reaction (or redox nature of AOx) has laid the basis of alcohol biosensors (Azevedo et al. 2005).

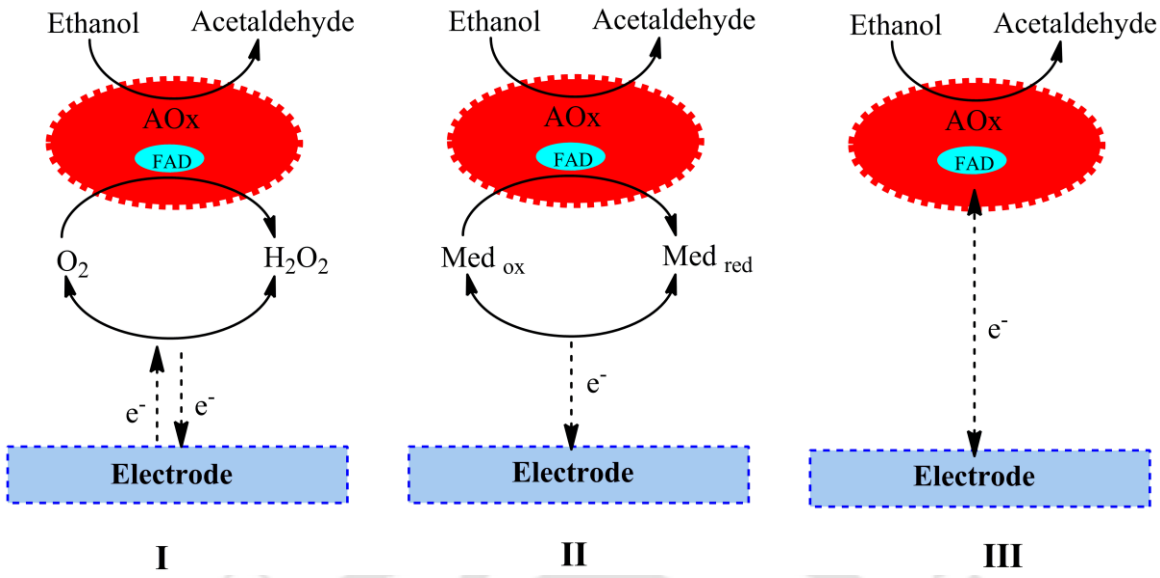

Scheme 1.1 Three generations of amperometric enzyme electrodes for sensing alcohol: **I:** 1st generation where either O_2 depletion or formation of H_2O_2 is measured. **II:** 2nd generation where an artificial mediator is used. **III:** 3rd generation where direct electron transfer between enzyme and electrode is used.

The general strategies used for the electrochemical sensing of alcohols are the measurement of oxygen consumption or H_2O_2 production, use of a diffusible or immobilized mediator, or by using direct electron transfer of the electrons from AOx to the electrode. Alcohol biosensors which involve detection of O_2 or H_2O_2 come under first generation of biosensors (Azevedo et al. 2005) (Scheme 1.1 **I**). Amperometric measurements based on the monitoring of oxygen consumption using a polarographic oxygen probe was initially developed by Clark (Clark and Lyone 1962). A negative potential (-0.7 V) is applied to the platinum cathode of the probe for a reductive detection of oxygen consumption. For developing the 2nd generation amperometric alcohol biosensors the redox species like, ferrocene derivatives, redox hydrogels, poly (neutral red), and ferricyanide derivatives have been exploited as the electron transfer mediators (Scheme 1.1 **II**) (Hasunuma et al. 2004; Boguslavsky et al. 1995; Vijayakumar et al. 1996). The advantage of using these mediators is

their low redox potential that substantially reduce the chance of interference caused by the co-existed electroactive species present in the sample. In order to function effectively, the mediators should be insoluble, nontoxic, and chemically stable and should possess good electrochemical properties. Leaching of these toxic mediators however makes them unsuitable for use *in vivo* detection systems. However, this problem can be overcome by wiring the AOx with the electron mediators. Nevertheless, wiring may cause conformational change of the enzyme that may impair the stability of the enzyme.

In recent years, alcohol biosensor research focussed on the direct electron transfer (DET) between AOx redox active site (FAD) and electrode surfaces (Das and Goswami 2013). The direct electron transfer results into the flow of current that is proportional to alcohol concentration in the sample. The electron transfer between the active site of AOx and the electrode is the limiting factor in the operation of the 3rd generation amperometric alcohol biosensors (Scheme1.1 **III**). The electronic communication between AOx and conventional electrodes is poor because of the deep embedment of FAD redox center in the protein shell that acts as an insulating barrier to DET (Goswami et al 2013). Consequently, for establishing better electrical contact between the AOx redox center and the electrode surfaces, different approaches have been proposed and one of them is the nanofabrication of the bioelectrode with highly conductive nanomaterials. In this regard MWCNTs was projected as a nanomaterial of great promise due to its clear effect on establishing DET, as witnessed from many amperometric biosensors successfully developed in the recent past (Agui et al. 2008; Vatsyayan et al. 2011; Das and Goswami 2013).

In 3rd generation electrochemical biosensors various electron transfer parameters are characterized by using direct electrochemistry techniques on the immobilized redox enzymes. Cyclic voltammetry (CV) is usually carried out with working electrodes at different potential scan rates (v) to obtain various electron transfer parameters. At first the redox potentials

(anodic potential (E_{pa}) and cathodic potential (E_{pc})) of the fabricated working bioelectrode is determined in an argon-saturated buffer solution at a fixed scan rate (for example: v = 50 mVs^{-1}). In DET if the peak separation (ΔEp) is > 59 mV, which is more than the peak separation of a reversible process (59 mV), represents a quasi-reversible redox process (Scott and Lukehart 2007). Moreover, with increase in scan rate, if the anodic (E_{pa}) and cathodic (E_{pc}) peak potentials shift to more positive and more negative values respectively increasing the ΔEp, further suggests a quasi-reversible process. Besides this, if the magnitudes of anodic (I_{pa}) and cathodic (I_{pc}) peak currents increased linearly with increasing scan rate the phenomenon is described as a surface confined redox process and indicates a thin-layer electrochemical behavior (Scott and Lukehart 2007). For a quasi-reversible wave, the relationship between peak potential and scan rate conform to the following equation (Laviron's equation) (Laviron 1974):

$$E_p = E^{o'} + \frac{RT}{\alpha nF} + \frac{RT}{\alpha nF} \ln v \qquad (1.1)$$

E is the peak potential (cathodic or anodic), $E^{o'}$ is the apparent standard potential. R is the thermodynamic gas constant (8.314 J K^{-1} mol^{-1}), F is the Faraday constant (96,500 C mol^{-1}) and T is the temperature (298 K). The symbols n and v are the electron transfer number and scan rate, respectively. The product of charge transfer coefficient (α) and n, αn is calculated from the slope of the E_{pa} versus ln$v$ plot.

The surface concentration of the ionic species (Γ) (mol cm^{-2}) on working bioelectrode can be estimated from the plot of peak current versus scan rate (v) using Brown-Anson model that is based on the following equation (Laviron 1979):

$$I_p = \frac{n^2 F^2 \Gamma A v}{4RT} \qquad (1.2)$$

Where *n* is the number of electrons transferred and *A* is the surface area of the electrode. The symbols *F*, *R* and *T* have their usual meanings. The heterogeneous electron transfer constant (k_s) of the bioelectrode could be obtained by the following equation (Laviron 1979):

$$\log k_s = \alpha\log(1-\alpha) + (1-\alpha)\log\alpha - \log\frac{RT}{nFv} - \frac{\alpha(1-\alpha)nF\Delta E_p}{2.3RT} \quad (1.3)$$

Where α is the charge transfer coefficient and k_s is the heterogeneous electron transfer rate constant and *R, T, F* and *n* having their usual significance.

1.5. Matrices for enzyme immobilization

A crucial step in the fabrication of any enzyme based biosensor is the immobilization of the enzyme molecules on the sensing surface (electrode in case of amperometric technique) since, the immobilization strategies for biomolecules are of paramount importance in order to preserve their biological activity. This is done with the help of an immobilizing material called matrix whose function is to hold the enzyme molecules on the electrode. The properties of the matrix being used, govern the efficiency of the fabricated biosensor in terms of sensitivity, selectivity and stability (Sarma et al. 2009). There are various properties of the matrix desirable for the successful immobilization of biomolecules on the electrode surface. The support matrix should have good mechanical stability, rigidity and good flow properties for enzyme stability and activity on storage (Park et al. 2010). Also it should be adaptable to different environments like different pH, temperature, ionic strength and chemical composition of the solvents. Apart from this, a good support material should be non-degradable and biocompatible. Different types of matrix materials have been utilized to immobilize enzyme for the construction of ethanol biosensor over the years. Conducting polymers, sol–gel/hydro-gels, nanomaterials and self-assembled monolayer are the most

common materials. Each of the matrix material has its own advantages and disadvantages. The final support matrix may consist of either a single component or multi components. Intensive research activities are continuously pursued to develop new matrices for immobilization of enzymes.

1.5.1. Conducting polymers

During the construction of amperometric enzyme electrodes attention is given to provide suitable architecture to the electrode for facile charge transfer from the biochemical reactions to the electronic circuit. To some extent, this can be controlled by applying suitable potential. However, some reactions, specifically those which involve biomolecules endure rather slow interfacial electron transfer even with large electrochemical driving forces. This problem can be mitigated by modifying a given electrode with a thin film of an electroactive polymer. These electroactive polymers or conducting polymers are become the materials of choice for the amperometric biosensor fabrication as they can act both as a binding matrix and as electron transfer mediator for the signal amplification of the biosensors (Ahuja et al. 2007; Sarma et al. 2009; Nambiar and Yeow 2011). Conducting polymers are the resonance stabilized π–conjugated organic polymers. They are also termed as "synthetic metals" since they mimic the electrical, electronic, magnetic and optical properties of metals. The conductivity in the conducting polymers is due to the delocalization of π - electrons providing the highway for charge mobility along the backbone of the polymer chain. Other than their conducting nature, they have other features like optical transparency, flexibility in chemical structure, controllable electrochemical properties, biocompatibility, ion selectivity and ease of handling (Zhao et al. 2009). Conducting polymers are traditionally synthesized by electrochemical (Basozabal et al. 2011), chemical (Gherras et al. 2012) and enzymatic polymerization (Kausaite-Minkstimiene et al. 2011) reactions. During the process of

electrochemical synthesis, the conducting polymers could be easily doped by various biomaterials including enzymes and the reactions have been identified as most specific for the preparation of films. The chemical and enzymatic approaches are more suitable for the preparation of conducting polymers based nanoparticles. Electrochemical and chemical syntheses of conducting polymers require high concentrations of monomers and involve toxic catalysts or strong oxidizing agents for polymerization and usually are performed at extremely low pH values (Li et al. 2012). Therefore enzymatic synthesis of conducting polymers is applied as an alternative method suitable for the formation of composite materials based on conducting polymers such as polyaniline (PANI), polypyrrole (Ppy), polythiophene, polyphenylene for the development of amperometric alcohol biosensors. PANI provides an excellent matrix for dispersing noble metals, which expands its usage, and has been used in the fields of catalysts and sensors (Xu et al. 2010). AOx immobilized on a perm selective electropolymerised polypyrrole modified gold electrode was used for an interference free detection of alcohol (Carelli et al. 2006). An amperometric alcohol biosensor was developed by immobilizing AOx through Polyamidoamine (PAMAM) dendrimers on a cysteamine modified gold electrode surface. Ethanol determination is based on the consumption of dissolved oxygen content due to the enzymatic reaction. The decrease in oxygen level monitored at -0.7 V vs. Ag/AgCl and correlated with the ethanol concentration in the samples (Akin et al. 2010). Immobilization of AOx was achieved in the copolymer of pyrrole with vinyl alcohol and thiophene side groups (PVATh-*co*-PPy/AOx) during electrochemical polymerization (Yildiz et al. 2007). AOx immobilized in resydrol polymer for ethanol detection was carried out by electrochemical deposition of the polymer film by applying the potentiostatic pulse profile (Shkotova et al. 2006). Alcohol biosensor based on conducting PPy, poly(3,4-etylenedioxythiophene) (PEDOT) and poly(3,4-ethylenedioxypyrrole) (PEDOP) were constructed during electro-polymerization of the

monomers in sodium dodecylsulfate (SDS) and phosphate buffer electrolysis medium (Turkarslan et al. 2010).

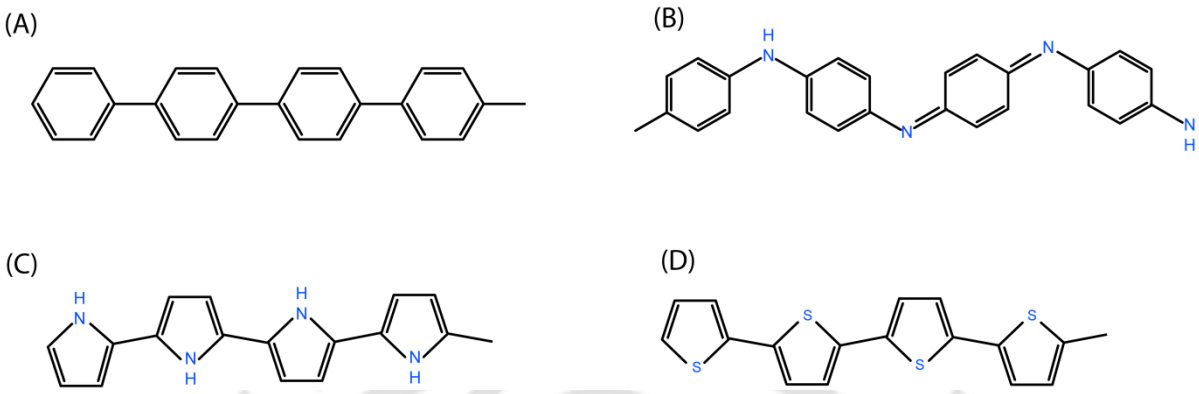

Figure 1.1 Chemical structures of conducting polymers. **A**: poly(*p*-phenylene), **B**: polyaniline, **C**: polypyrrole and **D**: polythiophene.

Photonic wiring of AOx onto conducting polymer of 4-(2,5-di(thiophen-2-yl)-1H-pyrrol-1-yl) benzenamine (SNS-NH_2) and carbon nanotubes (CNTs) modified gold slides was carried out for determination of short chain alcohols (Yildiz et al. 2014). Amperometric biosensors based on AOx immobilized on the conducting polymers of 3.4-ethylenedioxythiophene (PEDOT) and, 4,7-dithien-2-yl-2,1,3-benzothiadiazole (TBTD) were constructed and characterized for sensitive detection of alcohol (Tanriverdi et al. 2012). A homogenized mushroom (*Agaricus bisporus*) tissue based alcohol bioelectrode was also developed by immobilizing the tissue with gelatin and glutaraldehyde at dissolved oxygen probe (Akyilmaz et al. 2000). An amperometric enzyme electrode for the determination of alcohols was developed by immobilizing AOx in polyvinylferrocenium matrix on a Pt electrode surface (Gulce et al. 2002).

1.5.2. Sol-gels and hydro-gels

Sol-gel and hydrogel derived materials are another class of materials which are emerged as promising matrices for enzyme immobilization in biosensor fabrication (Yao and Takashima 1998; Tan et al. 2005). Sol-gel based materials possess physical rigidity, chemical inertness, tunable porosity, thermal and chemical stability, negligible swelling in aqueous and organic solutions etc. (Lev 1992). They also show good biocompatibility by allowing immobilization of large amount of enzymes with stable tertiary structures without denaturation (Lei et al. 2004). Tetraethylorthosilicate (TEOS) and tetramethoxysilane (TMOS) are effective precursors for the formation of sol-gels, which were used for the estimation of alcohol (Xu et al. 2005). Despite the many advantages of a sol-gel immobilization matrix, the brittleness of the sol-gel matrix is a major obstacle in their wide adoption as an immobilization matrix for biomolecules (Cho and Lee 1997). The sol-gel based inorganic-organic hybrid materials have found widespread applications (Haas 2000; Kajiwara and Krakovskyi 1995). These materials can effectively overcome the brittleness of inorganic sol-gel materials, and could be used to prevent unwanted substances from reaching the underlying surface and pre-concentration of analyte for electrochemical detection or trace electroanalysis (Wei and Collinson 1995). Hence various inorganic precursors such as (3-aoryloxypropyl) dimethoxymethylsilane (APDMOS), TEOS and TMOS for the formation of sol-gels were cross linked with organic polymer chitosan to prepare a new organic/inorganic sol-gel for enzyme immobilization. Another advantage of this new hybrid material is the widely present amino groups in chitosan molecules, providing a hydrophilic environment that is compatible with the biomolecules (Groboillot et al. 1993). Hydrogels are polar, uncharged water swellable, flexible materials which favor biocompatibility, due to their high water content (Brahim et al. 2002). When coated on electrode surface, these hydrogels act as antifouling agents and produce a hydrophilic interface from which water-soluble analytes can

readily diffuse from the aqueous bulk to the solid surface. The most widely used hydrogels are cross-linked polymers of poly (hydroxyethyl methacrylate) (pHEMA) of polyethylene glycol (PEG). Apart from these, the use of sol-gel and hydrogel based matrices have other benefits like their simple construction procedures and flexibility in controlling pore size and geometry. These matrices can easily be modified with various mediators, polymer additives etc. to furnish electrical conductivity to them so that these can be used in electrochemical biosensors (He et al. 2011). Composite materials of sol-gels and hydrogel based materials along with other matrices like polymers, conducting polymers and nanomaterials were also used in developing alcohol biosensors (Brahim et al. 2002; Tan et al. 2005; Wu and Choi 2003). Ethanol biosensors based on sol-gels and hydro-gels were described below. Vijayakumar and group had fabricated amperometric alcohol biosensors by co-immobilizing AOx with hydrogen peroxide reducing enzyme, HRP in a carbon paste matrix. An osmium containing three-dimensional redox hydrogel, (poly[1-vinyl imidazole osmium (4,4'-dimetyl-bipyridine)$_2$Cl])$^{+/2+}$ was used to "wire" enzymes (Vijayakumar et al. 1996). Smutok and group developed a sensitive amperometric ethanol bi-enzyme biosensor by co-immobilization of HRP with AOx in electrodeposition paint (EDP). Enzyme immobilization was performed by means of EDP with a first layer integrating HRP within an Os-complex modified anodic EDP in order to assure fast electron transfer between the enzyme and the electrode. On the top of this layer AOx was entrapped within a cationic EDP thus assuring fast substrate diffusion within the hydrogel layer concomitantly with a stabilization of the enzyme (Smutok et al. 2006). Castillo and group has fabricated an amperometric biosensor for alcohol using oxidase/peroxidase bienzyme systems using redox polymers poly(ethylene glycol) (400) diglycidyl ether (PEGDGE) and poly(vinylimidazole) complexed with Os(4,4' dimethylbipyridine)2Cl (PVI-dme-Os) (Castillo et al. 2003). Boujtita and group developed an AOx disposable ethanol biosensor based on a screen printed carbon electrode doped with a

redox hydrogel, cobalt pthalocyanine (Co-PC-SPCE) (Boujtita et al. 2000). Patel and co-workers carried out the fabrication of a screen-printed AOx sensor using poly(carbamoyl)sulfonate (PCS) hydrogel for low-cost detection of ethanol in wine samples (Patel et al. 2001). Although sol-gel and hydrogel based materials are proved to be promising they often face several drawbacks (Solanki et al. 2009) such as diffusional limitations through the porous network and poor reproducibility (Wang et al. 2003). The encapsulated enzyme may lose its catalytic efficiency due to the reduction of substrate binding and release rate by mass transport barrier of the sol-gel. Moreover, the biosensor based on these matrices may face unfavorable problem of enzyme leakage (Tan et al. 2005). For better confinement of enzyme, the matrix pore size has to be controlled. The concentration of a polymer solution for making a membrane should be optimized to generate pore size large enough to prevent the diffusion barrier and small enough to prevent enzyme leakage (Smith et al. 2002).

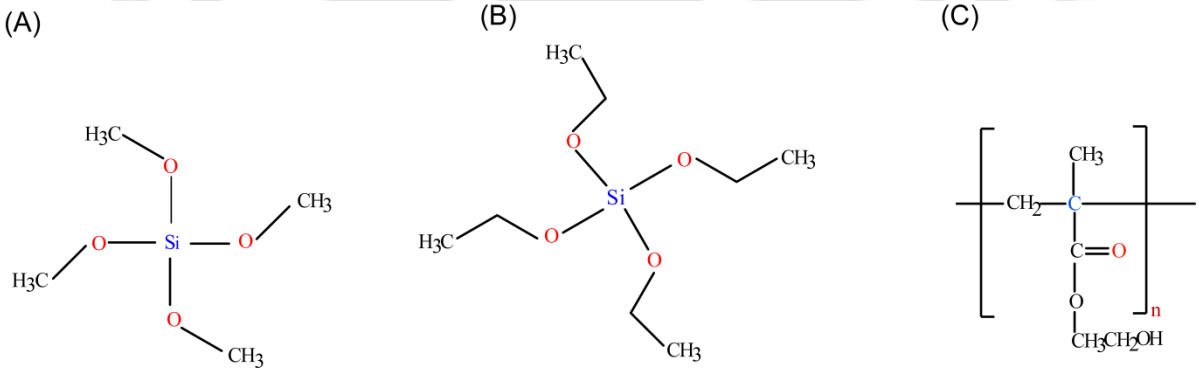

Figure 1.2 Chemical structures of the precursor sol-gel materials. **A:** Tetraethoxysilane, **B:** Tetraethylorthosilicate; **C:** Poly(hydroxyethylmethacrylate).

Santos and group fabricated a reagentless amperometric biosensor sensitive to ethanol. This sensor comprises a carbon paste electrode modified with ADH, NAD^+ cofactor

and Meldola's blue (MB) adsorbed on silica gel coated with niobium oxide. The amperometric response was based on the electrocatalytic properties of MB to oxidize NADH, which was generated in the enzymatic reaction of ethanol with NAD^+ under catalysis of ADH (Santos et al. 2003).

1.5.3. Self-assembled monolayers

Self-assembled monolayer (SAM) is a layer of molecular thickness formed by chemisorption of selected organic molecules on solid metal surfaces (Chaki and Vijayamohanan 2002). The organic molecules used to generate SAMs are generally bifunctional molecules of different terminal functional groups (sulfides, thiols amines, etc.) which can be tailored using various chemistries making them compatible for desired applications (Arya et al. 2009). Self-assembly technique offers several interesting perspectives in the field of biosensors. Functionalized SAMs can provide a reproducible and robust method of immobilizing desired biomolecules in the near vicinity of the electrode where some control over the orientation and distribution of the enzyme is afforded (Wink et al. 1997). Besides this, there are other numerous benefits of using SAMs in biosensor systems. Immobilization over SAMs modified surface can be achieved using either covalent or noncovalent coupling techniques requiring only minimal amount of biomolecule. The high degree of ordered and dense nature of SAMs mimics the membrane like cellular microenvironment and shield biomolecules from the sensor surface, preventing possible denaturation (Chaki and Vijayamohanan 2002). The improvements of detection limits and stability, the ability to regenerate the sensor, prevention of specific adsorption are other features using SAM (Nakaminami et al. 1999). SAM technology can be used to develop electrochemical, optical or piezoelectric sensors. In electrochemical biosensors, SAMs can be used for obtaining electroactive surface and can act as molecular wire between the

biomolecule and the electrode surface. Several reviews are available on the application of SAMs for biosensors (Chaki and Vijayamohanan 2002; Samanta and Sarkar 2011; Vijayamohanan and Aslam 2001). A couple of AOx biosensors based on SAMs were developed for sensitive detection of ethanol and methanol. Narvaez and group have developed a modular configuration consisting of gold electrodes (Au) on which transducing and biocatalytic modules are sequentially self-deposited through adsorption by electrostatic interactions. Alcohol sensors have been made by sequential and rational deposition of two different catalytic layers, one containing AOx and the other a modified HRP, and an electrochemical interface resulting in supramolecular structures that efficiently connect catalytic reactions, substrate and product diffusion and heterogeneous electron transfer steps. The electro chemical interface includes a positively charged redox polymer, which allows the electrical communication of the enzymes with the transducing surface, and a binder, which has the same structure as redox polymer without the osmium redox centers (Au/MPS/RP/HRPmod/Binder/AOX) (Narvaez et al. 2000). Hasunuma and group developed a self-assembled bienzyme oxidase and peroxidase sensor using a 11-ferrocenyl-1-undecanethiol as an electron mediator on gold electrode for determination of methanol on crude plant extracts (Hasunuma et al. 2004).

There are some limitations too identified on using SAM. Firstly, SAMs can decrease electron-transfer rates. Enzymes immobilized on SAMs are very much sensitive towards changes in pH, ionic strength and temperature: a minor change in one of these parameters may lose the biological activity. The chemical stability of some of the SAMs is not very good as monolayer can be chemically oxidized during the course of investigations. Electric field induced thermal desorption of monolayer is detrimental to biosensor applications. Due to high surface energy, hydrophobic SAM surface can accumulate several contaminants and

hence unwanted impurities can adsorb and block the analyte recognition sites (Chaki and Vijayamohanan 2002).

1.5.4. Nanomaterials

Nanotechnology has recently attracted extensive interest in the area of bioanalytical chemistry. Owing to their nanoscale dimensions, nanomaterials like nanoparticles (NPs), nanorods and nanotubes exhibit unique chemical, physical and electronic properties that are different from their bulk counterparts. The dimensional similarity between various nanomaterials and biomolecules made it possible to conjugate them into novel functional biomolecule-nanomaterial hybrid systems. These hybrid systems have synergistic properties originating from highly selective, catalytic and recognition properties of biomolecules and unique electronic, photonic, and catalytic features of nanomaterials (Guo and Dong 2009). This brings endless opportunities for interfacing biological recognition events with electronic signal transduction so as to design a new generation of bioelectronic devices. Different kinds of nanomaterials, and sometimes the same kind of nanomaterials can play different roles in different electrochemical sensing systems (Katz et al. 2004). Due to their high surface area, favorable electronic properties and electrocatalytic effect, nanomaterials modified electrodes provide a larger electroactive surface area for higher biomolecule loading (Asefa et al. 2009; Kim et al. 2008) and increased flow of electrons between the electrode and the biomolecules that probably help in decreasing the overpotential, amplifying biorecognition signal and increasing overall sensitivity of the biosensor. Also, due to their biocompatibility, they help in retaining the bioactivity of biomolecules on their surface which otherwise is frequently lost when biomolecules are directly immobilized on naked surfaces of bulk materials (Pingarron 2008). These properties of nanomaterials make them attractive immobilization matrix for construction of electrochemical enzyme biosensors. Metal nanoparticles (gold and platinum),

oxide nanoparticles (zinc oxide), carbon nanotubes are among the most widely used nanomaterials in the area of biosensors. There has been substantial progress in the past decade in biomolecule-NP hybrids for electrochemical biosensors that has established nanobioelectrochemistry as a mature scientific discipline. Several comprehensive reviews summarized important achievements in the field of electrochemical nanobiosensors (Hyun and Park 2011; Mi et al. 2009; Vaddiraju et al. 2010; Wang 2005).

Nanomaterials have found application in the development of alcohol biosensors. Carbon nanotubes and their composite with nanoparticles, owing to low potential detection of alcohol, high sensitivity and fast response, have gained much interest in application to alcohol biosensor. Morales and co-workers fabricated a nanocomposite based alcohol bioelectrode based on graphite powder, AOx and an epoxy resin (Morales et al. 1998). de Parda and group developed a composite graphite-Teflon electrode, in which the enzymes AOx and HRP, as well as the mediator ferrocene were incorporated into the electrode matrix for the reliable monitoring of alcohols in food and beverages (de Parda et al. 2003). A disposable amperometric ethanol biosensor was developed using screen-printed carbon electrodes mediated with a ferricyanide-magnetic nanoparticle mixture (Liao et al. 2006). Wu and group proposed a sensitive alcohol biosensor based on thionine-CNF nanocomposite with good dispersion. With a simple one-step electropolymerization of thionine-CNF nanocomposite and AOx, a stable poly(thionine)-CNF/AOx biocomposite film was created on electrode surface for detection of alcohol (Wu et al. 2007). Tsai and group fabricated a novel amperometric ethanol biosensor using ADH physically immobilized within poly(vinyl alcohol)-MWCNT composite by a freez thawing process (Tsai et al. 2007). Gouveia-Caridade and group fabricated an alcohol biosensor based on functionalized MWCNTs and AOx-BSA cross linked with glutaraldehyde (Gouveia-Caridade et al. 2008). Zhen and group

developed novel disposable amperometric biosensor strip for determination of blood alcohol concentration using nanocomposite film (GNPs-MWCNT-Nafion) (Zhen et al. 2011). Le and Tsai prepared an amperometric biosensor for the determination of ethanol using a nano biocomposite film of MWCNTs-Chitosan-ADH (Lee and Tsai 2009). Hydrothermally grown zinc oxide (ZnO) nanowires network modified with thin Au layer (~10 nm) sense the ethanol with maximum response at an operating temperature of 325 °C. Incorporation of Au not only enhances the sensor response but also improves the reaction kinetics towards ethanol. The response and recovery times for Au modified sensor films towards 50 ppm of ethanol at 325 °C were 5 and 20 s, respectively. This faster reaction kinetics has been attributed to the role of Au in improving the sensing properties as per the electronic sensitization mechanism and its nano-Schottky barriers type junction with ZnO (Ramgir et al. 2013). Santos and group studied MWCNT as transducer, stabilizer and immobilization matrix for the construction of amperometric biosensor based on ADH and MB. The amperometric response was based on the electro catalytic properties of MB to oxidize NADH, which was generated in the enzymatic reaction of ethanol with NAD^+ under catalysis of ADH (Santos et al. 2006). Manso and group fabricated a novel ethanol biosensor based on the bulk incorporation of ADH into a colloidal gold (Au coll)-MWCNTs composite electrode using Teflon as binding material (Manso et al. 2008). Recently Das and Goswami established direct electron transfer between AOx immobilized on MWCNTs and modified GCE (Das and Goswami 2013).

AuNPs have also been widely studied for developing enzyme based electrochemical biosensors. The favorable functional traits of these nanoparticles that drive these studies are their strong electrical and biocompatible properties. The other reason of using AuNPs in amperometric biosensors is their high surface to volume ratio, which is a common property of nanoparticles that serves to increase enzyme loading on the electrode surface for amplifying

the sensor signal and tailored wider detection range (Saxena et al. 2011). The coupling of AuNPs with the enzyme molecules is however, a critical issue to utilize the intended properties of the nanoparticles for achieving the desired level of response of the constructed biosensors. Moreover, the mode of coupling significantly influences the reproducible response characteristics of the constructed biosensors. For example, the high linker distance between the enzyme protein and AuNPs obtained by common chemical immobilization may interfer the electrocatalytic response of the biosensor, while the physical immobilization may impair the stable interaction between the enzyme and the AuNPs thus hindering the reproducible performance of the constructed biosensors (Saxena and Goswami 2012). However, analytical validation for the control of the surface characteristics under similar conditions has been a difficult task. Small variation in the density of the metal nanoparticles or the biomolecules that are attached to them would cause large variations between batches of measurements. As modification of the surface became more sophisticated with various nanomaterials immobilized onto a single surface, the reproducibility and repeatability of the measurements had to be sacrificed. The researchers are now working on automating surface modification techniques using nanomaterials (Kerman et al. 2008).

Although electrochemical biosensors have several positive attributes, their potential applications using complex matrices for analysis of real samples remain the major challenges for onfield applications. Complementary strategies involving nanomaterials are therefore the subject of intense study. We are in the early days of emerging technology of using nanomaterials to modify biosensors. Although many improvements are required in achieving reproducibile and sensitive biosensor, there is no doubt that a growing number of nanomaterial-based biosensors will soon be offered for diagnosis of diseases and monitoring following therapy (Kerman et al. 2008).

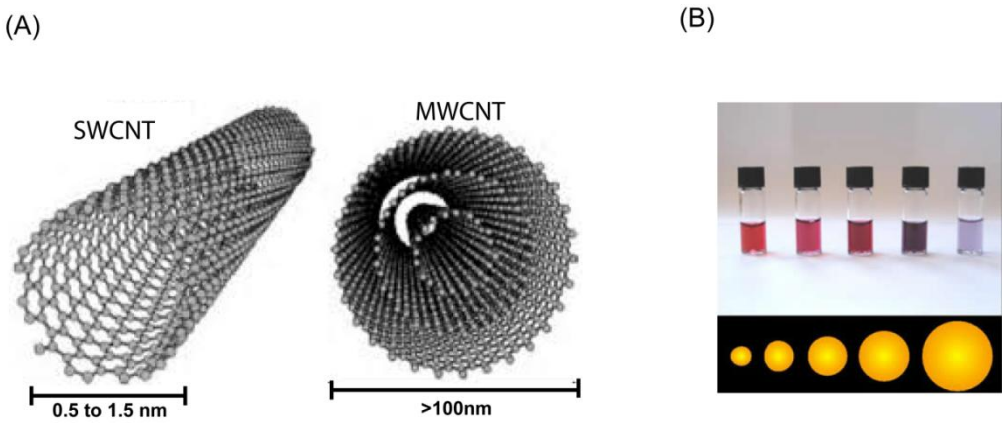

Figure 1.3 A: Schematic representations of single walled and multiwalled carbon nanotubes and **B:** Solutions of gold nanoparticles of various sizes. The size difference causes the difference in colors.

1.6. Methods for enzyme immobilization

The success of a biosensor relies on how well an enzyme binds to a desired biosensor surface and remains active during a desired application. The immobilization technique used to attach the biological material to a transducer surface is considered as one of the decisive steps that decide the operational behavior of a biosensor. Various factors influence the selection of immobilization method, such as biomolecule, transducer type, the nature of the analyte and the operating conditions of the biosensor (Luong et al. 1988). The method needs to be compatible with the biomolecule being immobilized and the matrix on which immobilization is to perform. The immobilization method should bring about high enzyme loading to ensure sufficient biocatalyst activities (Zhao and Jiang 2010). The immobilized biomolecules must also retain biological activity after immobilization, remain tightly bound to the surface and should not be desorbed during the use of the biosensor. The improper selection of immobilization technique can cause damage to the conformation of biomolecules

leading to the deactivation of biomolecular activity (Arya et al. 2008). Generally the choice of the matrix material decides the choice of the immobilization method. Commonly used methods include physical adsorption, entrapment, covalent binding using activators or cross-linkers and chemical crosslinking with gluteraldehyde or other bifunctional agents.

1.5.1. Entrapment

The method of entrapment is based on the localization of an enzyme within the interstitial spaces of a crosslinked and water-insoluble polymer matrix or semi-permeable membranes. This localization is independent of formation of bonds or chemical coupling between the enzyme and gel matrix or membranes. The matrix used for the entrapment should be tight enough to prevent the leakage of the biocatalyst and permeable enough for the substrate(s) or product(s) to diffuse into or out of the reaction medium. The advantages of the technique include extremely large surface area for contact between substrate and enzyme within a relatively small volume and the possibility of co-immobilizing different types of enzymes physically separated from each other in a single step. The technique does not alter the conformation of the enzyme where only aqueous solvents are used (Park et al. 2010). In the fabrication of an alcohol biosensor, entrapment of enzyme within a polymer or a membrane matrix has been widely used (Table 1.2). In most cases entrapment of a biomolecule is accomplished during polymeric gel or sol-gel preparation in a solution containing biomolecules. The entrapment can also be achieved using layer-by-layer or electrochemical polymerization techniques. Shkotova et al (2006) immobilized the AOx in resydrol polymer by using potentiostatic pulse profile consisting of 20 consecutive pulses of +1900 mV for 0.3s for ethanol detection. Kulys and Schmid (1991) have carried out the immobilization of AOx by entrapping against the electrode surface using a dialysis membranne.

Table 1.2 Alcohol biosensors based on entrapment immobilization of enzyme.

Biosensor configuration	Sensing element	Sensor Parameters	References
Pt/polyvinylferrocenium matrix	AOx	Linearity: 3.0 mM Detection limit: N.R Sensitivity: 9.1 µA mM^{-1} Stability: 94 % in 36 days	Gulce et al. 2002
Graphite rod/DMFc	AOx HRP	Linearity: 0.2-1.0 mM Detection limit: N.R Sensitivity: N.R Stability: N.R	Kulys and Schmid 1991
Pt/PEDOP	AOx	Linearity: N.R Detection limit: 170 mM Sensitivity: 0.021 µA mM^{-1} Stability: 20 % in 28 days	Turkarslan et al. 2010
Pt/Resydrol polymer	AOx	Linearity: N.R Detection limit: 2.75µM Sensitivity: N.R Stability: 4 % in 24 h	Shkotova et al. 2006
PVATh-co-PPy	AOx	Linearity: N.R Detection limit: N.R Sensitivity: N.R Stability: N.R	Yildiz et al. 2007
PVA-SbQ	AOx Catalase	Linearity: 0.75 mM Detection limit: 0.5 µM Sensitivity: 0.394 µs μM^{-1} Stability: 5 % in 16 weeks	Hnaien et al. 2010
Pt/Os-AP59/CP9	AOx HRP	Linearity: 2.0 mM Detection limit: N.R Sensitivity: 0.2 µA mM^{-1} Stability: 50 % in 14 days	Smutok et al. 2006
Pt/poly(carbamyl) sulfonate-hydrogel	AOx	Linearity: 0.01-3.0 mM Detection limit: 0.5 µM Sensitivity: 40 µA mM^{-1} Stability: 45 % in 8 days	Patel et al. 2001
Poly(thionine)-CNF	AOx	Linearity: 0.02-0.252 mM Detection limit: 1.7 µM Sensitivity: 4.1 µA mM^{-1} Stability: 4 % in 4 weeks	Wu et al. 2007

*Few values were normalized for making the units uniform for better comparision. The stability was reported as the decrease in biosensor response. Pt: Platinum, DMFc: 1, 1' dimethylferrocene, PEDOP: poly(3,4-ethylene dioxypyrrole), PVATh-co-PPy: Polypyrrole with vinyl alcohol and thiophene side chains, PVA:Polyvinyl-alcohol, SbQ: Strylpyridinium groups, Os: Osmium; AP: Anodic paint, CP: Cathodic paint, CNF: Carbon-nano fiber.

Smutok et al. (2006) developed a reagent less bienzyme alcohol biosensor by entrapping HRP and AOx in electrodeposition paints made up of acrylic acid and (dimethylamino)ethylmethacrylate (DMAEMA). Yildiz et al. (2007) immobilized AOx within conducting polymers of thiophene functionalized poly(vinyl alcohol) with pyrrole.

Hanaien et al (2010) developed a conductometric alcohol biosensor through immobilization of AOx in a photoreticulated poly(vinyl alcohol) membrane. Gulce et al. (2002) developed an enzyme electrode by immobilization of AOx in polyvinylferrocenium (PVC) matrix coated on a Pt electrode surface. Turkarslan et al. (2010) immobilized AOx within polypyrrole, poly(3,4-ethylenedioxythiophene) (PEDOT) and poly(3,4-ethylenedioxypyrrole) (PEDOP) through electropolymerization. Wu et al. (2007) immobilized the AOx on thionine-carbon nanofiber with a simple one-step electrochemical polymerization. Patel et al. (2001) carried out the immobilization of AOx within poly(carbamoyl)sulfate hydrogel exploiting the entrapment technique.

There are, however, some major drawbacks of the entrapment method. Firstly, the diffusional barriers as well as the steric hindrance to high molecular weight substrates make the method unsuitable for few enzymes acting on macromolecular substrates. This may slow down the reaction and the response time of the biosensor. Secondly, some loss of enzyme activity due to the production of free radicals during polymerization or leakage through the wide pores in the gel could occur.

1.5.2. Physical adsorption

Physical adsorption involves the direct adsorption of enzymes on the surface of matrix. This is a simple, economical, reversible and quick method for immobilizing an enzyme with the retention of its activity. In the immobilization method the interaction between enzyme and matrix is based on van der Waals forces, ionic binding or hydrophobic forces. Many substances adsorb enzymes on their surfaces, eg. alumina, charcoal, clay, cellulose, kaolin, silica gel, glass and collagen. The main advantage associated with direct adsorption onto solid surfaces is that it is simple and can be used under mild conditions with little or no conformational changes of the enzyme or destruction of its active center. There are

few reports where the immobilization based on physical adsorption method has been used for the development of alcohol biosensors (Table 1.3).

Table 1.3 Alcohol biosensors based on physical adsorption based immobilization of enzymes.

Biosensor Configuration	Sensing element	Sensor parameters	References
CPM/Os	AOx HRP	Linearity: 4.0 mM Detection limit: 10 µM Sensitivity: 1.31 µA mM^{-1} Stability: 10 % in 9 h	Vijayakumar et al. 1996
MWCNT-CHIT	ADH	Linearity: N.R Detection limit:0.52 µM Sensitivity:164.6 µA mM^{-1} Stability: 15 % in 30 min	Lee and Tsai 2009
PVA-MWCNT	ADH	Linearity: 1.5 mM Detection limit: 13 µM Sensitivity: 0.196 µA mM^{-1} Stability: 12 % IN 30 min	Tsai et al. 2007
Graphite/redoxpolymer/ SPPT/Gentamycine	AOx HRP	Linearity: 5 mM Detection limit: N.R Sensitivity: 0. 71 µA mM^{-1} Stability: N.R	Boguslavsky et al. 1995
MWCNT-Nf-AOx-PEI	AOx	Linearity: 0.08-0.42 mM Detection limit: 5 µM Sensitivity: 3.0 µA mM^{-1} Stability: 10 % in 4 weeks	Das and Goswami 2013
CPM-(graphite-Teflon)/ ferrocene	AOx HRP	Linearity: 0.01-0.75 mM Detection limit: 19 µM Sensitivity: 1.9 µA mM^{-1} Stability: No loss in 15 days	de Prada et al. 2003
GNPs-MWCNT-MB-Nafion	ADH	Linearity: 0.2-2.5 mM Detection limit: 5.0 µM Sensitivity: 0.093 µA mM^{-1} Stability: 5.8 % in 30 days	Zhen et al. 2011
Pt/porous Teflon membrane	AOx	Linearity: 0.10-30 mM Detection limit: 9.9 µM Sensitivity: 3.43 µA mM^{-1} Stability: N.R	Hammerle et al. 2011
Chitosan/eggshell membrane	AOx	Linearity: 0.06-0.8 mM Detection limit: 30 µM Sensitivity: N.R Stability: 13.4 % in 90 days	Wen et al. 2007.

*Few values were normalized for making the units uniform for better comparision. The stability was reported as the decrease in biosensor response. CPM: Carbon paste matrix, Os: Osmiun, MWCNT: multiwalled carbon nanotube, CHIT: chitosan, SPPT: Poly[N, N'-sulfono-(p-phenyleneterephthalamidel)], Nf:Nafion, PEI: Poly-ethylenimine, GNPs: Gold nanoparticles, MB: Meldola's blue.

Tsai and group have carried out the physical immobilization of ADH onto the poly(vinyl alcohol)-multiwalled carbon nanotube by freez-thawing process (Tsai et al. 2007). de Prada et al. (2003) developed a bienzyme sensor by physical inclusion of the enzyme and the mediator in the bulk of graphite-70 % Teflon cylindrical pellets. Das and Goswami (2013) developed a 3rd generation bioelectrode by immobilization of AOx using MWCNT and nafion nanocomposite. Lee and Tsai (2009) have carried out the immobilization of ADH on MWCNT-chitosan nanocomposite using physical adsorption of ADH for amperometric detection of ethanol. Hammerle et al. (2011) developed a gas alcohol sensor using by immobilization of AOx on a porous Teflon membrane coated with thin platinum. Zhen et al. (2011) used the layer-by-layer physical adsorption technique for measuring blood alcohol concentration using a disposable biosensor strip. Physical adsorption also has certain disadvantages. The immobilized enzyme may get desorbed from the matrix during operation due to changes in temperature, pH or ionic strength.

1.5.3. Covalent binding using activators or cross-linkers

The immobilization of biomolecules onto a matrix can also be achieved by binding of functional group of enzymes and matrix via covalent bonds. The bond is normally formed between functional groups on the carrier and groups on the enzyme not essential for catalytic activity (Aravamudhan et al. 2007a; Yang et al. 2006c). The support materials must possess reactive groups. If they do not, then the support can be activated by chemical means using cyanogen bromide, carbodimide, gluteraldehyde, aminosilane, diazonium salts, acid chloride, isocyanate, isothiocyanate derivatives etc. Chemically reactive sites of a protein are usually amino (NH_2) groups from lysine or arginine, carboxyl (COOH) groups from aspartic acid, glutamic acid, hydroxyl (OH) groups from serine, threonine, phenol residues of tyrosine, sulfhydryl (SH) group from cysteine and the imidazole group of histidine. This method has

several advantages like, it leads to very stable preparations with no release of enzyme into the solution. The covalent bonding between enzyme and carrier not only stabilizes the enzyme during catalytic reactions at higher temperature, it also allows the enzyme to withstand denaturants and organic solvents better. The covalent bonding has been employed to improve uniformity, density and distribution of the bound proteins, as well as reproducibility on the surfaces. There are few reports where the immobilization based on covalent binding method was used for the development of alcohol biosensors that exploit gluteraldehyde for the covalent immobilization of enzymes on a wide variety of matrices like nylon net (Verduyn et al. 1983), silicone/polycarbonate membrane (Lubrano et al. 1991), graphite powder (Johansson et al. 1993), propylamino-derivatised controlled pore glass (Azevedo et al. 2004) and other matrices (Guilbault et al. 1983) (Table 1.4). Kiralp et al (2008) covalently immobilized the AOx on magnetic beads of different sizes using suspension polymerization using ethyleneglycoldimethacrylate. Luo et al. (2007) crosslinked the ADH and NAD^+ on the screen printed electrode modified with meldola's blue for determination of serum alcohol. Carelli et al. (2006) developed an interference free alcohol biosensor based on AOx immobilized by glutaraldehyde co-crosslinking with BSA on a perm selective electropolymerized gold electrode. Vijayakumar et al. (1996) developed a bienzyme alcohol biosensor by co-immobilizing the AOx and peroxidase by covalent binding to graphite electrode with carbodimide. Castillo et al. (2003) developed an amperometric bienzyme sensor by immobiliozation of AOx and sweet potato peroxidase on hydrogel crosslinked with redox polymer. Hasunuma et al. (2004) developed a methanol bienzyme biosensor using the self assembly technique for real-time monitoring of methanol in crude plant samples.

Table 1.4 Alcohol biosensors based on covalent binding/cross-linking of enzyme on the electrode.

Biosensor configuration	Sensing element	Immobilization method	Sensor Characteristics	References
SPP/PVI-Os	AOx HRP	Cross-linking	Linearity: 0.002-2.0 mM Detection limit: 0.3 µM Sensitivity: 0.063 µA mM^{-1} Stability: 62.5 % in 6.6 h	Castillo et al 2003
Propylamino-CPG	AOx HRP	Covalent binding	Linearity: N.R Detection limit: N.R Sensitivity: N.R Stability: ~5 % in 14 h	Azevedo et al. 2004
CPM/PEI	AOx HRP	Covalent binding	Linearity: 0.25-2.0 mM Detection limit: 15 µM Sensitivity: 0.351 µA mM^{-1} Stability: 13 % in 8 h	Vijayakumar et al. 1996
11-FUT/ Au	AOx HRP	Covalent binding	Linearity: 0.0–0.0015 mM Detection limit: 10 µM Sensitivity: N.R Stability: No loss in 1 h	Hasunuma et al. 2004
CFE/MWCNT	AOx	Cross linking	Linearity: 1.4 mM Detection limit: 86 µM Sensitivity: N.R Stability: 70 % in 3 weeks	Gouveia-Caridade et al. 2008
Gelatin/GA	AOx	Cross linking	Linearity: 0.2-20 mM Detection limit: N.R Sensitivity: N.R Stability: N.R	Akyilmaz and Dinckaya 2000
Teflon/Gelatin/GA	AOx	Cross-linking	Linearity: 1 mM Detection limit: 50 µM Sensitivity: N.R Stability: 22 % in 154 days	Akyilmaz et al. 2003
Au/PPY_{ox}/glutaraldehyde-BSA	AOx	Crosslinking	Linearity: 0.75 mM Detection limit: 2.3 µM Sensitivity: 4.1 µA mM^{-1} Stability: 5 % in 6 h	Carelli et al. 2006
CFE/PNR	AOX	Cross linking	Linearity: 0-0.7 mM Detection limit: 29.7 µM Sensitivity: 0.70 µA mM^{-1} Stability: 12 % in 6 weeks	Barsan et al 2008
Pig Intestine/GA/BSA	AOX	Cross linking	Linearity: 1.0-10 mM Detection limit: 1000 µM Sensitivity: N.R Stability: N.R	Guilbault et al 1983
GA/silicone/PCM	AOX	Cross linking	Linearity: 4.3-108 mM Detection limit: 43 µM Sensitivity: N.R Stability: N.R	Lubrano et al 1991
Graphite powder/GA/PEI	AOX	Cross linking	Linearity: 2.0 mM Detection limit: 8.0 µM Sensitivity: N.R Stability: N.R	Johansson et al 1993

GA/Nylon net	Catalase	Cross linking	Linearity: 0.021-0.54 mM Detection limit: 21.7 µM Sensitivity: 0.032 µA/ppm Stability: N.R	Verduyn et al 1983
Magnetic beads/EGDMA	AOX	Cross linking	Linearity: N.R Detection limit: N.R Sensitivity: N.R Stability: N.R	Kiralp et al 2008
MB/BSA/GA/Nf	ADH	Cross linking	Linearity: 5.0 mM Detection limit: 110 µM Sensitivity: N.R Stability: 8.4 % in 30 days	Luo et al 2007

*Few values were normalized for making the units uniform for better comparision. The stability was reported as the decrease in biosensor response. SPP: Sweet potato peroxidase, PVI: Poly(vinylimidazole), Os: Osmium, CPG: Controlled pore glass, CPM: Carbon paste matrix, PEI: Polyethylenimine, 11-FUT: 11-ferrocenyl-1-un-decanethiol, Au: Gold, MWCNT: Multiwalled carbon nanotube, GA: Glutaraldehyde, EDC: 1-Ethyl-3-(3-di-methylaminopropyl)carbodiimide, PPY: Polypyrrole, BSA: Bovine serum albumin, PNR: Poly(neutral red), CFE: Carbon film electrode; PCM: Polycarbonate membrane; EGDMA: Ethyleneglycoldimethacrylate; Nf: Nafion.

The AOx and peroxidase were covalently attached to the electrode surface through EDC and NHS surface chemistry along with a mediator 11-ferocenyl-1-undecanethiol. Gouveia-Caridade et al. (2008) crossed linked the AOx-BSA with MWCNT using glutaraldehyde cross-linking. Akyilmaz and Dinckaya (2000) have cross-linked the AOx with gelatin for detection of alcohol in serum. Barsan and Brett (2008) electropolymerised a redox mediator (poly (neutral red)) on the carbon film electrodes and cross-linked the enzyme AOx using glutaraldehyde using BSA as a carrier protein.

Although the covalent binding offers stability, the conditions for this immobilization method are much more complicated and less mild than in the case of physical adsorption and entrapment methods. A loss of enzymatic activity due to its conformational changes is encountered if amino acids essential for the catalytic activity are involved in the covalent linkage to the support. Therefore, the binding reaction must be performed under conditions that do not cause loss of enzymatic activity (Arya et al. 2008). To protect the active site, the enzyme can be immobilized in the presence of a competitive inhibitor or substrate.

1.7. Alcohol biosensors based on optical and other transduction principles

The alcohol biosensors reported till date, are mostly electrochemical. However, various alcohol biosensors based on optical detection methods have also been reported. Few reports on lifetime–based (Chang et al. 1997), chemiluminescence (Xie et al. 1992) and fluorescence-based (Mohr and Spichiger-Keller 1997; Mohr et al. 1997; Blum et al. 2001; Orellana et al. 1995) alcohol sensors were introduced utilizing various alcohol-sensitive dyes. Although promising, these sensors suffer from dye leaching, cross-sensitivity to pH, and low specificity. They also lack high temperature stability and are subject to interference due to autofluorescence. Later Petrova and group developed ratio metric optical alcohol sensor that operates in the red-infrared region of the visible spectrum. It utilizes Nile Blue Chloride, a fluorescent dye with an excitation maximum at λ_{650nm}. The dye is physically entrapped stably in a PEG dimethacrylate hydrogel. The dye exhibits two emission peaks, which allows for ratiometric measurements (Petrova et al. 2007) that circumvent many problems usually encountered in the intensity-based methods (Kermis et al. 2002; Kostov and Rao 1999). Morisawa and Muto reported a simple optical fiber sensing system for alcohol detection in liquors. In this sensor head, a mixture polymer of novolac resin and polyvinylidenefluoride with a ratio of 9:1 was coated as a sensitive cladding layer on the plastic fiber core made of polystyrene-(PS-) coated polycarbonate. Using this sensor head and a green LED light source, alcohol concentration in several kinds of liquors from beer to whisky were measured with a fast response time of less than 1 minute (Morisawa and Muto 2012). A wide range of substrates were used, including chromogenic, fluorogenic and luminogenic substrates for the fabrication of optical ethanol biosensors. One of the most popular substrates used is ABTS. The oxidised form of ABTS has a bluish green colour and is usually detected around $\lambda_{415\ nm}$. In this method AOx and HRP were immobilized on the inside surface of a 96-well microtitre plate. Ethanol containing samples were added to the AOx microtitre plate and after the

reaction (30 min), a sample was transferred to the HRP plate, which already contained the chromogen, ABTS (Ukeda et al. 1999). Another currently used chromogen is 4-aminoantipyrine (4-AAP), which is used in combination with another reducing substrate such as phenol, 4-hydroxybenzo-sulfonate and 8-hydroxyquinoline (Salgado et al. 2000; Azevedo et al. 2004; Rodionov et al. 2002). Recently Verma and Gupta have developed a fiber optic surface plasmon resonance (SPR) based ethanol sensor using ADH and nicotinic acid. The sensor works on the spectral interrogation technique and operates in the visible range of the spectrum (Verma and Gupta 2014). Mitsubayashi and group have developed an optical bio-sniffer for ethanol vapours by immobilizing AOx onto a tip of a fibre optic oxygen sensor coated with an oxygen sensitive ruthenium complex. The bio-sensing principle is based on quenching of the ruthenium complex, in the presence of O_2 molecules (both liquid and gas-phases) (Mitsubayashi et al. 2003). Other optical biosensors were constructed by co-immobilisation of AOx and O_2 sensitive dyes, e.g. ruthenium complex derivative on a PVC membrane. However, it has limitations particularly, low accuracy and reproducibility due to difficulty in measuring oxygen precisely (Lau et al. 1999). A fibre-optic chemiluminescence method for the determination of ethanol in beverages has been proposed. In this method, the H_2O_2 produced was determined by measuring the luminescence of the oxidation of luminol, by H_2O_2, using $K_3Fe(CN)_6$ as a catalyst (Xie et al. 1992). Recently, other methods have also been reported to follow the oxidation of alcohols by AOx. In this method H_2O_2 produced has been detected using PANI, where H_2O_2 oxidized the PANI film, by recording the colour change from green to blue. The biosensor was constructed as a dip stick format for visual and simple use (Kuswandi et al. 2014). Besides this, the SPR technique has also been used as optical transducers for developing alcohol biosensors (Sih and Wolf 2005). A conductometric biosensor has been developed for the determination of short chain primary aliphatic alcohols through immobilization of AOx from *Hansenula* sp. and bovine liver catalase in a

photoreticulated poly(vinyl alcohol) membrane at the of integrated microelectrodes (Hnaien et al. 2010). Ajay and Srivastava had reported a conductometric sensor using microtubules of polyaniline as transducer cum immobilization matrix, capable of detecting ethanol in liquid phase. ADH and its coenzyme NAD^+ were used to improve the selectivity of the sensor. The sensor concept is based on the protonation of the polyaniline by the hydrogen ion produced in the enzyme-catalyzed reaction, leading to changes in the electrical conductance of the polyaniline (Ajay and Srivastava 2007). A potentiometric oxygen electrode with immobilized *S. ellipsoideus* was also successfully used to produce a microbial biosensor for the determination of ethanol with an extended response range (Rotariu et al. 2004). Korpan and group reported a conductometric biosensor for ethanol detection based on whole yeast cells. A membrane with yeast cells immobilized in 2 % Ca-alginate gel was attached on gold planar electrodes. Changes in conductivity due to the specific consumption of ethanol by yeast cells were registered by the computer-controlled sensor system (Korpan et al. 1994). Williams and Hupp demonstrated that silicate-encapsulated yeast ADH can be employed as a sensor for short chained alcohols in standard aqueous, harsh nonaqueous, and gas-phase environments (Williams and Hupp 1998).

1.8. Chemical and physical sensors for alcohol

Chemosensors are another big group of devices aimed at simplifying the classical methods of alcohol determination in beverages. A few reports based on chemical, optochemical and physical methods for detection of ethanol are furnished below. Bozkurt and group used fluorescence-based optochemosensor for determination of ethanol content in beverages of various sources in a wide range of concentrations based on 5,10,15,20-tetra-phenyl porphyrin (TPP) doped on PVC film. Response is based on the quenching of the TPP fluorescence by ethanol as a result of electrostatic attraction (Bozkurt et al. 2010). The sensor

linearly responds to ethanol in the concentration range from 1 to 75 vol. % and was applied to the determination of ethanol in various kinds of wines and whisky. Mohr and group have synthesized a group of chromogenic reactants that reversibly interact with alcohols resulting in a change in absorbance. When chromogenic reactants embedded in plasticised PVC membranes, 4-(N, N-dioctylamino)-4 %- trifluoroacetyl-azobenzene (ETH^T 4001) showed a significant signal change on exposure to aqueous ethanol solution with a decrease in absorbance at around $\lambda_{490\ nm}$ and an increase in absorbance at around $\lambda_{430\ nm}$ (Mohr et al. 1998). Sasaki et al. (2006) synthesized a Chlorophyll derivative possessing a trifluoroacetyl group at the 3-position and used as a new chemosensor for alcohols determination. Simon and group investigated the Porous glass films with immobilized solvatochromic dyes to develop an optochemical sensor for determination of ethanol in water. Depending on the polarity of a solvent, i.e content of ethanol in water, the immobilized indicators changed their fluorescence properties. Sensing films were prepared by immobilizing the dyes with a sol-gel process (Simon et al. 1995). Ashok and group reported a chemometric prediction for the toxicity and quality of liquors using an optofluidic sensor based upon Waveguide Confined Raman Spectroscopy (WCRS). The WCRS sensor was used to predict ethanol concentration with an accuracy of 0.7 % by volume using a Partial Least Square based chemometric model (Ashok et al. 2013). Fong and group reported a fluorescence sensors based on a trifluoroacetophone compound doped in ethyl cellulose (EC) thin films for the detection of methanol, ethanol, and 2-propanol vapors. Thin-film sensors were prepared with 4 dibutylamino-4'-(trifluoroacetyl)stilbene (Chromoionophore IX or CIX) as the fluorescent dye and its solution in EC was spin-coated onto glass slides. The luminescence intensity of the dye ($\lambda_{555\ nm}$) was quenched when exposed to alcohol vapor (Fong et al. 2014). Hajian and group have recently reported that nanostructure flowers of Pt and Pt-Ru electrodeposited on indium tin oxide (ITO) covered glass as a model catalyst to study the electro oxidation of

ethanol. The electrocatalytic properties of Pt/ITO and nanostructured flower like Pt-Ru/ITO electrodes for ethanol oxidation have been investigated by cyclic voltammetry at room temperature and showed that the existing Ru improves catalytic activity of the Pt based electrode for ethanol oxidation (Hajian et al. 2015). The transition metals are capable of establishing reversible interactions with other atoms; some metal complexes may act as receptors for different types of molecules. This behavior was exploited to form complex-analyte supramolecules and increased the selectivity of several sensor types (Elosua et al. 2006). The application of a lipophilic fluorescent reagent, fluorescein octadecyl ester, in a fiber-optic sensor for the determination of aliphatic alcohols in a range 10–60 vol.% was reported (Zeng et al. 1994). The formation of hydrogen bonds between chromoionophore and alcohol molecules is responsible for changing the sensor-relative fluorescence intensity. The application of lipophilic trifluoroacetophone derivatives in optical alcohol sensors was reported by Simons group (Seiler et al. 1991; Spichiger et al. 1992). Plasticized PVC films doped with trifluoroacetophenone derivatives selectively extract alcohols from the sample solution into the organic membrane phase where the reversible formation of hemi-acetals occurs. Entrapment of fluorescent molecules in PVC films allows the investigation of both photophysical and photochemical properties and sensor applications (Wang et al. 2006; Isha et al. 2007). Chiam and group fabricated an optical microfiber sensor coated with conducting polymer, PANI for detection of various types of alcohols such as methanol, ethanol, 1-propanol and 2-propanol (Chiam et al. 2014). Optical sensors for alcohols based on fluorescence enhancement of fluorescein or malachite green and fluorescence quenching of polyaromatic-substituted 1,3-oxazoles and thiazoles were reported (Orellana et al. 1995). Elosua and group reported an optical fibre sensor coated with a complex of Au and Ag $\{[Au_2Ag_2(C_6F_5)_4(C_6H_5N)_2]\}$ for detecting volatile alcoholic compounds. The recognition layer of the sensor was a nanometer-scale Fizeau interferometer, doped with the complex

which, in the presence of methanol, ethanol and isopropanol vapours, showed vapochromic behaviour. The vapochromism is manifested by a change in the colour and the refractive index. The solvents coordinate with the Ag metal centres and break the Ag–Ag and Ag–Au bonds, which give the complex its initial colour (orange to red). The sensing part was deposited on an optical fibre using the ESA method (electrostatic self-assembly method) (Elosua et al. 2006). In addition to above, a variety of methods were developed for the detection of ethanol vapors using optical sensing mechanism (Penza et al. 2004; Manera et al. 2004; Arakawa et al. 2010; Yebo et al. 2010; Manivannan et al. 2012; Kladsomboon and Kerdcharoen 2012; Anoshkin et al. 2013; Klini et al. 2014).

Chapter 2

Alcohol Oxidase from *Pichia pastoris*

Chapter 3

Amplification of Alcohol Oxidase Activity

CHAPTER 3

Amplification of alcohol oxidase activity by entrapping activator within protein matrix

3.1 Overview

Significant research has been carried out to improve the functional properties of enzymes for the efficient use of these biocatalysts in different aspects of food, beverage, cosmetic, pulp, dairy, pharmaceutical, and biofuel industries, diagnostic and therapeutic applications through either rational (Chical et al. 2005) or random approaches (Dalby 2011). In order to develop efficient enzyme based biosensors, a high activity of the enzyme is essential to realize sustainable stability and sensitivity of the constructed device. The inclusion of highly active enzyme also obviates the need of loading excessive amount of catalyst on the electrode surface for maintaining a stable function of the device. The activation of enzyme is usually performed by adding soluble activator in the reaction medium or by binding the activator to the enzyme using the conventional methods (cross linking, covalent and adsorptive binding) (Cooper et al. 1990; Mateo et al. 2007), which however, succumb to some limitations for developing operationally stable device. For example, a mere physical adsorption of the activator may not lead to a stable device, while the covalent coupling may decline the enzyme activity rapidly due to possible change in the conformation

of the protein. Additionally, the procedure involving simple mixing of the activator with the enzyme protein warrants an additional step of supplementing the activator to the sample solution at the time of operation, thereby hampering independent operation of the biosensor. Hence we focused on developing activity amplified AOx as the biorecognition element by stably entrapping a known chemical activator within the protein matrix using a novel protein unfolding-refolding technique prior to use the enzyme on the electrode surface.

The *in-vitro* protein unfolding generally performed by the addition of high molar concentrations of Guanidinium hydrochloride (GdnHcl) or urea to the protein sample (Mari et al. 1998; Venkatesha et al. 1998; Dragani et al. 1999). The reactivation (refolding) of proteins is usually performed by diluting the denaturant with appropriate amount of desired buffer or removal of denaturant by dialysis (Parisi et al. 2003) which however decreases the activity of the enzyme. Here, first we explored the aid of a low frequency MW radiation based technique for partial unfolding of the AOx protein and then investigated a simple low temperature-based technique for refolding the protein into its native state and simultaneous entrapment of the activator present in the solution within the protein matrix. Extensive research has been carried out on the effect of low frequency MW on protein conformation, aggregation and folding-unfolding of globular proteins (Copty et al. 2006; de Pomerai et al. 2003; Bohr and Bohr 2000). However, the studies on the regeneration of native structure of MW treated denatured proteins are not yet adequately known. In the present study we established that the partially unfolded AOx protein obtained at low MW exposure time could be reverted back to its native conformation with functionally active state by applying a simple incubation technique. We explored this phenomenon to entrap the AOx activator, ferrocene within the protein matrix and evaluated detailed kinetic parameters of the activator entrapped enzyme protein and presented in this chapter.

3.2. Experimental Approaches

3.2.1. Reagents and stock solutions

AOx (32 U·mg^{-1}protein), HRP (1080 U·mg^{-1} solid), MWCNT (OD 10–15 nm, length 0.1–10 μm), (±)–10–camphorsulfonic acid, vectaSpin microcentrifuge tube filter (20 K MWCO), ferrocene, 5 % (w/v), Nafion117 in isopropanol and 50 % (w/v) polyethylenimine (PEI) in water, Sephacryl S-300 bead solution (M_r Cut off 500-1500 KDa), N-bromosuccinimide (NBS) and ABTS were bought from sigma Aldrich (USA). (±)-10-camphorsulfonicacid (CSA) was supplied along with the spectropolarimeter. 30 % Hydrogen peroxide (H_2O_2), potassium dihydrogen phosphate (KH_2PO_4), di potassium hydrogen phosphate (K_2HPO_4), dimethyl sulphoxide and methanol were obtained from Merck and all other chemicals were of analytical grade and used as received without any further purification.

A stock solution of ethanol (10 mM) was prepared in deionized water. The ferrocene stock solution (10 mM) was freshly prepared in 30 % DMSO before experiment. The stock solution of ABTS (2 mM) was freshly prepared in 50 mM KPBS just before the experiments. A stock solution of 0.06 % v/v (±)-10-camphorsulfonicacid (CSA) was freshly prepared in deionized water for calibrating spectropolarimeter instrument. AOx (14 mM) and HRP (70 μM) stock solutions were freshly prepared in 50 mM KPBS, pH 7.5 and 7.0, respectively prior to being used. All solutions were prepared in deionized water (15 MΩ) from Millipore water purification system (Millipore, Bedford, MA).

3.2.2. Enzyme assay

The AOx activity was measured by following HRP-coupled assay (Kemp et al. 1988) described under the section 2.2.2.

3.2.3. Microwave treatment of AOx

The MW radiation was provided from a standard magnetron of a microwave oven (LG MC-8089 TLR, LG Electronics India) operating at 2.45 GHz and 0 - 900 W, and 1 s-100 min. The sample holders containing the AOx (0.1 $mg \cdot mL^{-1}$) was inserted into the MW oven and irradiated for time intervals in the range of 10 s-60 s, at 900 W and 2.45 GHz (Scheme 3.1 A). After radiation treatment, the enzyme samples were quickly studied for residual enzyme activities, tryptophan (Trp) fluorescence emission intensities, changes in the secondary structure and subunit dissociation of enzyme.

3.2.4. Preparation of ferrocene entrapped AOx

A total 0.1 $mg \cdot ml^{-1}$ of AOx (50 mM KPBS, pH 7.5) was added to 0.3 mM ferrocene at room temperature (RT). A mixture of AOx enzyme and free ferrocene was treated with MW at 2.45 GHz, 900 W for 10 s and incubated for overnight at 4 °C. The refolded AOx samples in presence of ferrocene were loaded onto vectaSpin microcentrifuge tube filter (20 K MWCO), and subjected to 10,000x*g* for 10 min. The protein retained on the membrane was washed with KPBS several times for removal of the residual surface bound ferrocene and centrifugation was repeated twice to collect the ferrocene entrapped AOx (FcAOx) from the membrane surface. The FcAOx was totally denatured by exposing to MW for 1 min and then centrifuged twice at 10,000x*g*. The filtrate fractions were pooled and collected for spectral analysis to measure the ferrocene entrapped within the protein matrix.

3.2.5. Modification of tryptophan by NBS

Aliquots of purified AOx 3ml (0.5 $mg \cdot ml^{-1}$) in 0.1 M sodium acetate buffer, pH 4.0, were titrated with 5 µl aliquots of freshly prepared 0.1 M, N-bromosuccinimide (NBS) at RT. The NBS mediated inactivation was monitored spectrophotometrically by following the decrease in absorbance at λ_{278nm}. The number of Trp residues oxidized per molecule of

enzyme was calculated by using molar absorption coefficient of 5500 M^{-1} cm^{-1} according to Spande and Witkop (Spande and Witkop 1967).

$$n = \frac{A_{278} \text{ x } 1.317}{5500 \text{ X Enzyme molarity}} \quad (3.1)$$

n = Number of Trp residues modified per molecule of enzyme, 5500 = molar extinction co-efficient of Trp at λ_{278nm}.

3.2.6. Fabrication of FcAOx bioelectrode

A GCE (diameter = 0.5 cm) was cleaned, first by polishing it with alumina powder, then washed it ultrasonically with 70 % ethanol and water separately for 15 min each and finally drying in air. The cleaned GCE was dip coated three times with 1 % (nafion) Nf, with intermittent drying after each coating step. Nf dip coating is applied for the better attachment of the Nf-MWCNTs matrix onto the surface of the Au electrode. 1 mg MWCNTs were dispersed in 100 µl of 5 % Nf and sonicated for 20 min to obtain a stable homogeneous suspension. 10 µl of this mixture was dropped on Nf-coated GCE and dried. For preparing GCE–Nf–MWCNTs–FcAOx–PEI bioelectrode, 12 µl of freshly prepared FcAOx solution was dropped on Nf–MWCNTs-modified GCE electrode, dried and covered with 8 µl PEI (5 %) layer. GCE–Nf–MWCNTs–AOx–PEI bioelectrode was prepared by applying 12 µl (50 µM) AOx onto MWCNTs–Nf coating. The fabricated bioelectrodes were immersed in 50 mM KPBS (pH 7.5) for 15 min prior to being used. When not in use, the bioelectrodes were stored in 50 mM KPBS (pH 7.5) at 4 ºC.

3.2.7. Apparatus and measurements

Spectrophotometric measurements were done on a Cary 300 bio Uv-vis spectrophotometer (Varian, USA) using 1 cm path length quartz cuvette at 25 °C.

Fluorescence measurements were done on a LS-55 spectrofluorometer (Perkin Elmer, USA) at 25 °C. Spectra, each with an average of four scans, were recorded in the scan range of λ_{300nm} - λ_{430nm} by exciting the sample at λ_{295nm} using a slit width of 5 nm and step size of 0.5 nm. The concentration of enzyme used was 0.1 mg·ml^{-1} and background fluorescence was corrected. CD spectra were recorded using a J-815 spectropolarimeter (JASCO, Japan) calibrated with 0.06 % (w/v) aqueous solution of (±)–10–camphorsulfonic acid. The spectra were determined from λ_{240nm} - λ_{190nm}, in 0.1 cm path length suprasil quartz cuvette, at a scan rate of 100 nm·min^{-1}, 1 nm intervals, a time constant of 1 s, and average of 3-4 scans. The temperature of the cell (–15 °C to +90 °C) was controlled by using a peltier temperature control unit. The spectra were corrected for baseline and the secondary structure analysis was performed by using Jasco SSE-protein secondary structure estimation program supplied with the instrument (Yang et al. 1996). Gel filtration experiments were carried out at RT on a Sephacryl S-300 (10/50) (M_r Cut off 500-1500 kDa) column using an ACTA FPLC device (GE Healthcare). Sedimentation velocity experiments were performed with optima XL–A/XL–I analytical ultracentrifuge (Beckman, USA) equipped with absorption and interference optics. Using an An50–Ti rotor, the samples were centrifuged at 82,575x*g* (20 °C). Scans were acquired at λ_{280nm} and interval of 180 s. Differential pulse voltammetry (DPV) was performed in a three-electrode configuration with an Autolab PGSTAT 1212 (Eco Chemie, Netherlands). The working electrodes were GCEs or modified GCEs. Ag/AgCl (3 M KCl) and platinum (Pt) rod served as reference and counter electrodes, respectively. KPBS (50 mM, pH 7.5) was used as the supporting electrolyte. All potentials were measured and reported relative to the Ag/AgCl reference electrode. All experiments were performed at RT. During the DPV measurements, the electrolyte solution was constantly purged with argon gas.

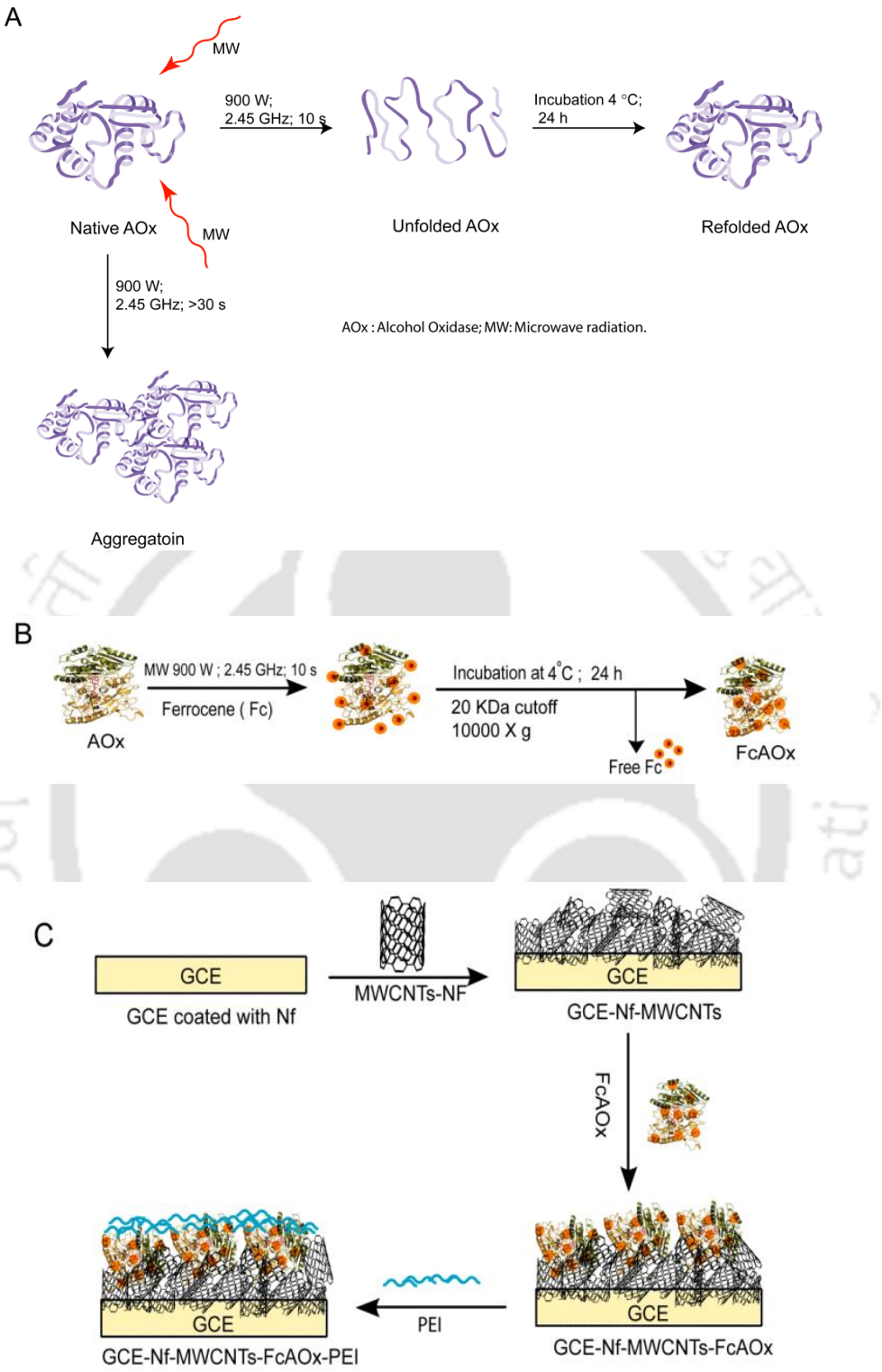

Scheme 3.1 A: MW radiation induced unfolding and refolding of AOx protein. **B**: Schematic representation for the preparation of FcAOx using MW based unfolding and refolding technique. **C**: Electrode fabrication procedure for electrochemical characterization of FcAOx using DPV.

3.3. Results and Discussion

3.3.1. Unfolding – refolding of AOx upon microwave irradiation

Scheme 3.1A shows the schematic diagram for the unfolding and refolding of AOx. The activity of AOx sharply declined with the increasing MW treatment time, and at 30 s of treatment nearly 15 % original activity was retained (Figure 3.1A). The rate of decrease in AOx activity with MW treatment time was linear till the 30 s of treatment time and was calculated as 13.28 $U \cdot s^{-1}$ (Inset of Figure 3.1A). The observed inactivation of AOx by MW exposure suggests that the structure of AOx is directly affected by the electromagnetic field. The initial burst phase of inactivation was parallel to the increase in Trp fluorescence emission of AOx (Figure 3.1B), which indicates growing exposure of the Trp residues from the buried protein matrix due to unfolding of protein with increasing MW treatment time. The rate of increase in Trp fluorescence with increasing the treatment time was 10.61 $au \cdot s^{-1}$ (Inset of Figure 3.1B). A red shift of 0.5 nm, 1.5 nm, 2.5 nm, 3.5 nm and 5 nm after excitation of the protein at λ_{295nm} for the respective 10 s, 20 s, 30 s, 40 s and 60 s of MW treatments indicates the progressive unfolding of the AOx protein. The CD spectra of the native AOx in the far UV-region showed a deep negative double maximum at λ_{208nm} and λ_{222nm} and a positive peak at λ_{192nm} indicating the presence of α-helical conformation in AOx (Figure 3.2A). The estimated secondary structure content of AOx was similar to that of previous study which showed 32 % α-helix and 41 % β-sheet (Boteva et al. 1999). Since α-helical and β-sheet fractions were found to account for ~74 % of the secondary structural content, the native AOx can be considered as a protein with highly ordered secondary structural content and stable conformation. A significant decrease in β-sheet with increasing MW treatment time on AOx protein was observed. Nearly 6 % and 41 % β-sheets of the native enzyme disappeared after the MW treatment for 10 s and 60 s, respectively.

Table 3.1 The secondary structural composition of AOx protein after MW treatment for different time periods.

MW exposure time	% secondary structure			
	α-helix	β-sheets	turns	random
0 s	32.7	41.8	5.6	19.6
10 s	37.0	39.1	4.2	20.2
20 s	36.7	37.6	3.1	21.0
30 s	42.1	34.5	2.8	21.6
40 s	45.3	30.7	1.6	22.4
60 s	22.9	24.5	—	38.5
10 s + renatured[a]	32.1	41.3	5.4	21.5

[a]Incubating at 4 °C for 1 h after exposing with MW for 10 s

However, there was a significant increase in α-helix content with increasing MW treatment till 40s of treatment time. Nearly 13 % and 38 % of the *α*-helix content of the native protein increased after the MW treatment for 10 s and 40 s, respectively. Whereas, at 60 s of MW treatment the *α*-helical structures were decreased by nearly 30 % and the turns were completely disappeared with the concomitant increase in the random structures (Table 3.1). The results indicate that the intrinsic structure of the protein is extensively damaged by the MW energy beyond 40 s of the treatment time. The subunits of AOx protein did not detached during MW irradiation. The unfolding transition monitored by observing the variation of ellipticity at λ_{222nm} and Trp fluorescence emission at $\sim\lambda_{340nm}$ against different MW exposure time shows that the unfolding of AOx under MW irradiation occurs without forming any intermediate protein structure (Figure 3.2B). To confirm the fact, we performed size exclusion chromatography of AOx protein treated with MW for different time period. As shown in Figure 3.3, the protein treated for 0 s, 10 s and 30 s was eluted as single peak with corresponding retention time of 21.2-22.0 min. The protein treated for 40 s generated two distinct peaks with retention times of 17.1 min and 21.4 min. The decrease in retention time implies that a fraction of the native protein lost its globular structure due to distorted secondary structure caused by MW and possible partial aggregation of the structurally

distorted proteins. The protein obtained by the increased MW treatment time of 60 s eluted as a single peak with retention time of 17.1 min, indicating complete denaturation and possible associated aggregation of the protein. The increasing unfolding of AOx protein with the prolong MW treatment exposes hydrophobic residues of the protein that may facilitate intermolecular interaction and aggregation of the proteins. The findings confirmed that the MW treatment did not dissociate the AOx protein to stable independent/isolated subunits as evident from the void of any peaks with retention time longer than that of the native protein. Kinetic measurements were carried out to examine the catalytic properties of the enzyme after different MW treatment times using native sample as reference (Table 3.2).

Table 3.2 Kinetic activity data of AOx treated with MW for different time periods.

MW exposure time	K_m (µM)	V_{max} (µM s^{-1})	K_{cat} (s^{-1})
0 s (Native AOx)	2137±81	0.63±0.03	0.22±0.04
10 s	2705±65	0.17±0.02	0.43±0.02
20 s	3951±47	0.11±0.01	0.26±0.01
30 s	6832±24	0.05±0.05	0.09±0.01
10 s + renatured[a]	2234±21	0.59±0.02	0.19±0.01

The values represent S.E.M (n = 3) of three different experiments. [a]Incubating at 4 °C for 1 h after exposing with MW for 10 s

The enzyme solutions exposed to 10 s MW treatment showed 26.5 % increase in K_m and 26.9 % decrease in V_{max} from the native state, whereas with further increase in exposure time (20 s and 30 s) led to extensive abbaration in the kinetic parameters (K_m, V_{max} and K_{cat}) of the enzyme. Refolding experiments were performed to answer the question whether AOx protein treated with low frequency MW could revert to its native structure. Refolding was carried out by using a simple incubation technique as described below. The MW treated protein sample was incubated at 4 °C under static condition for 24 h to bring back the distorted conformation of the AOx obtained by the MW treatment for different time period to the native state. Recovery of AOx enzyme activity was measured as follows. The defined volume of irradiated enzyme solution at different exposure time was incubated by following

the above incubation conditions and the activity of enzyme was measured for every 10 min interval using ABTS method as described in the section 3.2.2. From activity experiment's as shown in Figure 3.4A it was observed that an activity recovery of 50 % ± 7 %, 75 % ± 2 % and 95 % ± 5 % were obtained by incubating the 10 s MW treated protein at 4 °C for 15, 25 and 45 min, respectively. The refolding experiments analyzed with spectroscopic measurements were done by following the above incubation conditions and monitored for changes in band position at λ_{222nm} and λ_{215nm} for CD spectra and Trp emission maximum at λ_{340nm}. The CD spectroscopic data and fluorescence emission spectra of Trp at λ_{340nm} showed that the distorted secondary structure of AOx generated by the MW exposure for 10 s reverts back closer to the native conformation when the treated sample was incubated at 4 °C for 60 min (Figure 3.4B and C). The renaturation under similar incubating condition for the samples initially treated with MW for 20 s and 30 s was partial whereas, it was void for the samples treated for more than 40 s as confirmed by CD analyses. The denatured protein obtained by 10 s MW treatment was refolded following the technique described above and the kinetic parameters of the resulting refolded protein was found to be closer to the native enzyme.

3.3.2. Characterization of FcAOx

Scheme 3.1B shows the schematic diagram for the preparation of AOx enzyme conjugate. The enzyme activity was significantly increased by the addition of ferrocene to enzyme (0.14 mM) at 25 °C. The maximum activity of the enzyme was found at 0.3 mM of ferrocene (Figure 3.5A). The rate of increase in the activity for 0.3 mM of ferrocene was 83.8U/ml. The partially unfolded protein obtained by MW treatment of AOx for 10 s when refolded in presence of 0.3 mM ferrocene, the latter was entrapped within the protein matrix and generated FcAOx. The concentration of ferrocene isolated by denaturing the FcAOx protein was determined at λ_{446nm} (ε_{446} = 1065 $M^{-1}cm^{-1}$). The molar ratio of ferrocene to AOx

in FcAOx was found to be ~2.6:1. Sedimentation velocity data obtained as absorbance at λ_{280nm} versus cell radius was fitted using continuous sedimentation co-efficient distribution *c(s)* analysis with SEDFIT (Schuck et al. 2003), giving a residual profiles in the range from -0.02 to +0.02 (Figure 3.5B and C). The *c(s)* distribution curves for native and ferrocene entrapped enzymes at 20 °C (Figure 3.5D) exhibited intense major peaks, indicating non interacting homogenous systems for both the enzyme fractions. The molecular weight (M_w) and sedimentation coefficients (s) of the native AOx and FcAOx were determined using a range of 's' values from 15-25 s, and frictional ratio (f/f_0) of 1.2. The fit obtained yielded the 'M_w' and 's' values of 575 kDa, 18.7 s and 582 kDa, 19.4 s for AOx and FcAOx, respectively. Increase in 'M_w' and 's' of the FcAOx by 7 kDa and 0.7 s respectively, indicated stable entrapment of ferrocene molecules within the AOx protein. The molar ratio of ferrocene to AOx in FcAOx discerned from the study was 3:1. The CD analysis of AOx and FcAOx in KPBS validate a comparable characteristic: narrow negative peaks at λ_{222nm} and λ_{208nm} and more intense positive peak at λ_{194nm} with α-helical conformation. There was no significant difference in the secondary structure composition of AOx and FcAOx (Figure 3.5E). Scheme 3.1C shows the schematic diagram for the fabrication of FcAOx bioelectrode. The electrochemical characterization of native AOx bioelectrode using DPV showed a FAD peak (I_{pa}) at -0.51 V (Munteanu et al. 2008) (Figure 3.5F, curve a) and ferrocene electrode displayed a peak at +0.23 V, characteristic for Fe^{III} in (Fe^{III}/Fe^{II}) system (Wu et al. 2010) (Figure 3.5F, curve b). FcAOx immobilized electrode displayed a pair of peaks at -0.51 V and +0.23 V, corresponding to FAD and ferrocene in AOx (Figure 3.5F, curve c), signifying the stable entrapment of ferrocene within the protein matrix of AOx. The kinetic parameters for AOx were significantly improved upon addition of ferrocene in the assay mixture. However, the magnitude of the kinetic values was improved further when FcAOx was used instead of using a mere mixture of AOx with free ferrocene to catalyze the reaction. The K_m

and K_{cat} of the FcAOx were 1519±31.7 µM and 0.209±0.01 s^{-1}, respectively; while the corresponding values of the parameters for the native AOx with externally added ferrocene were 1869±55.6 µM and 0.154±0.01 s^{-1}. The K_m and K_{cat} for native AOx were 2237±61.9 µM and 0.142±0.01 s^{-1}, respectively. Thus, the efficiency (K_{cat}/K_m) of the AOx was increased by ~30 % and ~116 % by using free and entrapped ferrocene, respectively. The results confirmed that the activating role of ferrocene is facilitated by its entrapment in the AOx protein matrix.

The pH stability of FcAOx was studied in the pH range of 3-11 (Figure 3.6A) and identified pH 7.5 as the optimum, which conform to the pH stability of the native AOx. The storage stability of FcAOx in KPBS at 4 °C was studied and found that ~92 % of the activity was retained at the end of 30 days of incubation of the sample (Figure 3.6B). Successive washing of the FcAOx conjugate with KPBS even for 12 times did not alter the ferrocene concentration in the conjugate.

3.3.3. Mechanism of MW mediated heat transfer to AOx protein

Correlation between solutes in water is determined not only by their direct interaction, but also by the ability of water to hydrate the solutes. Hydration of hydrophobic and ionic solutes is therefore an important topic in electrochemistry, geochemistry and especially biology, where it is common for protein structures to be stabilized by the charges held together by bridging water molecules. The problem is not trivial, even at infinite dilution with respect to the solute where subtle competition between solute-water and water-water interactions exists. Temperature is considered to be the most important thermodynamic parameter and the ability of water to solvate a solute depends on it. An interesting question is how the fundamental degrees of freedom, such as translation and rotation contribute to hydration. A biologically important situation arises when water molecules are irradiated with

MWs of appropriate frequency to excite their rotational motion. It has been shown that MWs induce heating by excitation of rotational motion in water molecules. Excess rotational kinetic energy is then transferred to translational degrees of freedom. The MW radiation effect observed here is probably mediated by the water molecules attached to the protein surface. The protein bound water absorbs MW radiation in the range of 1-15 GHz (Dawkins et al. 1979; Feldman et al. 2003) as compared to the free water molecules that absorb at 19 GHz (Copty et al. 2006). The MW frequency of 2.45 GHz used in this investigation is thus fall in the range for protein bound water absorption band. Thus MW treatment induces the conformational changes by stimulating the coherent intrinsic dynamics in globular protein molecules through the hydration layer surrounding the globular protein. The MW energy received by the protein bound water molecules perturbed the peptide bond energy of the AOx protein that triggered the rapid conformational change to the protein molecules that skip any intermediate structural transition state of the protein.

3.3.4. Mechanism of ferrocene interaction with AOx

Studies were carried out to elucidate the mechanism of ferrocene interaction within AOx protein. The effect of salt on the activity of native AOx and FcAOx were separately studied. The activity of FcAOx was decreased at elevated salt concentrations, whereas the activity of native AOx was unaltered within the salt concentration range used (Figure 3.7A). The results infer that interaction between ferrocene and protein in FcAOx is electrostatic in nature, since high salt concentration is known to nullify molecular electrostatic interactions (Shields and Farrah 1983). Ferrocene strongly quenched the Trp fluorescence intensity (emission at $\lambda_{344nm,}$ excitation at $\lambda_{295\ nm}$) of AOx protein in a concentration dependent manner (Figure 3.7B). The quenching effect was increased linearly at the rate of 5.82 au·s^{-1} with MW treatment time indicating the enhanced interaction of ferrocene molecules with the exposed

Trp residues in the gradually unfolded AOx protein (Figure 3.7C). Furthermore, Trp residue(s) are involved in the catalytic activity of AOx as evident from the loss of more than 50 % of the enzyme activity when as many as three Trp residues were modified by NBS (Figure 3.7D). The nature of the isobestic point at λ_{263nm} (Figure 3.7E) and decrease in the Trp fluorescence intensity (Figure 3.7F) infers that the loss of activity is due to the Trp modification rather than structural changes or modification of tyrosine residues (Paus 1978). The results signify that a maximum of three Trp residues play a critical role in the enzyme activity. It is likely that the ferrocene molecules are retained in the protein matrix by the Trp residues through π-stacking interactions between the indolic ring of Trp and the cyclopentadienyl rings of ferrocene and thereby accelerating the catalytic activity of the AOx. π-stacking is known to contribute to the interactions between small aromatic molecules and proteins (Babine and Bender 1997). However, to understand the exact role of ferrocene and its interaction with the Trp residues on the activity of AOx the active site configuration of the AOx needs to be elucidated, which is however beyond the scope of this work and will be dealt, separately when the x-ray crystallography data on *Pichia pastoris* AOx will be available.

3.4. Conclusions

Studies on protein folding and unfolding are known to provide critical information on the structure and function of proteins. This investigation has established that MW mediated unfolding of the protein is a reversible phenomena and the reversibility is effectual at low MW exposure time (10 s) on the protein. The unfolding process enacted by the MW radiation occurs rapidly without passing through any intermediate transition state under the time scale units employed. The reversible refolding techniques demonstrated through this investigation has clear advantages over the conventional chemical based approach owing to its direct

nature that void the separation steps for the protein involved in chemical denaturant based approach. This MW based technique was utilized for stable entrapment of chemical activator ferrocene in the protein matrix of AOx for enhancing biocatalytic activity of the enzyme. The activated enzyme showed a two-fold increase in efficiency (k_{cat}/k_m) and no significant change of its secondary structure. The activator molecules were stably entrapped in the AOx protein matrix in a molar ratio of ~3:1 through electrostatic interaction with the Trp residues involved in the functional activity of the enzyme as demonstrated by advanced analytical techniques.

Figures

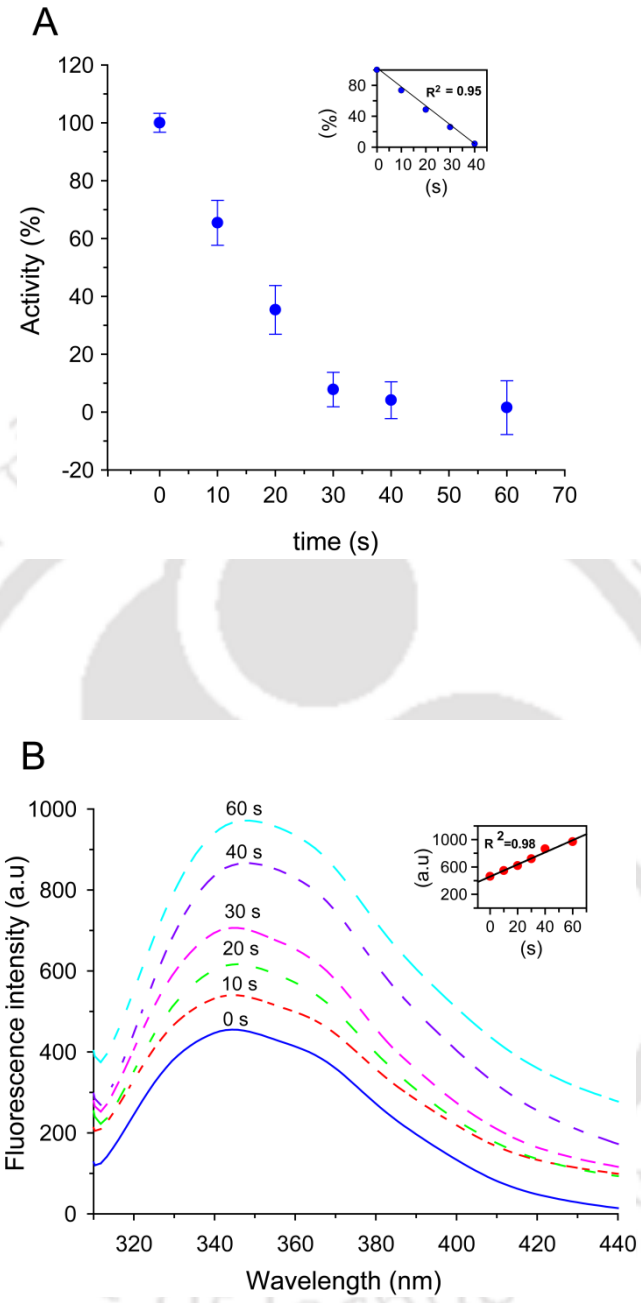

Figure 3.1 Unfolding studies of AOx upon MW irradiation. **A:** Activity of AOx after exposing to 2.45 GHz MW radiation as a function of time, **B:** Trp fluorescence emission spectra of AOx at different MW irradiation time intervals in comparison with control (0 s) excited at $\lambda_{295\ nm}$.

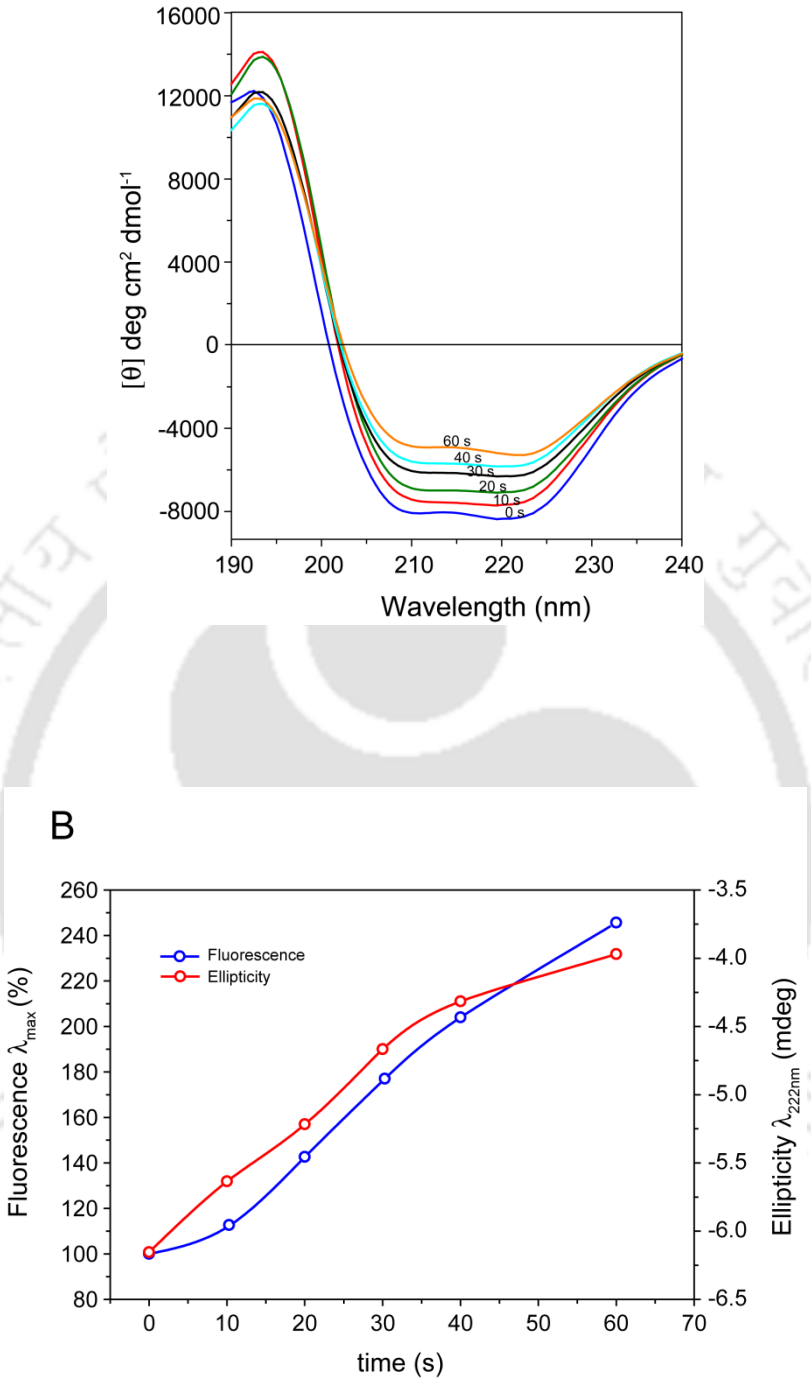

Figure 3.2 Unfolding studies of AOx upon MW irradiation: **A:** The far-UV CD spectra of AOx at different MW treatment time intervals in comparison with control (0 s), **B:** Unfolding transition curves of AOx as a function of MW treatment time by following fluorescence maxima at λ_{340nm} and ellipticity (mdeg) at λ_{222nm}.

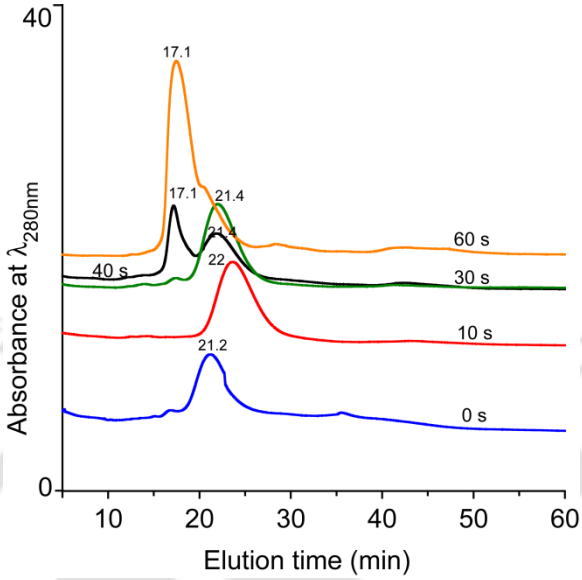

Figure 3.3 Sub unit dissociation studies of AOx upon MW treatment, monitored by gel filtration chromatography. Native AOx with a final concentration of 0.1 $mg \cdot ml^{-1}$ in the phosphate buffer was treated with MW for different time periods (0 s, 10 s, 30 s, 40 s and 60 s) and the protein was applied on to Sephacryl S 300 column equilibrated with 50 mM phosphate buffer. The elution profile was monitored in time scale at $\lambda_{280\ nm}$. The numbers above the peaks correspond to the elution time of the protein in min.

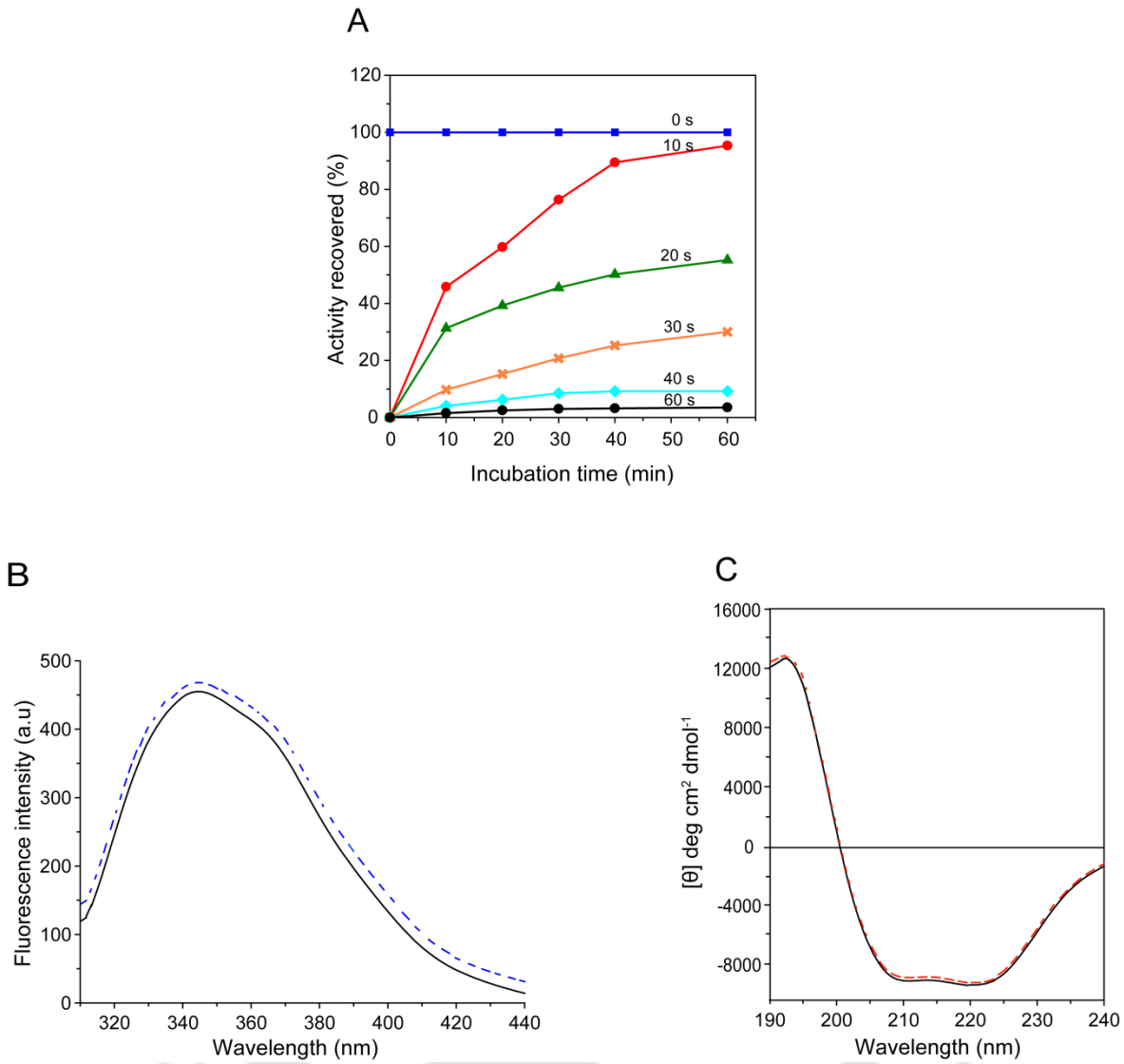

Figure 3.4 Refolding studies of MW treated AOx protein. **A:** The percentage of AOx activity recovered in comparison with control (0 s) after incubating the MW treated enzyme samples at 4 °C for 1h. The numbers on the curves indicates the time of exposure for MW. **B:** The Trp fluorescence emission spectra of native AOx and the refolded AOx obtained by incubating the 10 s MW treated enzyme at 4 °C for 24 h. **C:** The far-UV CD spectra of native AOx and the refolded AOx obtained by incubating the 10 s MW treated enzyme at 4 °C for 24 h.

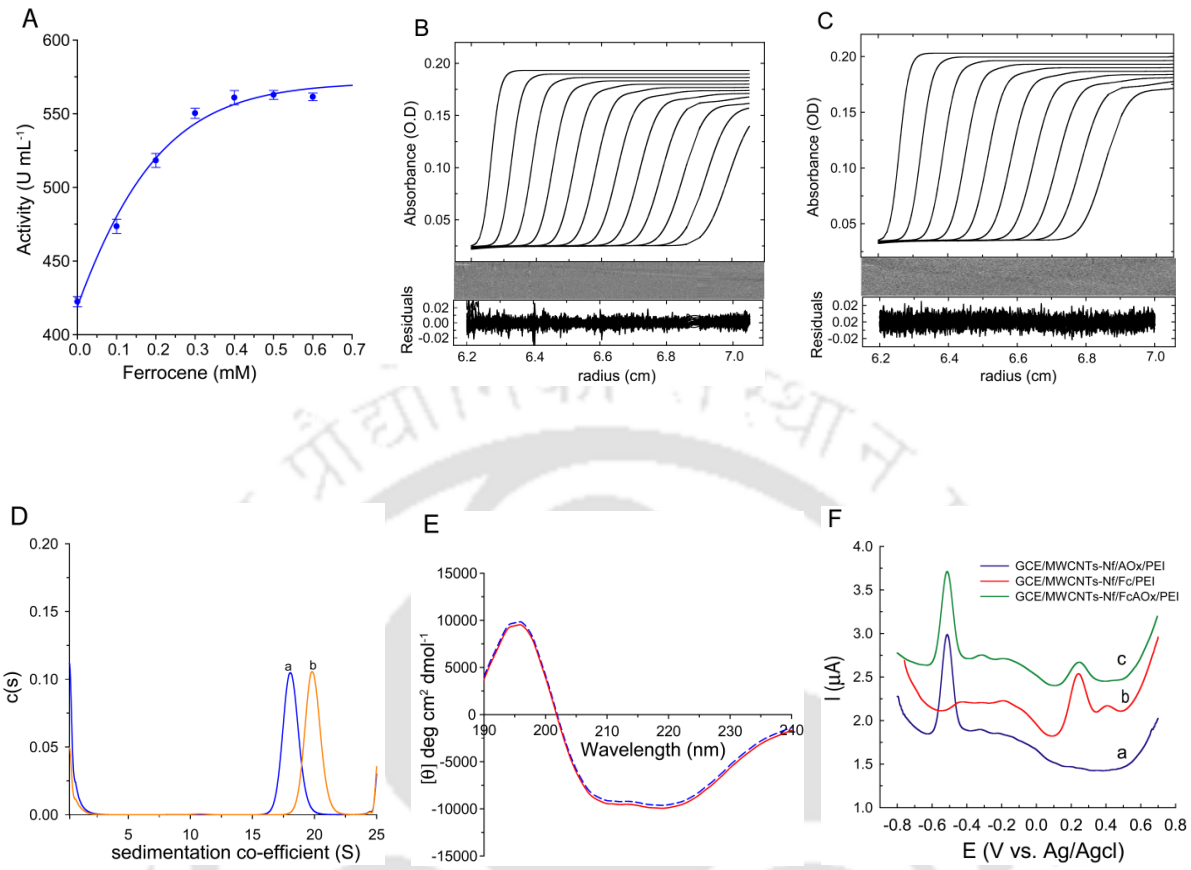

Figure 3.5 Characterization of FcAOx. **A:** Effect of ferrocene on the activity of AOx, **B** and **C:** Simulated sedimentation velocity absorbance profiles of AOx and FcAOx conjugate obtained at 82,575x*g* and 20 °C, scanned at λ_{280} nm, radial data interval of 0.003 cm, time interval of 180 s. **D:** Continuous sedimentation co-efficient *c(s)* distribution analysis of the simulated data from sedimentation velocity experiment showing 's' values for (a) AOx and (b) FcAOx, simulated parameters: partial specific volume = 0.73 mL g^{-1}, frictional ratio f/f_0 = 1.2 and buffer density of 1.0 g cm^{-2}. **E:** Far UV-CD spectra of native AOx (solid line) and FcAOx (dashed line). **F:** DPV of differently modified electrodes showing (a) GCE-MWCNT-Nf-AOx-PEI (b) GCE-MWCNT-Nf-Fc-PEI and, (c) GCE-MWCNT-Nf-FcAOx-PEI.

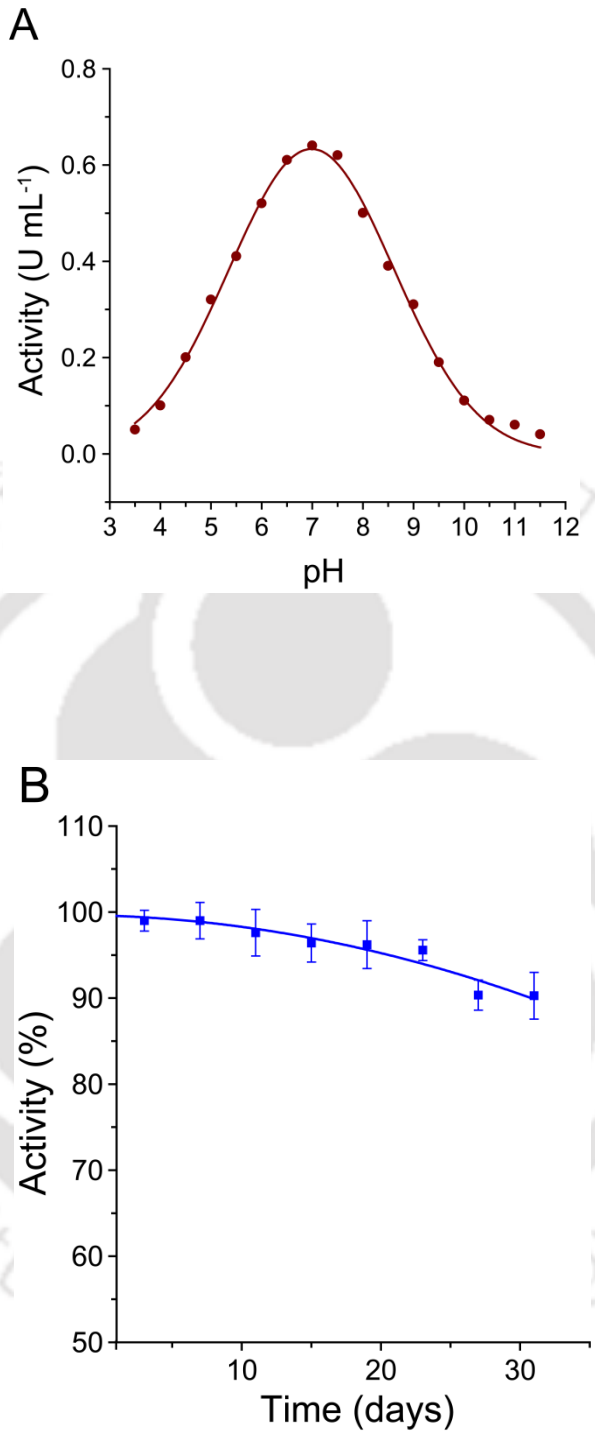

Figure 3.6 Stability of FcAOx. **A:** Activity as a function of pH and **B:** time in days at pH 7.5, 4 °C. The different buffers (each at 50 mM) used was sodium acetate (pH 3.5 - 5.5), potassium phosphate (pH 6.0 - 7.5), tris-HCl (pH 8.0 - 9.0) and glycine-NaOH (pH 9.5 - 11.5).

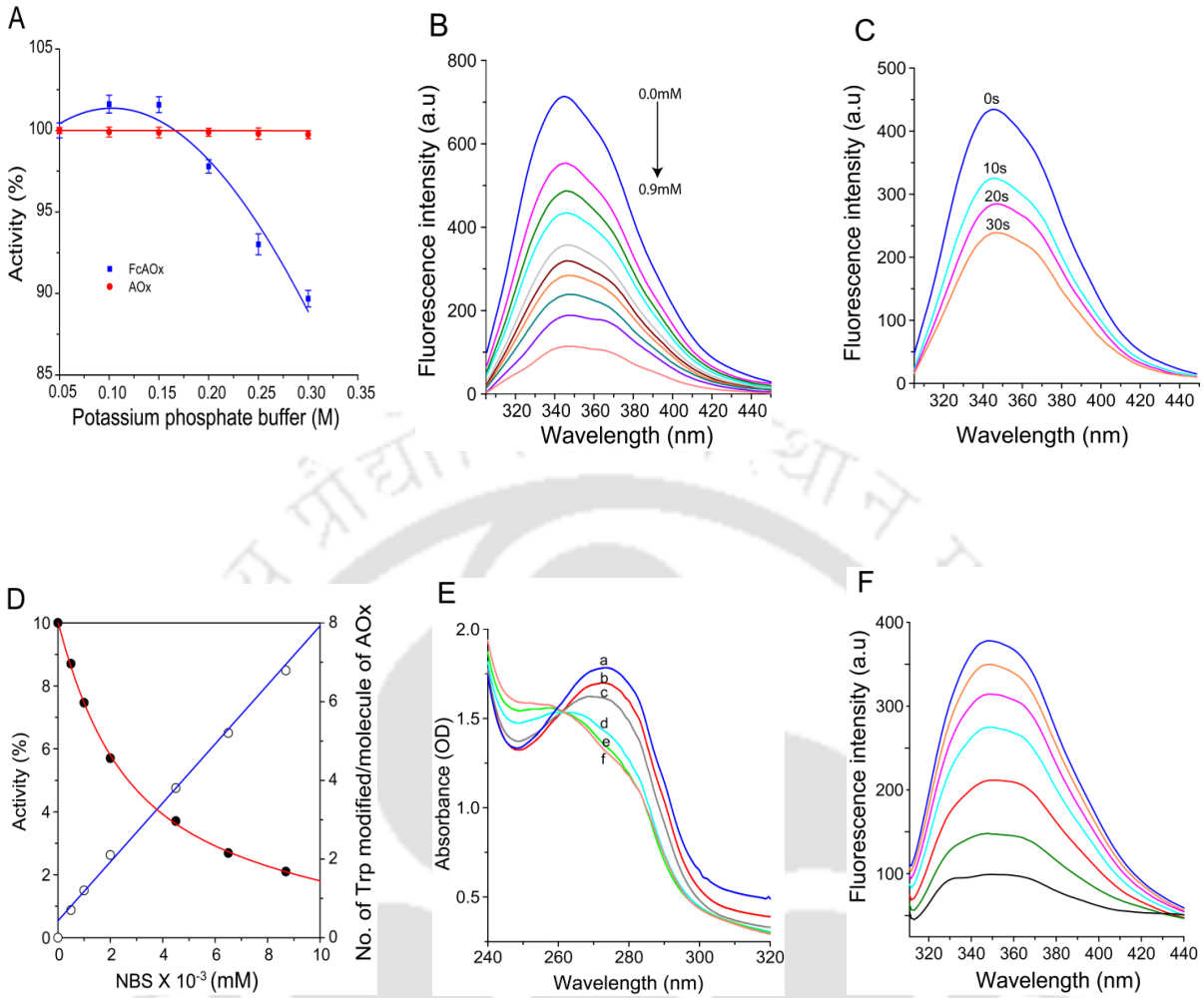

Figure 3.7 Studies on the mechanism of ferrocene interaction with AOx protein. **A:** FcAOx activity as a function of ionic strength as salt concentration of potassium phosphate buffer (pH 7.5). **B:** Trp fluorescence emission spectra of AOx when mixed with different concentrations of ferrocene in a 0.1 mM gradient as indicated by the arrow line. **C:** Trp fluorescence emission spectrum of AOx treated with the MW for 0 s, 10 s, 20 s and 30 s in presence of 0.3 mM ferrocene in KPBS. **D:** AOx activity versus NBS concentration during the oxidation of Trp residues. The number of Trp residues oxidized was calculated from the decrease in absorbance at λ_{278nm}. **E:** Absorption spectra of native (a) and NBS modified AOx (b, c, d, e, f). Enzyme concentration was 14 µM in 0.1 M sodium acetate buffer, pH 4.0. The test volume was 1.0 ml. **F:** Fluorescence emission spectra (Excitation at λ_{295nm}) of AOx with successive addition of NBS from lower (blue) to higher (black) concentration.

Chapter 4

Ferrocene Activated Alcohol Oxidase as Biorecognition Element

CHAPTER 4

Ferrocene activated alcohol oxidase as biorecognition element for developing alcohol biosensor

4.1. Overview

Alcohol oxidase (AOx) based biosensors described so far are yet to address adequately the drawbacks, like low sensitivity, poor stability, and narrow linear range of detection for their practical applications. The factors responsible for these limitations are attributed to poor signal transduction, degradation or denaturation of enzyme, leaching of mediator and low loading of kinetically active enzymes on the bioelectrodes. We proposed to develop a novel amperometric alcohol biosensor with increased sensitivity, stability and linear range of detection using activity pre-amplified AOx as biorecognition element. The biocatalytic activity of the AOx may be amplified by entrapping ferrocene, which is an activator for AOx (Kumar and Goswami, 2008), stably in the protein matrix, following the simple MW based technique described in the previous section. We also proposed to use the third generation principle of signal transduction where the electrons involved in the redox process are shuttled directly between the active site of the enzyme and the electrode to generate the specific response (Barton et al., 2004). The key advantages credited to the biosensors based on the direct electron transfer (DET) principle are high operational stability due to mediator independent operation and interference free detection of analytes caused by the low over potential involved in the reaction. However, the major obstacle for developing

DET principle based biosensor is the deeply buried redox centre in the protein of many redox enzymes that hampers the electron flow between the enzyme and the electrode. Nano-fabrication of bioelectrode with highly conductive nanomaterials is emerging as a tool of choice due to its clear effect on establishing DET. In this regard MWCNT is projected as a nanomaterial of great promise as witnessed from many amperometric biosensors successfully developed in the recent past (Agui et al., 2008; Vatsyayan et al., 2011). The AOx with amplified activity is proposed to immobilize on a sol-gel chitosan layer assembled on HRP in a MWCNT matrix on the electrode surface. In this bi-enzyme sensor, the H_2O_2 formed by the AOx catalyzed oxidation of alcohol is bioelectrocatalytically reduced by HRP through DET mechanism to generate the response. MWCNT provides high electroactive surface for facile electron exchange between the electrode and HRP. The silica-sol gel chitosan (SG-Chit) matrix provides biocompatible support for stability of the bi-enzyme complex on the electrode surface, desired porosity for easy diffusion of analyte and preconcentration of the analyte for electrochemical detection (Wang et al., 2003). Polyethylenimine (PEI), a polycationic polymer has been used to stabilize the FcAOx immobilized on the SG-Chit film. The fabricated bioelectrode utilizing the HRP-FcAOx system has been characterized and a detailed account on response of the bioelectrode for the substrate alcohol in real samples is presented in this chapter.

4.2 Experimental Approaches

4.2.1. Reagents and stock solutions

AOx from *Pichia pastoris* (32 U·mg^{-1} protein), HRP (1080 U·mg^{-1} solid), MWCNT (OD 10–15 nm, length 0.1–10 μm), chitosan from crab shells (≥75 % deacetylated), Tetraethoxysilane (TEOS), (±)–10–camphorsulfonic acid, vectaSpin microcentrifuge tube filter (20 K MWCO), ferrocene, ABTS, 5 % (w/v), Nafion117 in isopropanol and 50 %

(w/v), polyethylenimine (PEI) in water were purchased from Sigma Aldrich. Methanol, dimethyl sulphoxide, K_2HPO_4, KH_2PO_4 and 30 % H_2O_2 was bought from Merck. All other chemicals were of analytical grade and used as received without any further purification.

Stock solution of ethanol (20 mM) was prepared in deionized water. The stock solution of ABTS (2 mM) was freshly prepared in 50 mM KPBS just before the experiments. AOx (14 mM) and HRP (70 µM) stock solutions were freshly prepared in KPBS, pH 7.5 and 7.0, respectively prior to being used. All solutions were prepared with deionized water (15MΩ) from Millipore water purification system (Millipore, Bedford, MA).

4.2.2. Enzyme assay

The AOx activity was measured by following HRP-coupled assay (Kemp et al. 1988) as described under the section 2.2.2

4.2.3. Preparation of sol-gel chitosan solution (SG-Chit)

A 0.5 % chitosan (Chit) solution was prepared by dissolving 0.5 g Chit in 100 mL of 1.0 % (v/v) acetic acid solution with magnetic stirring for about 2 h. A stock solution of SG-Chit was prepared by mixing 14 µL of TEOS, 30 µL of methanol, and 1.2 mL of 0.5 % Chit solution in a 2 mL PVC tube. The mixture was sonicated for 30 min until a clear and homogenous solution has formed and subsequently stored at RT for 3 h. The stock solution was freshly prepared just before the fabrication of biosensor.

4.2.4. Fabrication of GCE-MWCNT-Nf-HRP-SG-Chit-FcAOx-PEI bioelectrode

Scheme 4.1A shows the schematic diagram on the fabrication of the bioelectrode. A GCE (diameter 0.5 cm) was cleaned by polishing with alumina slurry, then washed ultrasonically with 70 % ethanol and water separately for 5 min each and finally allowed to dry under clean air at RT. A total 3 mg of MWCNTs was dispersed in 300 µL of 5 % Nf and sonicated for 20 min to obtain a stable homogenous suspension. A total 6 µL of MWCNT-Nf

solution was dropped onto the GCE and allowed to dry under clean air at RT. Once dried, 5 µL of HRP from stock solution was layered above the MWCNT and dried for overnight at 4 °C. Once dried, 5 µL of SG-Chit was dropped above the HRP layer and allowed to dry for 2 h under clean air at RT, and finally 5 µL of FcAOx (0.1 $mg \cdot mL^{-1}$) was layered over the SG-Chit layer, dried for overnight at 4 °C and covered with 5 µL of 5 % (v/v) PEI solution. The fabricated bioelectrode was again dried under clean air at RT and stored in KPBS at 4 °C when not in use.

4.2.5. Apparatus and measurements

Spectrophotometric measurements were done on a Cary 300 bio Uv-vis spectrophotometer (Varian, USA) using 1 cm path length quartz cuvette at 25 °C. The Cyclic voltammetry (CV) was performed in a three-electrode configuration with an Autolab PGSTAT 1212 (Eco Chemie, The Netherlands). The working electrodes were GCE or modified GCEs. Ag/AgCl (3M KCl) and Pt rod served as reference and counter electrodes, respectively. KPBS (50mM, pH 7.5) was used as the supporting electrolyte. All potentials were measured and reported relative to the Ag/AgCl reference electrode. All experiments were performed at RT. During the CV measurements, the electrolyte solution was constantly purged with argon gas. Electrochemical impedance spectroscopy (EIS) measurements were performed in a background solution of 5 mM $K_3Fe(CN)_6/K_4Fe(CN)_6$ (1:1) and 0.1 M KCl in KPBS (50 mM, pH 7.5) within the frequency range of 0.05 Hz to 10 kHz. The amplitude of the alternate voltage was 5 mV. Field emission scanning electron microscopy (FESEM) images were obtained on a scanning electron microscope (Zeiss, USA) using the following setting conditions: 3-5 KeV EHT, 50 mm aperture.

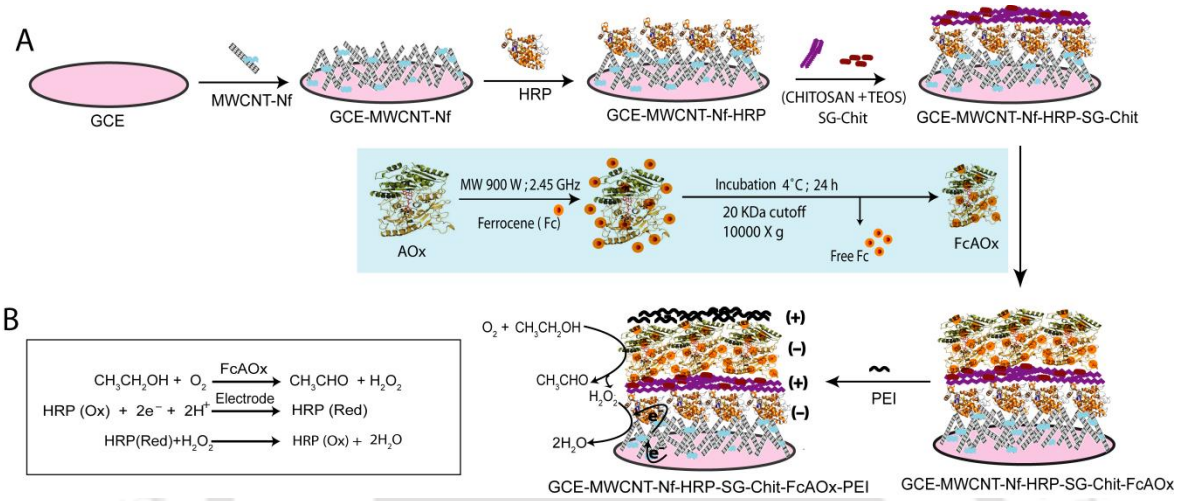

Scheme 4.1 Fabrication scheme of GCE-MWCNT-Nf-HRP-SG-Chit-FcAOx-PEI bioelectrode: **A:** Electrode fabrication process at GCE surface. **B:** The principal reactions catalyzed by FcAOx and HRP at electrode surface.

4.3. Results and discussion

4.3.1. Morphological characterization of the bioelectrode using FESEM

Figure 4.1 shows the FESEM images of GCE-MWCNT-HRP-SG-Chit-FcAOx-PEI electrode, revealing the stepwise changes in the electrode surface morphology at different stages of bioelectrode fabrication. As shown in figure 4.1A, smooth bare GCE surface transformed into a porous thread like morphology when MWCNTs-Nf was layered on it. The porous nature of the MWCNT-Nf (figure 4.1B) was diminished upon addition of HRP on the film. Further, when a layer of SG-Chit was applied on the film to fabricate GCE-MWCNT-HRP-SG-Chit bioelectrode, the surface morphology changed to an uneven form with a rough surface, which provides an effective electrode surface area for increased immobilization of biomolecules. The surface of GCE-MWCNT-HRP-SG-Chit electrode changes to globular morphology after the immobilization of FcAOx revealing successful immobilization of enzyme (Figure 4.1C). Finally when a layer of PEI was applied on MWCNT-HRP-SG-Chit-FcAOx film, the surface morphology changed to smooth even form (Figure 4.1D). Stability of the immobilized layers on the electrode surface occurred under the influence of electrostatic interaction between the negatively and positively charged layers in the electrode surface as shown in the Scheme 4.1A.

4.3.2. Electrochemical characterization of the bioelectrode using EIS

Figure 4.2A represents the results of EIS studies carried out with electrodes in 5 mM $K_3Fe(CN)_6/K_4Fe(CN)_6$ (1:1) and 0.1 M KCl in KPBS (50 mM, pH 7.5). Nature of the obtained impedance spectra, presented as Nyquist plots reveals that polarization at the electrode surface is due to a combination of kinetic and diffusion processes. The EIS was also validated the formation of different layers on the electrode surface by change in the electron transfer kinetics between the bulk electrolyte and the electrode surface. The value of electron

transfer resistance (R_{et}) at the electrode surface can be estimated directly from the diameters of Nyquist plots. The bare GCE exhibits a line with small semicircle diameter with R_{et} of 140 Ω (Figure 4.2A, curve a). The semicircle disappeared upon layering of MWCNT onto the GCE, implying highly conductive MWCNT film facilitates the charge transfer with the electrode (Figure 4.2A, curve b). Reappearance of a semicircle line with R_{ct} of 311 Ω (Figure 4.2A, curve c) upon layering of HRP/SG-Chit on the MWCNT-Nf film indicates the formation of the HRP/SG-Chit film that reduces the charge transfer on the electrode surface. The increase in impedance was expected as the protein immobilization increases the R_{et} values by blocking the route for charge transfer from the electrolyte solution to the electrode surface. The R_{et} of the GCE-MWCNT-Nf-HRP-SG-Chit electrode was further increased to 390 and 410 Ω (Figure 4.2A, curve d and e) when FcAOx/AOx and PEI were stepwise layered on it, indicating the formation of these successive layers with increasing charge transfer resistance on the electrode surface.

4.3.3. Response mechanism of the fabricated bioelectrodes

CV of bare GCE and modified GCE was done in an argon-saturated KPBS (50 mM, pH 7.5) at 50 mV s^{-1} (Figure 4.2B). No clear redox peaks were observed for bare GCE and GCE-MWCNT-Nf (Figure 4.2B, curve a) suggesting that MWCNT-Nf layer is electro-inactive in this potential window. The GCE-MWCNT-Nf-HRP-SG-Chit bioelectrode generated by immobilization of HRP and SG-Chit on MWCNT-Nf film displayed a pair of redox peaks at -0.23 V and -0.34 V, which are characteristic for the direct electrochemistry of HRP (Zhao et al. 2008) (Figure 4.2B, curve b). Following the immobilization of FcAOx and PEI over GCE-MWCNT-Nf-HRP-SG-Chit film, the generated bioelectrode (Figure 4.2B, curve c) displayed a pair of redox peaks similar to that of curve b with increased peak currents. The formal potential [$(E_{pa} + E_{pc})/2$] of the redox couple at bioelectrode GCE-

MWCNT-HRP-SG-Chit-FcAOx-PEI was -0.28, which is nearly conforming to the previous reports for HRP (Fe^{III}/Fe^{II}) on direct electrochemistry (Wu et al. 2010). The redox potential of HRP was further confirmed from the increase in anodic and cathodic peak current by the addition of ethanol to the modified electrode (Figure 4.2B, curve d). The bioelectrode reactions involved the formation of H_2O_2 by FcAOx biocatalysis of substrate alcohol followed by HRP-catalyzed reduction of the liberated H_2O_2 through MWCNT supported direct electron transfer mechanism.

4.3.4. Response characteristics of the fabricated bioelectrode towards alcohol

The optimum pH 7.5 identified for the bioelectrode response conformed to the pH optimum for biocatalytic reaction of AOx (Suye et al. 1997). Figure 4.3A illustrates a typical current-time plot (at -0.34 V) on successive step addition of alcohol dose. The magnitude of the cathodic current was increased linearly with increasing ethanol concentration and reached saturation at 3000 µM of ethanol for FcAOx bioelectrode (Figure 4.3B, curve ii) and 1800 µM for AOx bioelectrode (Figure 4.3B, curve i). The response characteristics obtained from FcAOx based bioelectrode are compared with AOx-based bioelectrode and observed that all the response characteristics were substantially improved when FcAOx was used in the bioelectrode (Table 4.1). The biosensor responses for various alcohols (each at 0.05 mM) were tested. Considering the activity on methanol as 100 %, the activity on ethanol (71 %), 1-propanol (<9.2 %), 1-butanol (<1 %) and benzyl alcohol (<1 %) were recorded and as expected, the current response decreased with increasing the aliphatic chain length of the alcohol molecules. A comparative analysis on the performance of various prominent 1st (Lee and Tsai 2009; Patel et al. 2001), 2nd (de parda et al 2003; Hasunuma et al. 2004; Smutok et al. 2006; Gouveia-Caridade et al. 2008; Jimenez et al. 2014; Manso et al. 2008; Tsai et al. 2007) and 3rd generation (Das and Goswami 2013) alcohol biosensors reported so far showed

that the present FcAOx based biosensor offers improved operational stability, wide dynamic range of response with lower minimum concentration in the range, and improved detection limit. The ADH based biosensor (Lee and Tsai 2009) though showed marginally higher sensitivity of 164.6 μA mM^{-1} cm^{-2}, the other critical performances namely, stability, detection limit and dynamic range obtained by the present biosensor are improved. The cause of improved detection limit and sensitivity of the FcAOx based biosensor is ascribed to the amplified activity of the AOx obtained by entrapping the activator ferrocene in it and the DET mechanism involved in the signal transduction of the biosensor.

Table 4.1 Response characteristics of bioelectrodes.

Response characteristics	Bioelectrode	
	GCE-MWCNT-Nf-HRP-SG-Chit- FcAOx/PEI	GCE-MWCNT-Nf-HRP-SG-Chit- AOx/PEI
Linear range (μM)	5–3000	5–1800
Correlation co-efficient, *r*	0.9976	0.9951
Detection limit (DL)* (μM)	2.32±0.018	4.61±0.050
Sensitivity (μA mM^{-1} cm^{-1})	150±0.25	90±0.31
SD limit (μA)	0.117±0.02	0.140±0.05
Response time (s)	20	35

**DL = (3 X SD/Sensitivity)*; (where SD is the estimated standard deviation for the points used to construct the calibration curve and the *sensitivity*, its slope).

The improved kinetic parameters, such as lower K_m value of the FcAOx substantially contributed to the aforementioned improved functional activities of the biosensor as evident from the comparative analysis of the performance with native AOx based biosensor shown in table 4.1. The electrostatic interaction principle utilized by us for the physical immobilization of the enzyme on the biocompatible SG-Chit based electrode surface provided a significant operational stability and reproducibility on the response of the biosensor.

4.3.5. Stability and interference studies

The operational stability of the electrode was investigated for 28 successive measurements with 3 mM of alcohol (the highest response in the linear range) during a period

of 5 h. Our results demonstrated that the bioelectrode still maintained 90 % of its initial activity at the end of 28 measurements (Figure 4.4A). The reproducibility of the bioelectrode was estimated from the response to various alcohol concentrations at three bioelectrodes prepared by similar procedure. The results showed the acceptable reproducibility with a relative standard deviation (RSD) of 2 % for the bioelectrode. The storage stability of the bioelectrode was examined by carrying out the response measurements at a regular interval of three days and found that the bioelectrode retains ~90 % of the original response even after five weeks when stored at 4 °C and pH 7.5 (Figure 4.4 B). The half-life ($t_{1/2}$) of the biosensors under the above storage condition was ~184 days. To study the selectivity of the sensor towards alcohol, the effect of some potential interfering agents present in real samples namely, ascorbic acid, lactic acid, glucose, urea and uric acid, on the biosensor response was studied in 50 mM KPBS (pH 7.5) at -0.34 V. The response of the sensor was examined by exposing it separately to these interferents, with analyte in 1:1 ratio (Figure 4.4C). The selectivity co-efficient (SC) of ~1 for each interferent estimated using the formula, SC = I_{c+i}/I_c, where I_{c+i} and I_c are response for alcohol in the presence and absence of each interferents, respectively infers that these compounds did not significantly affect the biosensor response.

4.3.6. Analysis of commercial alcohol samples

The ethanol content ($mg \cdot mL^{-1}$) in three different beer samples (A, B, and C) was determined (at -0.34 V) using the GCE-MWCNT-Nf-HRP-SG-Chit-FcAOx-PEI biosensor by the multiple standard addition method without any pretreatment of the samples and found to be 0.39±0.014, 0.43±0.021 and 0.41±0.017 for sample A, B and C, respectively. The concentrations of ethanol in the same samples were also measured by gas chromatography and found to be 0.41±0.016, 0.44±0.015 and 0.40±0.012 for the samples A, B, and C,

respectively. The comparison of the data was done by paired t-test (Sigma 11) and no significant difference were found (P = 0.709) between the results obtained by the methods. The study validates the reliability of the existing biosensor for sensitive and quantitative analysis of industrial samples.

4.5. Conclusions

The amplified biocatalytic activity of AOx achieved by stable entrapment of chemical activator ferrocene in the protein matrix has been successfully exploited to develop an efficient biosensor using direct electrochemistry as governing principle for interference free detection of alcohol in real sample. The overall performance of the fabricated biosensor improved in terms of stability, linear detection range and sensitivity for detection of alcohol in liquid sample. The constructed biosensor exhibited good correlation with the standard analytical method, suggesting its application potential in alcohol industries.

Figures

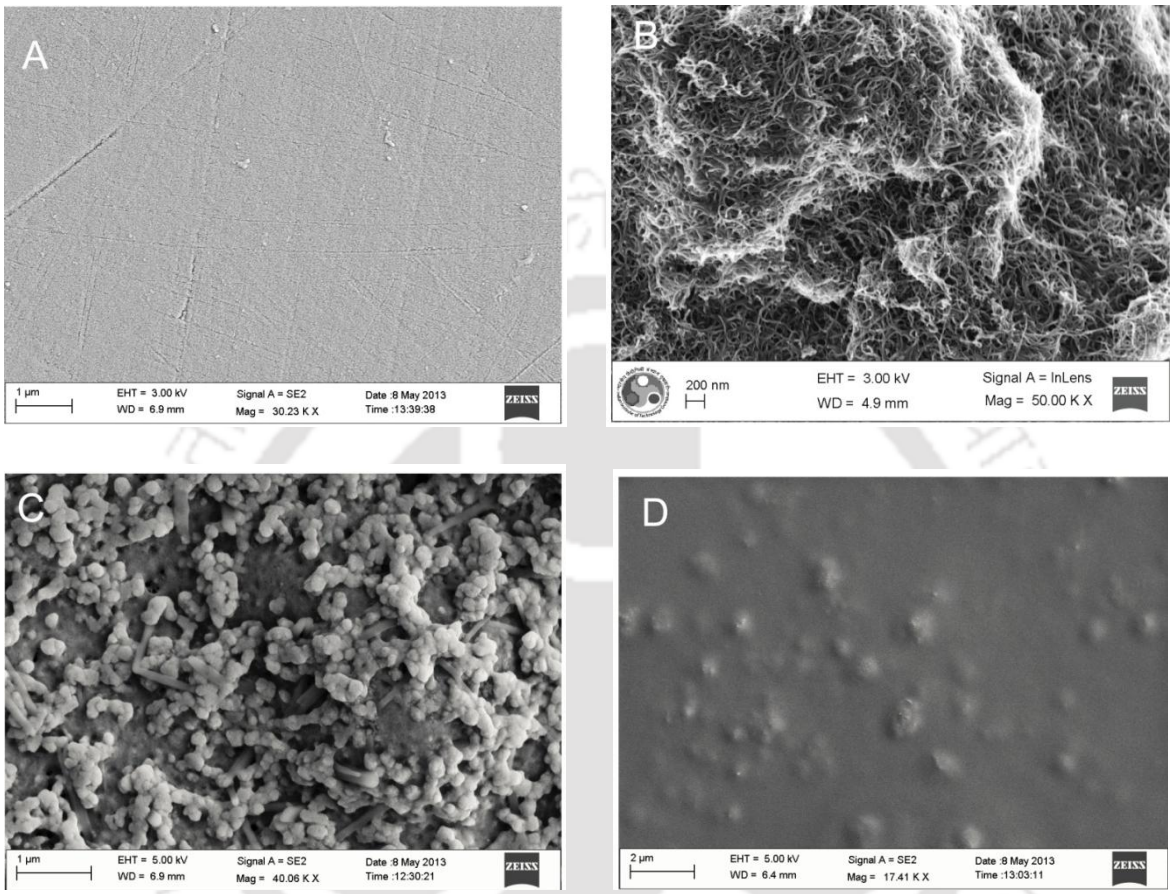

Figure 4.1 FESEM images at major stages of GCE-MWCNT-Nf-HRP-SG-Chit-FcAOx-PEI bioelectrode fabrication. **A:** GCE, **B:** GCE-MWCNT-Nf, **C:** GCE-MWCNT-Nf-HRP-SG-Chit-FcAOx, **D:** GCE-MWCNT-Nf-HRP-SG-Chit-FcAOx-PEI with EHT 3-5 kV.

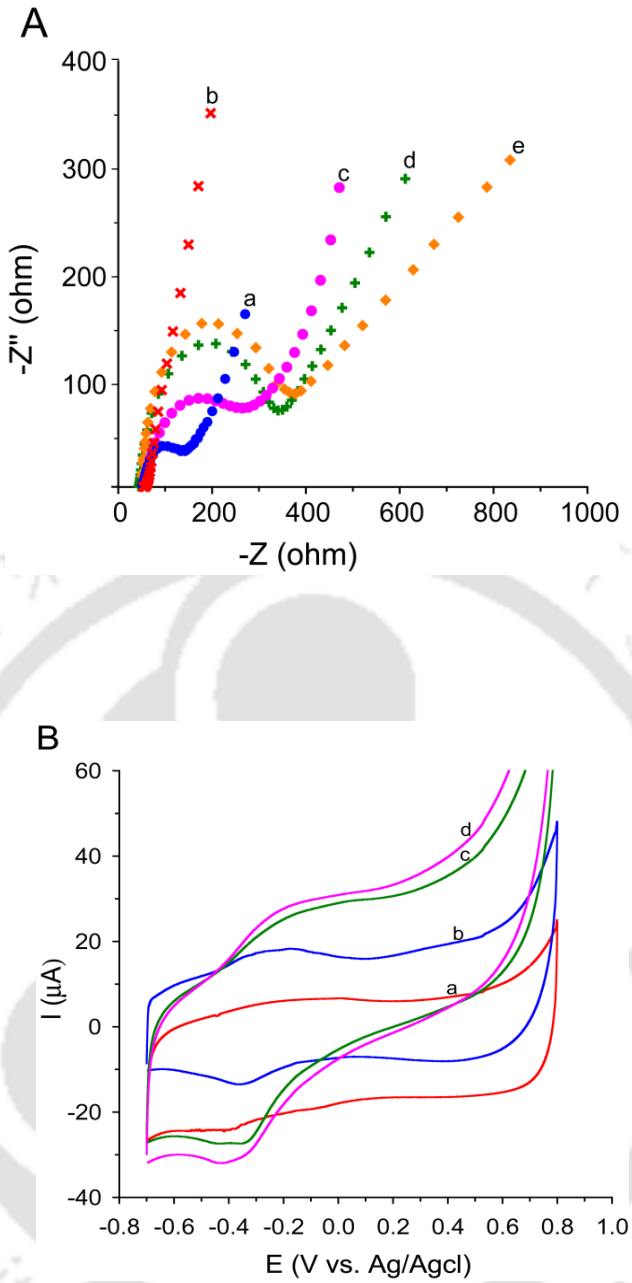

Figure 4.2 CV and EIS studies at major steps of GCE-MWCNT-Nf-HRP-SG-Chit-FcAOx-PEI bioelectrode fabrication. **A:** EIS of (a) GCE, (b) GCE-MWCNT-Nf, (c) GCE-MWCNT-Nf-HRP-SG-Chit, (d) GCE-MWCNT-Nf-HRP-SG-Chit-FcAOx-PEI, (e) GCE-MWCNT-Nf-HRP-SG-Chit-AOx-PEI electrodes in 5 mM $K_3Fe(CN)6$ /$K_4Fe(CN)6$ (1:1) and 0.1 M KCl in KPBS. **B:** CV of (a) GCE-MWCNT-Nf, (b) GCE-MWCNT-Nf-HRP-SG-Chit, (c) GCE-MWCNT-Nf-HRP-SG-Chit-FcAOx-PEI, (d) GCE-MWCNT-Nf-HRP-SG-Chit-FcAOx-PEI with 5 µM ethanol in an argon gas purged solution of 50 mM KPBS (pH 7.5) at a scan rate of 50 mV s^{-1}.

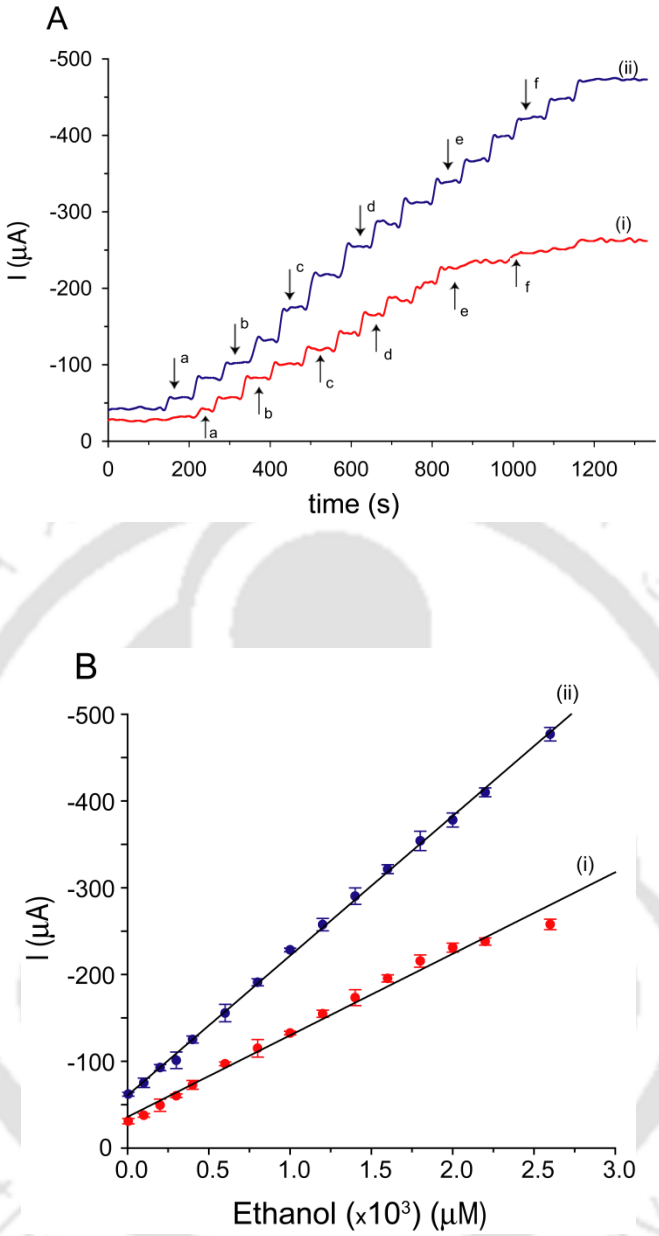

Figure 4.3 Current vs. time plot of the modified GCE. **A:** Chronoamperometric current responses of the GCE-MWCNT-Nf-HRP-Chit-SG-FcAOx-PEI and GCE-MWCNT-Nf-HRP-Chit-SG-AOx-PEI bioelectrodes for successive addition of alcohol (a) 5 µM (b) 50 µM (c) 100 µM (d) 500 µM (e) 1000 µM (f) 3000 µM. **B:** Response curves of the bioelectrodes (a) GCE-MWCNT-Nf-HRP-Chit-SG-FcAOx-PEI, (b) GCE-MWCNT-Nf-HRP-Chit-SG-AOx-PEI with increasing ethanol concentration in argon purged solution of KPBS. The operating potential used was -0.34 V (vs. Ag/AgCl electrode).

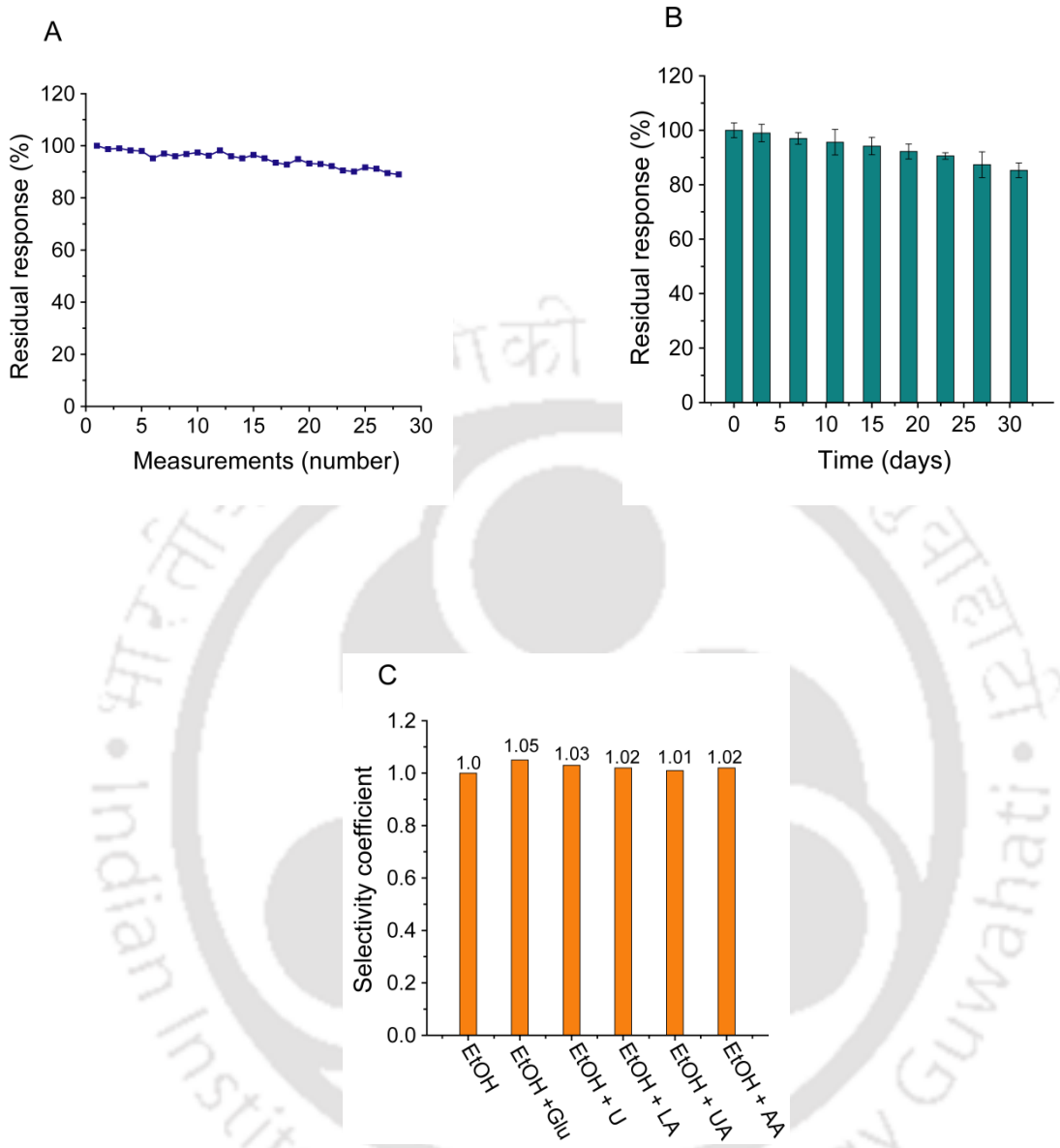

Figure 4.4 Stability of the GCE-MWCNT-Nf-HRP-SG-Chit-FcAOx-PEI bioelectrode. **A:** Operational stability and **B:** storage stability of the fabricated GCE-MWCNT-Nf-HRP-SG-Chit-FcAOx-PEI electrode. Each datum point represents the average of the analysis of triplicate values (n =3), with the range indicated with error bars. **C:** Interference studies with GCE-MWCNT-Nf-HRP-SG-Chit-FcAOx-PEI bioelectrode: (EtOH: Ethanol, Glu: glucose, U: urea, LA: lactic acid, UA: uric acid, AA: ascorbic acid.

Chapter 5

Gold Nanoparticle Activated Alcohol Oxidase as Biorecognition Element

CHAPTER 5

Gold nanoparticle activated alcohol oxidase as biorecognition element for developing alcohol biosensor

5.1. Overview

Biocatalytic activation of AOx by entrapping the activator ferrocene within the protein matrix as described in the previous chapter, though found highly effective in improving substantially the critical functional parameters of the constructed biosensor upon its inclusion as biorecognition element the technique demands additional steps alongside loss of enzyme in the fabrication process of the biosensensor. Therefore a simple method of AOx activation has been sought for the fabrication of amperometric alcohol biosensor. We focused on gold nanoparticles (AuNPs) for developing enzyme based electrochemical biosensors. The favorable functional traits of these nanoparticles that drive these studies are their strong electrical and biocompatible properties. The other reason of using AuNPs in amperometric biosensors is their high surface to volume ratio, which is a common property of the nanoparticles that serves to increase the enzyme loading on the electrode surface for amplifying the sensor signal and tailored wider detection range (Saxena et al. 2011). The wide utility of these nanoparticles has prompted to explore different synthesis routes that fit well with their intended applications. Focus has recently been laid on the green synthesis

route for their production using a variety of biological materials, though the synthetic mechanism in most of the cases yet to be adequately explored (Zhong et al. 2004; Si and Mandal 2007; Hussain et al. 2009; Shankar et al. 2005). Since the stability of the AuNPs formed in the reaction medium is an important criterion for their efficient collections and utilizations, hence studies on the application of various conditions and substances to prepare stable colloidal AuNPs have also received substantial research interest (Bajpai et al. 2007; Spirin et al. 2005; Rangnekar et al. 2007). The coupling of AuNPs with the enzyme molecules is however, a critical issue to utilize the intended properties of the nanoparticles for achieving the desired level of response for the constructed biosensors. Moreover, the mode of coupling significantly influenced the reproducible response characteristics of the constructed biosensors. For example, the high linker distance between the enzyme protein and AuNPs obtained by common chemical immobilization may interferes the electrocatalytic response of the biosensor, while the physical immobilization may impair the stable interaction between the enzyme and the AuNPs thus hindering the reproducible performance of the constructed biosensors (Saxena and Goswami 2012). An affable coupling for the desired functional properties may be difficult to achieve when the enzyme used is a labile protein such as alcohol oxidase (AOx), which is a multimeric protein with Mw of ~600 kDa. To overcome the aforementioned disadvantages and to increase the dynamic range and stability of the biosensor in comparison with ferrocene activated AOx based bienzyme sensor, the protein mediated *in-situ* synthesised and stabilized AuNPs as activating and enhanced enzyme loading material for amperometric alcohol biosensor was developed. In this approach the synthesis and stabilization of the AuNPs on the AOx protein surface were performed in single step by exploiting a spontaneous native reaction process driven by the enzyme itself under alkaline environment (pH 8.5). The AOx coupled AuNPs were encapsulated with polyaniline (PANI), synthesised by oxidative polymerization of aniline

using H_2O_2 generated *in-situ* from the AOx catalysed oxidation of alcohol. PANI offers a great advantage for immobilization of enzymes because of its biocompatibility, stability and controllable electrochemical properties (Zhao et al. 2009). In this amperometric enzyme sensor, the H_2O_2 formed by the AOx-AuNPs catalyzed oxidation of alcohol was used as redox indicator to generate the Faradic current response. The fabricated bioelectrode has been characterized and its response characteristics for the substrate ethanol in real samples has been evaluated and presented here.

5.2. Experimental Approaches

5.2.1. Reagents and stock solutions

AOx from *Pichia pastoris* (32 $U \cdot mg^{-1}$protein), HRP (1080 $U \cdot mg^{-1}$ solid), $HAuCl_4$, chitosan from crab shells (≥75 % deacetylated), aniline, uric acid, ascorbic acid, lactic acid, urea, (±)–10–camphorsulfonic acid, ABTS, Nafion117 (Nf) (5 % w/v in isopropanol) were purchased from Sigma Aldrich. Ethanol, K_2HPO_4, KH_2PO_4 and H_2O_2 (30 % v/v) were purchased from Merck. All other chemical were of analytical grade.

Chitosan stock solution (0.2 % w/v) was prepared by dissolving 0.2 g chitosan powder in 100 ml of 1.0 % glacial acetic acid solution. Aniline was purified by passing 1.5 ml of aliquots through a neutral Al_2O_3 column (5 cm long, 0.4 cm diameter) to remove all colored components. Stock solutions of AOx (14 mM) and HRP (70 µM) were freshly prepared in 50 mM KPBS, pH 7.5 and 7.0, respectively prior to being used. The stock solution of ABTS (10 mM) was freshly prepared in 50 mM KPBS just before the experiments. All solutions were prepared with deionized water (15 MΩ) from Millipore water purification system (Millipore, Bedford, MA).

5.2.2. Enzyme assay

The AOx activity was measured by following HRP-coupled assay (Kemp et al. 1988) as described under the section 2.2.2.

5.2.3. Preparation of AOx stabilized AuNPs (AOx-AuNPs)

All glassware was washed with Aqua Regia (HCl: HNO_3, 3:1 v/v), and rinsed with ultrapure water. A total 0.1 ml of aqueous $HAuCl_4$ solution (1 mM) was added to 0.1 ml of AOx solution (1 $mg \cdot mL^{-1}$) under shaking at 37 °C. An aliquot of NaOH (~5 µL, 1 M) was then added to the solution after 5 minutes to adjust pH 8.5. The reaction solution was kept in shaking incubator at 37 °C for 24 h for the formation of the AuNPs.

5.2.4. Preparation of PANI/AOx-AuNPs nanocomposites

A bulk solution consisted of 200 mM aniline, 1 $mg \cdot mL^{-1}$ AOx stabilized AuNPs and 20 mM ethanol were allowed to stand at 4 °C in dark. The progress of the polymerization of aniline to PANI was evaluated at λ_{450nm} (Scheme 5.1B). PANI was synthesized by oxidative polymerization of aniline using H_2O_2 generated from the AOx catalysed oxidation of alcohol. During this process, cation or cation radical sites generated in monomer (polymer) molecule initiated the polymer growth (Sapurina and Shishov 2012). After 24 h of reaction time, the solution was centrifuged at 5000xg for 3 min. The precipitated nanocomposites were collected and again transferred into 200 µL of the same buffer and then subjected to 5000xg for 3 min. The washing buffer solution was removed and PANI/AOx-AuNPs particles were collected and stored in 200 µL of KPBS, pH 7.5 for further use.

5.2.5. Fabrication of bioelectrode

Scheme 5.1A shows the schematic diagram for the fabrication of the bioelectrode. A GCE (diameter 0.5 cm) was cleaned by polishing it with alumina powder, washing it

ultrasonically with 70 % ethanol and water separately for 15 min each and finally drying in air. 100 µL of 0.2 % chitosan was mixed with 200 µL of PANI/AOx-AuNPs and the resulting solution was deposition on a GCE through a step drying process using 3 µL of the solution at a time for 3 times to prepare GCE/chit/PANI/AOx-AuNPs. After complete drying, 5 µL of Nf (5 % v/v) was layered over it and then allowed to dry at RT to produce GCE/Chit/PANI/AOx-AuNP/Nf. Prior to measurements, the surface of the modified electrodes was thoroughly washed with distilled water. The fabricated bioelectrodes were stored at 4 °C when not in use.

5.2.6. Apparatus and measurements

Uv-vis spectroscopic measurements were carried out with a CARY 300 BIO (Varian, USA) spectrophotometer with a scan range of λ_{300nm}-$\lambda_{800\ nm}$, using 1 cm path length quartz cuvette at 25 °C. CD measurements were carried out by using a Jasco J-815 spectropolarimeter calibrated with 0.06 % (w/v) aqueous solution of (±)–10–camphorsulfonic acid. The spectra were recorded at a scan rate of 50 nm min^{-1} in a 0.1 cm path length suprasil quartz cuvette from λ_{190nm} - $\lambda_{240\ nm}$, a bandwidth of 1 nm with 4 accumulations and a time constant of 4 s. The spectra were corrected for baseline and the secondary structure analysis was performed by using DICHROWEB (Whitmore and Wallace 2008). Transmission electron microscopy (TEM) images were acquired with a 200 kV electron microscope (JEOL JEM, 2100). The Fourier transform infrared spectroscopy (FTIR) measurements were conducted on a Perkin Elmer spectrometer operated at a resolution of 4 cm^{-1}. DLS and zeta potential measurements were carried out in a Zetasizer Nano Instrument system (Malvern Instruments Ltd., England). Data were acquired at 20 °C, repeated 20 times and averaged. The viscosity was set to 1 cP at a scattering angle of 90° and resulting autocorrelation function was analyzed by the integrated control software to obtain size and charge

distributions. Gel filtration experiments were carried out at RT on a Sephacryl S-300 (10/50) (M_r cut off 500 - 1500 KDa) column using an ACTA FPLC device (GE Healthcare). The column was equilibrated with 3 bed volumes of 50 mM KPBS (pH 7.5). Sedimentation velocity experiments were performed with Beckman optima XL–A/XL–I analytical ultracentrifuge equipped with An50–Ti rotor and the operation conditions were: 82,575x*g*, 20 °C, Scans at λ_{280nm} and interval of 180 s. Data obtained as absorbance at λ_{280nm} versus cell radius were fitted using continuous sedimentation co-efficient distribution *c(s)* analysis with SEDFIT (Schuck 2003). CV and EIS were performed with an Autolab PGSTAT 1212 (Eco Chemie, Netherlands).

A three-electrode system was employed with platinum rod as a counter electrode, Ag/AgCl (saturated KCl) as reference electrode, and GCE or modified GCE as the working electrode. All potentials were measured and reported relative to the Ag/AgCl reference electrode. During the CV measurements, the electrolyte solution was constantly purged with argon gas. EIS measurements were performed in a background solution of 5 mM $K_3Fe(CN)_6/K_4Fe(CN)_6$ (1:1) and 0.1 M KCl in KPBS (50 mM, pH 7.5) within the frequency range of 0.05 Hz to 10 kHz. The amplitude of the alternate voltage was 5 mV. All experiments were performed at RT. AFM was performed using an ambient air scanning probe microscope (Agilent Technologies 5500, USA). Images were recorded with typical contact mode using Picoscan 5 software. The amperometric determination of ethanol in commercial samples was performed by the multiple standard addition method. The samples were diluted with KPBS, pH 7.5 in appropriate concentration and passed through 0.22 µM filter disc before analysis. The enzyme loading of the electrode was determined in terms of number of enzyme units retained per unit surface area (U cm^{-2}) of the electrode. The enzyme units were calculated using a spectrophotometric rate determination method involving the measurement of H_2O_2 generation accompanying the oxidation of alcohol (Kemp et al. 1988).

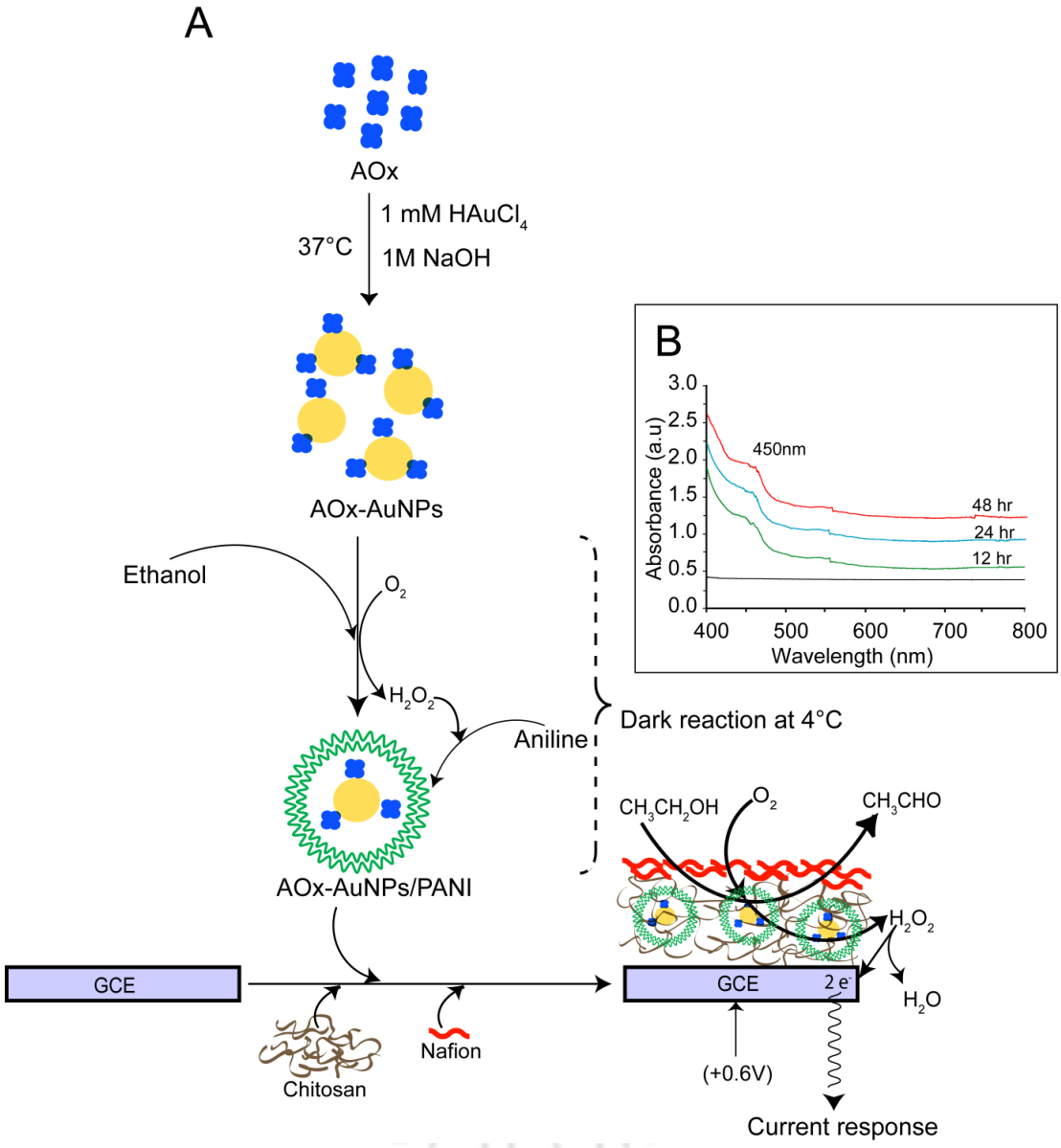

Scheme 5.1 A: Fabrication scheme of GCE/Chit/PANI/AOx-AuNPs/Nf. **B:** Formation of PANI in KPBS: Reaction mixture containing 1mg·mL^{-1} of AOx, 20 mM of ethanol and 200 mM of monomer aniline. The duration of polymerization was studied for 12 h, 24 h and 48 h. Formation of the PANI is implied by the peak generated at the λ_{450nm}.

The AOx immobilized electrode was immersed and incubated for 10 min at RT in a reaction mixture containing ethanol (0.2 mM), HRP (87 nM), ABTS (2 mM) in total 1 mL KPBS (50 mM, pH 7.5). The electrode was removed and the appearance of dye formed during the reaction was measured at λ_{405nm}. The enzyme loading (U cm^{-2}) was calculated using the following formula:

$$U\ cm^{-2} = \Delta A/0.2\ \varepsilon_{405} at \qquad (6.1)$$

Where, 'ΔA' is the change in absorbance in time t of incubation of the AOx immobilized electrode and 'a' is the area of the electrode. The molar extinction coefficient of $ABTS^{2-}$ dye at λ_{405nm} (ε_{405}) is taken as 18.4 mM^{-1} cm^{-1}.

5.3. Results and Discussion

5.3.1. Characterizations of AOx-AuNPs

The Uv-Vis spectra of the solution obtained by mixing AOx with $HAuCl_4$ did not show any characteristic localized surface Plasmon resonance (SPR) peak at λ_{540nm} for AuNPs even after incubating the mixture for several hours (Figure 5.1A, curve a). The solution however, when adjusted to pH 8.5 with 1 M NaOH and incubated for 6 h at 37 °C, a prominent SPR peak appeared (Figure 5.1A, curve b). The intensity of the SPR peak was increased with increasing the incubation period of the reaction mixture (Figure 5.1A, curve c). Above findings demonstrated that AOx protein could initiate the reduction of $AuCl_4$ to the formation of AuNPs under alkaline environment. The CD spectra of AOx and AOx-AuNPs conjugate (SEC purified) showed comparable characteristics: a narrow negative peak at $\lambda_{222\ nm}$ and $\lambda_{208\ nm}$, more intense positive peak at $\lambda_{194\ nm}$ with α-helical conformation (Figure 5.1B). A minor difference in the secondary structural composition between AOx and AOx-AuNPs occurred possibly due to the interaction of the charged AuNPs with the AOx. The synthesized AuNPs was analyzed with TEM. The average AuNPs size (diameter, D) was calculated by

considering ~100 particles from multiple TEM pictures of the sample acquired from different locations of the TEM grid. One representative TEM picture of the synthesized AuNPs is presented in Figure 5.1C. The images showed the average particle size of 22 nm with a spread range of 18-24 nm. DLS analysis of the reaction mixture incubated for 24 h showed a poly-dispersed particles size in 3 major peaks: the highest intensity at 37± 2.1 nm assigned to the AOx-AuNPs conjugates (Figure 5.1E); the low intensity 10.4 ± 1.5 nm sizes assigned to the unreacted native protein (Figure 5.1D), and peak in the range of 22-26 nm was attributed to the low aggregation of AOx protein. In SEC, the AOx was eluted as single peak with retention time of 21±1.2 min. Whereas AOx and AuNPs mixture (pH 8.5) incubated for 6 h, 12 h and 24 h were eluted as two peaks with retention time of 17.5±0.5 min and 21±0.5 min, respectively. The high intensity peak at 17.5±0.5 min corresponds to the AOx-AuNPs and the low intensity peak at 21±0.5 corresponds to the unreacted AOx (Figure 5.1F). The decrease in the retention time implies the formation of AOx-AuNPs conjugates. The sedimentation coefficients (s) of AOx and AOx-AuNPs (SEC purified) were determined by using a range of 's' values from 15-20 s, and frictional ratio (f/f_0) of 1.2. The fit showed the 's' values of 18.2 ± 0.2 s and 18.6 ± 0.1 s for AOx and AOx-AuNPs incubated for 24 h, respectively (Figure 5.2A). Increase in 's' of AOx-AuNPs by 0.3 s indicated the successful formation of AuNPs conjugated AOx. The pH stability of the AuNPs conjugated AOx was studied at pH 3.0 - 11.0 (Figure 5.2B) and found the conjugate was less stable at higher acidic (<pH 6.5) and alkaline (>pH 10.0) conditions as the SPR absorbance at these pH conditions decreased with time. The conjugate showed stable absorbance (at λ_{540nm}) at pH 8.5 for 24 h. The AOx-AuNPs also showed good stability in NaCl concentration in the range 10^{-5} M to 10^{-1} M (Figure 5.2C). The AOx (p*I* 4.5) showed a zeta potential of -30 mV at pH 7.5 (Figure 5.2D). The zeta potential recorded for AOx-AuNPs was -57 mV, implying the possible contribution of negative charge of AuNPs into the conjugate potential (Figure 5.2E).

The FT-IR spectral (Figure 5.3) analyses of the pure AOx and the AOx-AuNPs pellets shown that the characteristic amide band at 1600–1700 cm^{-1} (mainly CO stretch) is related to the secondary structure of the protein (Burt et al. 2004). The amide-I (1632 cm^{-1}) and amide-III bands (1262 cm^{-1}) of AOx were only marginally shifted to 1630 cm^{-1} and 1261 cm^{-1}. The results indicate that there were no significant changes in the secondary structure of the AOx protein after its conjugation with the AuNPs. The band at 1744 cm^{-1}, which is assigned to the $-COO^-$ of acidic amino acids such as, aspartic and glutamic acid residues, was disappeared in AOx-AuNPs implying the potential involvement of $-COO^-$ group of AOx protein in complexing and thus, stabilizing the AuNPs (Liu et al. 2013**)**. A strong band at 2550 cm^{-1} corresponds to the sulphydryl groups (–SH) of cysteine (Aryal et al. 2006) was diminished in AOx-AuNPs indicating involvement of cysteine of AOx protein in reducing $AuCl_4^-$ to AuNPs under alkaline conditions. Additionally a band at 1400-1450 cm^{-1} has been masked in AOx-AuNPs which was assigned to the vibrations of Trp residues. The K_m and K_{cat} determined for AOx were 1.92 ± 0.02 mM and 0.165 ± 0.02 s^{-1}, respectively. The K_m and K_{cat} for the AuNPs conjugated AOx were 1.72 ± 0.01 mM and 0.170 ± 0.01 s^{-1}, respectively. Thus, the efficiency (K_{cat}/K_m) of the AOx was increased by 18 % in AOx-AuNPs. There were no significant changes on the kinetic parameters for the AOx when it was merely mixed with the AuNPs prepared by citrate reduction method. The results confirmed the activating role of AuNPs for AOx in the self assembled enzyme-nano conjugate system.

5.3.2. Morphological characterization of bioelectrode with atomic force microscopy

3D AFM images were recorded to characterize the morphological changes of the electrode surface obtained after each major steps of fabrication. Figure 5.4A shows the image of the plane bare GCE. The AuNPs synthesized by citrate reduction method (Frens 1973; Turkevich et al. 1951) were homogenously distributed over the electrode surface (Figure

5.4B). The electrode surface with AOx-AuNPs (Figure 5.4C) film was transformed to a heterogeneous character with a mixture of globular structure for protein and particle structure similar to AuNPs as in Figure 5.4B. When PANI encapsulated AOx (Figure 5.4D) and AOx-AuNPs (Figure 5.4E) were assembled on the GCE the apparent sizes of the globules were increased further with a clear heterogeneity and protrusions across the whole surface for the later inferring significant increase in electrode surface area relevant for greater immobilization of biomolecules. The diameter of the clusters showed 250 nm and 287 nm for PANI/AOx and PANI/AOx-AuNPs, respectively. The images indicate that the PANI encapsulated AOx-AuNPs nanocomposite was successfully incorporated on the electrode surface. The surface morphology changed to smooth even form when chitosan and nafion were added for the formation of the film in GCE/Chit/PANI/AOx-AuNP/Nf electrode (Figure 5.4F).

5.3.3. Electrochemical characterization of the fabricated electrodes

5.3.3.1. Cyclic voltammetry

CV of bare GCE and modified GCE was done in a KPBS (50 mM, pH 7.5) at 50 mV s^{-1} to monitor changes in their electrochemical behaviour introduced at different steps of electrode modification. No clear peaks were observed for bare GCE (Figure 5.5A, curve a) and GCE modified electrodes GCE/Chit/PANI/AOx/Nf and GCE/Chit/PANI/AOx-AuNPs/Nf (Figure 5.5A, curve b, and c) suggesting that PANI/AOx-AuNPs layer is electro-inactive in this potential window. The addition of ethanol on GCE/Chit/PANI/AOx-AuNPs/Nf bioelectrode however, generated a broad oxidation peak at around +0.6 V (Figure 5.5A, curve d), which is attributed to the oxidation potential of H_2O_2 (Patel et al. 2001; Xian et al. 2006) formed by the electro-catalytic oxidation of ethanol. The Faradic current at +0.6 V increased with increasing ethanol concentration on the modified electrode (Figure 5.5, curve e).

5.3.3.2. Electrochemical impedance spectroscopy

EIS was employed to further monitor the charge properties on the bioelectrode surface during the stepwise assembly of the electrode. The impedance spectra presented as Nyquist plots ($-Z''$ vs Z') obtained on different modified electrodes in a solution of 5 mM $K_3Fe(CN)_6/K_4Fe(CN)_6$ (1:1) and 0.1 M KCl (50 mM, KPBS pH 7.5) (Figure 5.5B). The value of the charge-transfer resistance (R_{ct}) at the electrode surface can be estimated directly from the diameters of the high frequency semicircle. The bare GCE exhibits a line with small semicircle diameter with R_{ct} of 171 Ω (Figure 5.5B, curve a). The semicircle disappeared upon layering of PANI onto the GCE, implying highly conductive PANI film facilitates the charge transfer with the electrode (Figure 5.5B, curve b). Reappearance of a semicircle line with R_{ct} of 450 Ω (Figure 5.5B, curve c) upon layering of PANI/AOx and Nf on the GCE film indicates the successful formation of the film, which increases R_{ct} due to the formation of a ferrocyanide transport-blocking layer on the electrode. The R_{ct} of the GCE was drastically increased to 950 Ω (Figure 5.5B, curve d) when Chit/PANI/AOx/Nf were layered on it. This implies that the assembled chitosan/Nf layer generated an obstruction to the electron transfer of the electrochemical probe at electrode surface. The R_{ct} of the electrode decreased to 690 Ω when Chit/PANI/AOx-AuNPs/Nf was layered on the electrode surface (Figure 5.5B, curve e), implying that AuNPs play an important role in accelerating the electron transfer process.

5.3.4. Response characteristics of GCE/PANI/AOx-AuNPs/Nf bioelectrode towards ethanol

From a typical current-time plot (Figure 5.6A, ii and iii) it revealed that the peak current increased linearly (R^2= 0.9731) with increase in ethanol concentrations in the range of 10 µM – 4.7 mM for the bioelectrode GCE/PANI/AOx-AuNPs/Nf. The limit of detection

(*DL*) and sensitivity of the bioelectrode for ethanol were 7±0.027 µM and 68.3±0.35 µA mM^{-1} cm^{-2}, respectively; where *DL = (3 × SD)/sensitivity*, and *SD* (*n = 3*) is the standard deviation for the points used to construct the calibration curve and the sensitivity, its slope. The sensitivity and linear range of the GCE/Chit/PANI/AOx-AuNPs/Nf biosensor (Fig 5.6B, curve iii) was higher than the bioelectrodes that void AuNPs (Fig 5.6B, curve i and ii). The reason is attributed to the increased loading of ~12 % catalytically active AOx on the electrode surface supported by the enhanced immobilization surface area due to the AuNPs. Additionally, the interfacial layer of AuNPs likely to play supporting role in enhancing the kinetics of the enzyme as reported previously (Section 5.3.3) and facilitating the electron hopping from the redox indicator (H_2O_2) to the electrode surface due to its high conductive property.

Table 5.1: Response characteristics of the bioelectrode

Response characteristics	Bioelectrodes	
	GCE/Chit/PANI/AOx-AuNPs/Nf	GCE/Chit/PANI/FcAOx-AuNPs/Nf
Linear range (µM)	10-4700	8-5500
Correlation co-efficient, r	0.9731	0.9836
Detection limit (DL) (µM)	7±0.027	4±0.012
Sensitivity (µA mM^{-1} cm^{2})	68.3±0.35	91.0±0.51
Standard deviation (SD) limit (µA)	0.18±0.01	0.12±0.02
Response time (s)	5.0	2.0

The values were expressed as mean ± SD (n = 3)

A comparative analysis on the performance of various prominent alcohol biosensors was carried out (Patel et al. 2001; de parda et al. 2003; Hasunuma et al. 2004; Smutok et al. 2006; Tsai et al. 2007; Gouveia-Caridade et al. 2008; Manso et al. 2008; Lee and Tsai 2009; Das and Goswami 2013; Jimenez et al. 2014; Soylemez et al. 2014). The operational and storage stability of the constructed biosensor are comparable to and even improved than many of the reported prominent biosensors. The dynamic detection range of the biosensor was far wider than most of the alcohol biosensors reported so far except an ADH-based

biosensor reported recently (Jimenez et al. 2014). However, the lowest detection concentration in the dynamic range obtained by us (0.01 mM) is far lower than the aforesaid ADH-based biosensor (0.9 mM). The ultralow detection limit of the constructed biosensor is considered as beneficial for detecting precisely very low concentration of alcohol in real samples. The overall performance of the biosensor is improved than the previously reported alcohol biosensors. The cause of improved stability and linear range of the present biosensor is ascribed to the amplified activity and high loading of the AOx obtained by its conjugation with activator AuNPs and the highly favorable conformation to AOx provided by the PANI film involved in the fabrication process. The improved kinetic parameter of the AOx-AuNPs had substantially contributed to the aforementioned improved functional activities of the biosensor. The encapsulation of AOx conjugates within enzymatically synthesized conductive PANI nanoparticles offered a significant storage, operational stability and reproducible response of the biosensor.

5.3.5. Operational and storage stability

A freshly prepared GCE/Chit/PANI/AOx-AuNPs/Nf bioelectrode was taken and the variation in its current response towards ethanol was monitored as a function of time and the number of measurements. For a period of 5 h, 32 measurements of a 4 mM ethanol solution were performed by the electrode. After each measurement, the bioelectrode was washed with KPBS. Results demonstrated that the bioelectrode maintained 93.7 % of its initial activity at the end of 25 measurements (Figure 5.7A). The response of three bioelectrodes prepared by similar procedure to various alcohol concentrations was examined and found acceptable reproducibility with a relative standard deviation (RSD) of ~2.4 % for the response. The storage stability of the bioelectrode was examined by carrying out the response measurements at a regular interval of three days and found that the bioelectrode retains ~93 % of the original

response even after five weeks when stored at 4 °C and pH 7.5 in 50 mM KPBS (Figure 5.7B). The half-life ($t_{1/2}$) of the biosensors under the above storage condition was ~302 days.

5.3.6. Interference study

The effect of potential interfering agents in alcohol determination present in real samples namely, ascorbic acid (AA), lactic acid (LA), acetic acid (Acet. A), butyric acid (BA), tartaric acid (TA), malic acid (MA), citric acid (CA), glucose (Glu), urea (U) and uric acid (UA), on biosensor response was studied in 50 mM KPBS (pH 7.5) by exposing the sensor separately to these compounds with ethanol in 1:1 ratio. Selectivity co-efficient (SC) of the fabricated bioelectrode for each interferent was calculated using the formula, SC = I_{c+i}/I_c, where I_{c+I} and I_c are bioelectrode response at +0.6 V for ethanol in the presence and absence of each interferents, respectively. The results showed that these compounds did not significantly affect the biosensor response as evident from the selectivity co-efficient (SC) of ~1 for each of the compounds (Figure 5.7C).

5.3.7. Determination of ethanol in beverage samples

The ethanol content (% v/v) in three different beverage samples was determined (at +0.6 V) using the GCE/Chit/PANI/AOx-AuNPs/Nf biosensor and found to be 4.5±0.14, 13.4±0.21 and 52±0.17 % for beer, wine and spirit, respectively. The concentrations of ethanol in the same samples were also measured by gas chromatography and found to be 4.4±0.15, 13.5±0.12 and 51.8±0.2 % for beer, wine and spirit, respectively. The comparison of the data was done by paired t-test (Sigma 11) and no significant difference was found (P = 0.709) between the results obtained by the methods. The study validates the reliability of the existing biosensor for sensitive and quantitative analysis of alcohol samples.

5.4. Conclusions

A stable AOx protein surface stabilized AuNPs synthesized by exploiting the native chemical drive of the protein molecules under alkaline condition was developed for the first time. In this nano-conjugate the intimately associated AuNPs found to enhance the kinetic activity of the AOx enzyme. The AOx-AuNPs conjugates encapsulated with PANI synthesised by exploiting a localized AOx catalysed oxidative reaction, implanted stably on the GCE by using chitosan and Nafion polymers. This nanocomposite bioelectrode based biosensor showed high operational and storage stability and wide linear current response against ethanol with very a low detection limit. The linear range is thus sufficient for quantitative analyses of alcohol in clinical, forensic and many other practical applications where sensitive detection of alcohol is important. The biosensor was also effectively used for determination of ethanol in commercial beverage samples. The overall performance of the constructed biosensor validates the potential application of the bioelectrode fabrication concept for developing a commercially viable biosensor device.

Figures

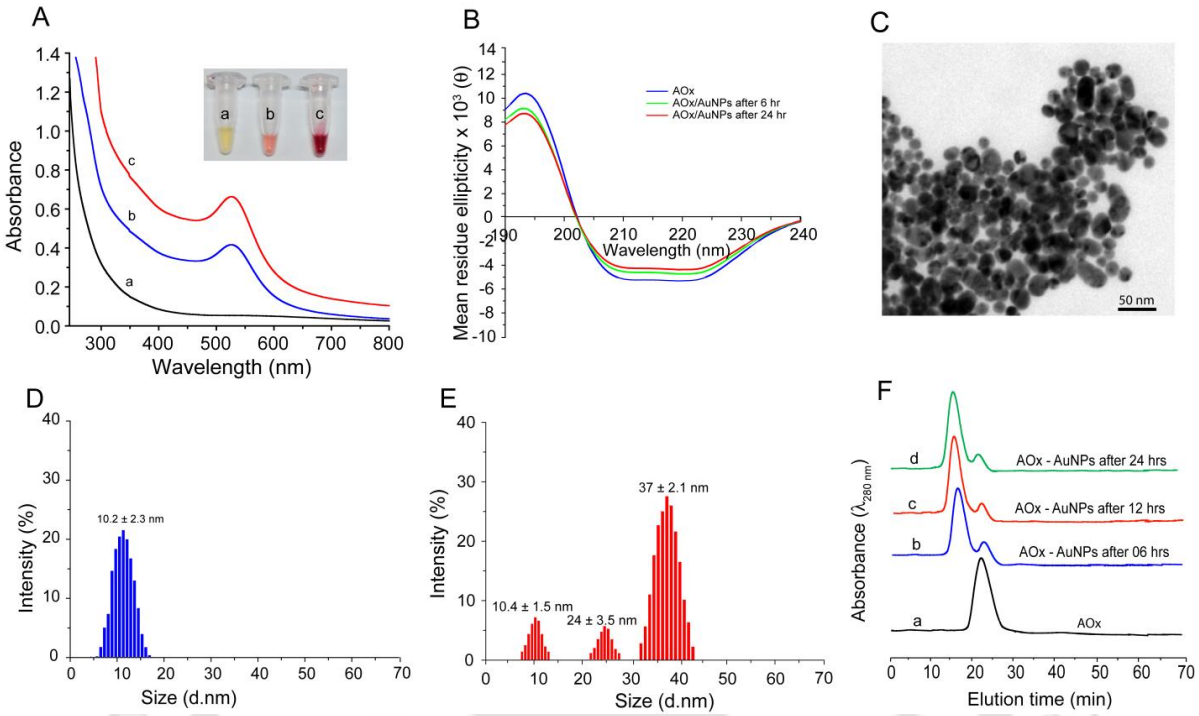

Figure 5.1 Characterization of AOx stabilized AuNPs. **A:** Uv-vis Spectra: (a) AOx mixed with $HAuCl_4$, pH 7.5 and incubated for 24 h; (b) AOx mixed with $HAuCl_4$ adjusts to pH 8.5 with 1 M NaOH and incubated for 6 h and (c) 24 h. Concentration of AOx and $HAuCl_4$ in the analyses was 1 mg·mL^{-1} and 1 mM, respectively. **B:** far UV-CD spectra of native AOx (blue line), and AOx stabilized AuNPs obtained after 6 h (green line) and 24 h of incubation (red line). **C:** TEM image of AOx stabilized AuNPs. **D:** DLS studies of the AOx and **E:** Reaction solution after 24 h incubation of the AOx with $HAuCl_4$ in KPBS at 20 °C, pH 7.5. (F) SEC of AOx (a) and reaction mixture containing AOx-AuNPs incubated for 6 h (b) 12 h (c) and 24 h (d).

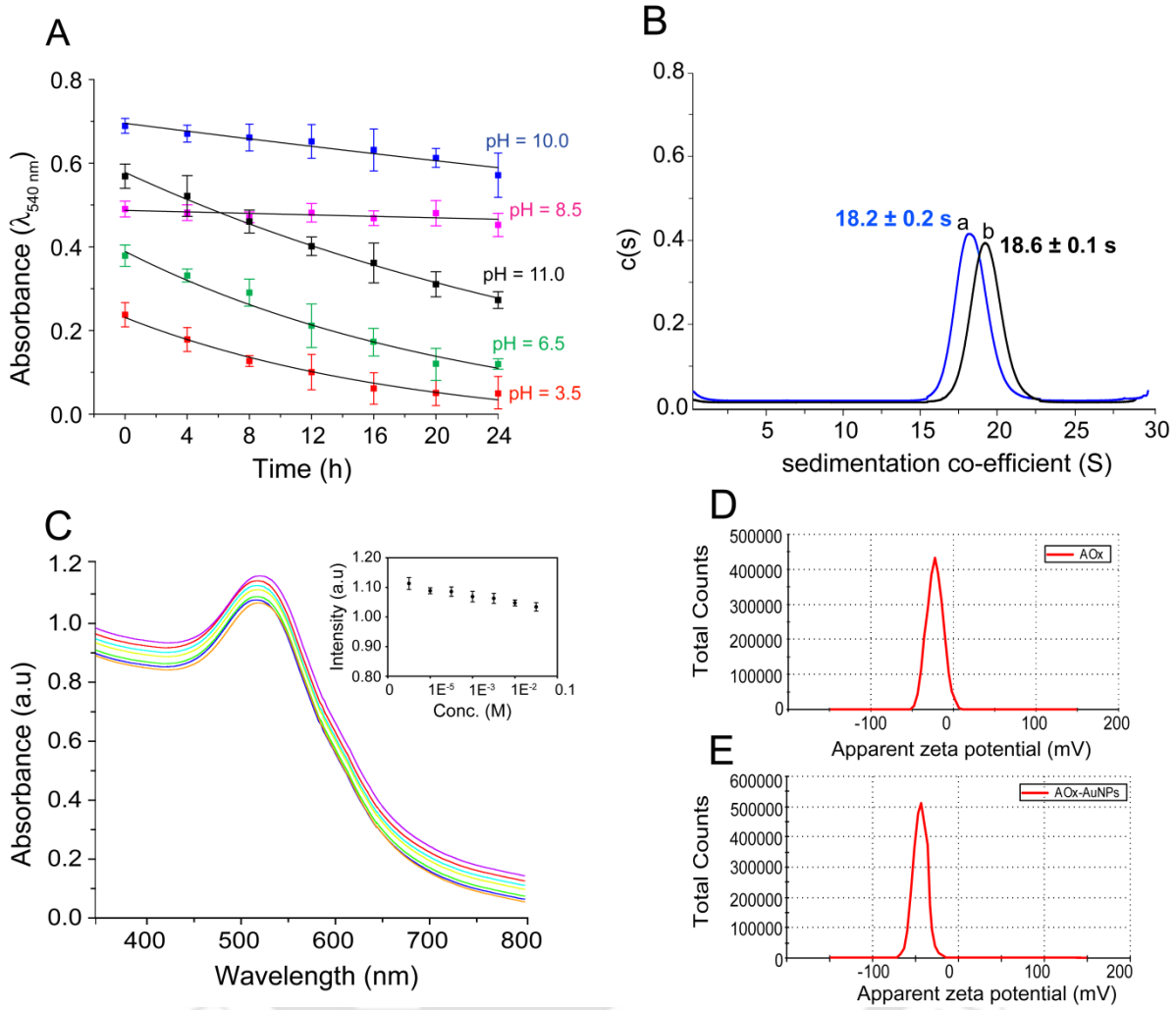

Figure 5.2 Characterization of AOx stabilized AuNPs. **A:** pH stability studies of the AOx stabilized AuNPs. The different buffers (each of 50 mM) used were sodium acetate (pH 3.5), potassium phosphate (pH 6.5), tris-HCl (pH 8.5) and glycine-NaOH (pH 10.0-11.0), **B:** *c(s)* distribution analysis of the simulated data from sedimentation velocity experiment at 4 °C in KPBS showing 's' values for (a) pure AOx and (b) AOx-AuNPs fractions obtained from SEC. The data were fitted using the parameters $\bar{\upsilon}$ = 0.73 ml/g and ρ = 1.00 g/cm^3. **C:** Effect of NaCl addition on AOx capped AuNPs. Inset shows the intensity of SPR (λ_{540nm}) at various concentrations of NaCl. The peak with highest intensity at λ_{540nm} is the peak where no NaCl was added. **D:** Zeta potential distribution curves of AOx and AOx-AuNPs (SEC purified) at pH 7.5 and 20 °C.

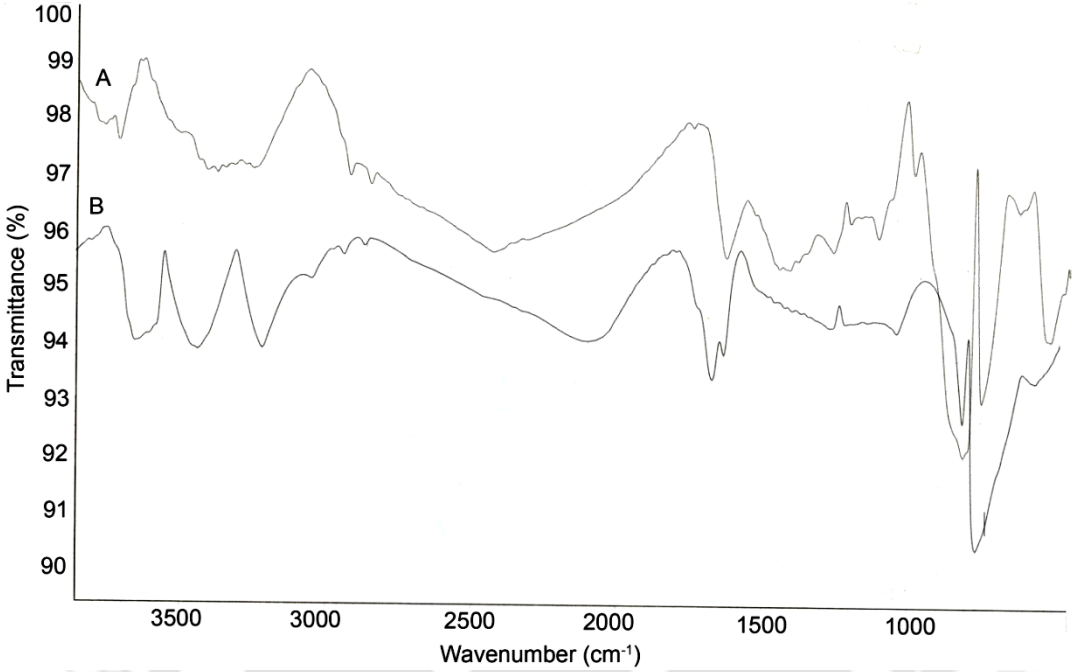

Figure 5.3: FT-IR spectral characteristics of AOx (**A**) and AOx-AuNPs (**B**).

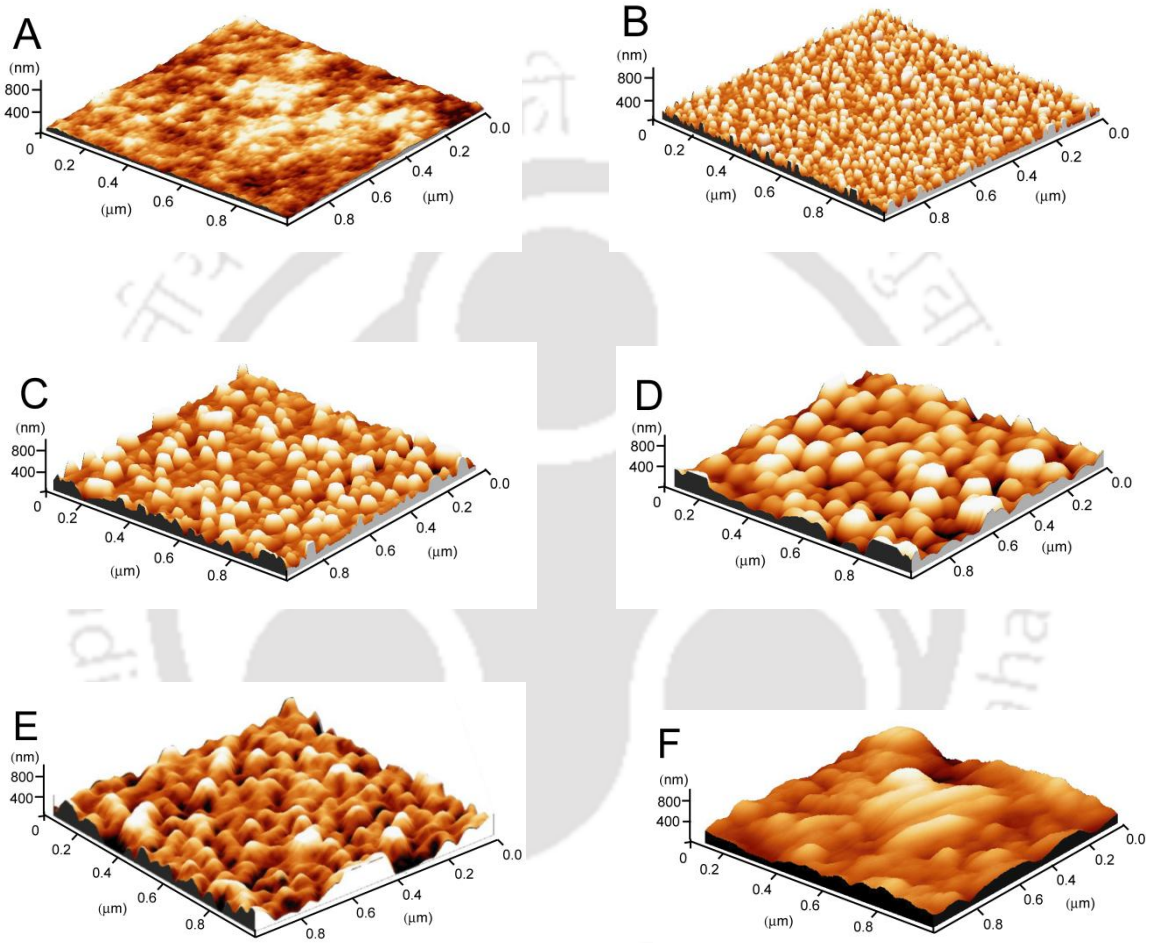

Figure 5.4 AFM images at major stages of GCE/Chit/PANI/AOx-AuNPs/Nf bioelectrode fabrication. **A:** GCE, **B:** GCE/AuNPs, **C:** GCE/AOx-AuNPs, **D:** GCE/PANI/AOx, **E:** GCE/PANI/AOx-AuNP and **F:** GCE/Chit/PANI/AOx-AuNP/Nf.

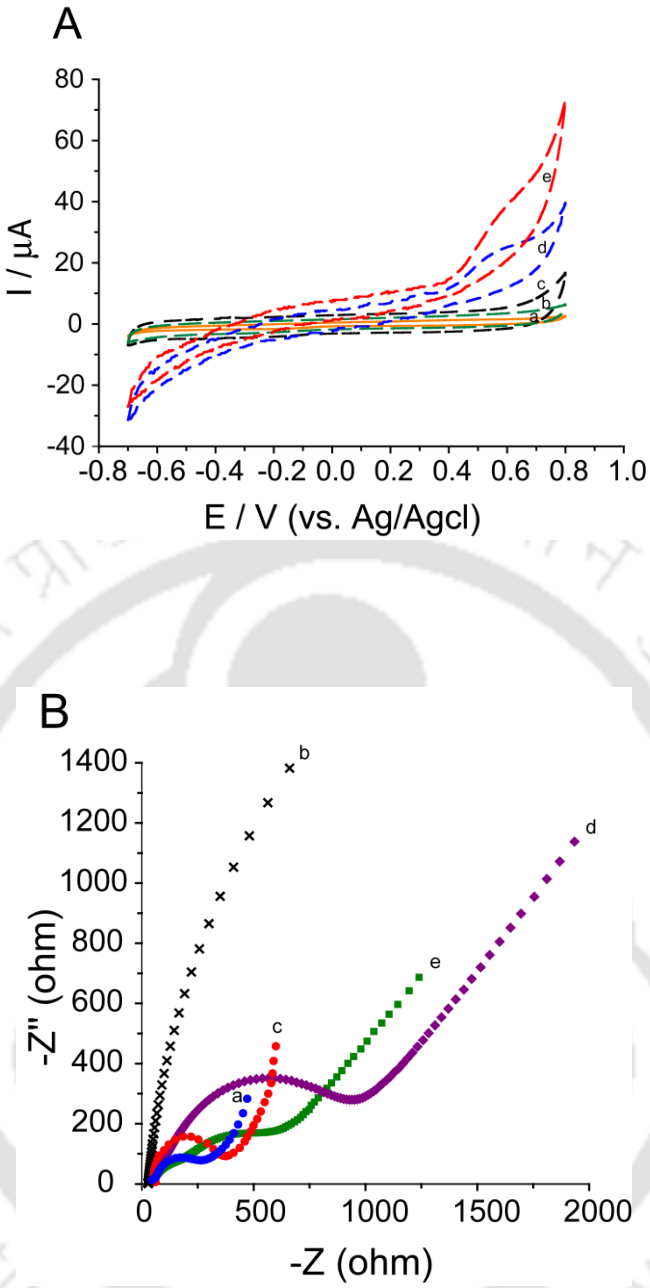

Figure 5.5 CV and EIS studies at major stages of GCE/Chit/PANI/AOx-AuNPs/Nf bioelectrode fabrication. **A**: CV of GCE (a), GCE/Chit/PANI/AOx/Nf (b), GCE/Chit/PANI/AOx-AuNPs/Nf (c), GCE/Chit/PANI/AOx-AuNPs/Nf with 5 µM (d) and 50 µM (e) ethanol in 50 mM KPBS (pH 7.5) at a scan rate of 50 mV s^{-1}. **B**: EIS of GCE (a), GCE/PANI (b), GCE/PANI-AOx/Nf (c), GCE/Chit/PANI/AOx/Nf (d) and GCE/Chit/PANI/AOx-AuNPs/Nf (e) electrodes in 5 mM $K_3Fe(CN)_6/K_4Fe(CN)_6$ (1:1) and 0.1 M KCl in 50 mM KPBS.

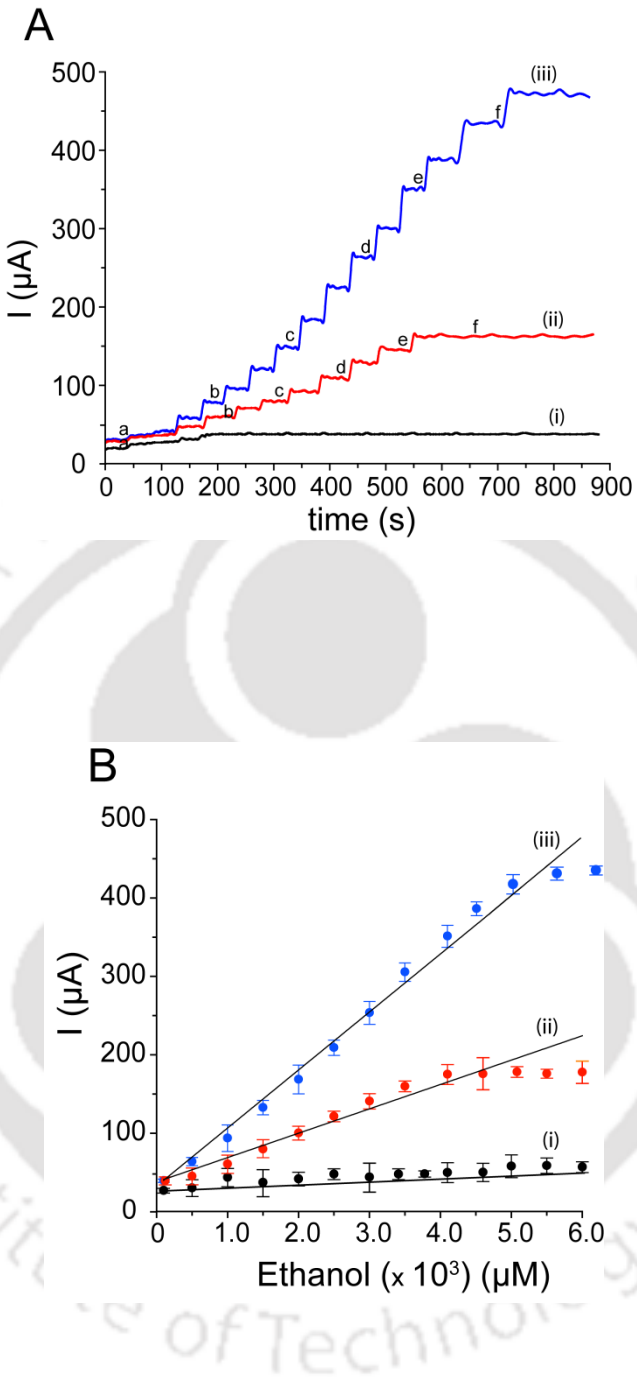

Figure 5.6 Current vs. time plots for the modified GCE electrodes. **A**: Chronoamperometric current responses of the GCE/AOx/Nf (i), GCE/chit/PANI/AOx/Nf (ii) and GCE/Chit/PANI/AOx-AuNPs/Nf (iii) bioelectrodes at (a) 5 µM (b) 50 µM (c) 500 µM (d) 1.5 mM (e) 3 mM (f) 6 mM successive addition of alcohol. **B**: Response curves of the GCE/AOx/Nf (i), GCE/Chit/PANI/AOx/Nf (ii) and GCE/Chit/PANI/AOx-AuNPs/Nf (iii)

bioelectrodes with increasing ethanol concentration from 5 µM to 6 mM. The operating potential used was + 0.6 V (vs. Ag/AgCl electrode).

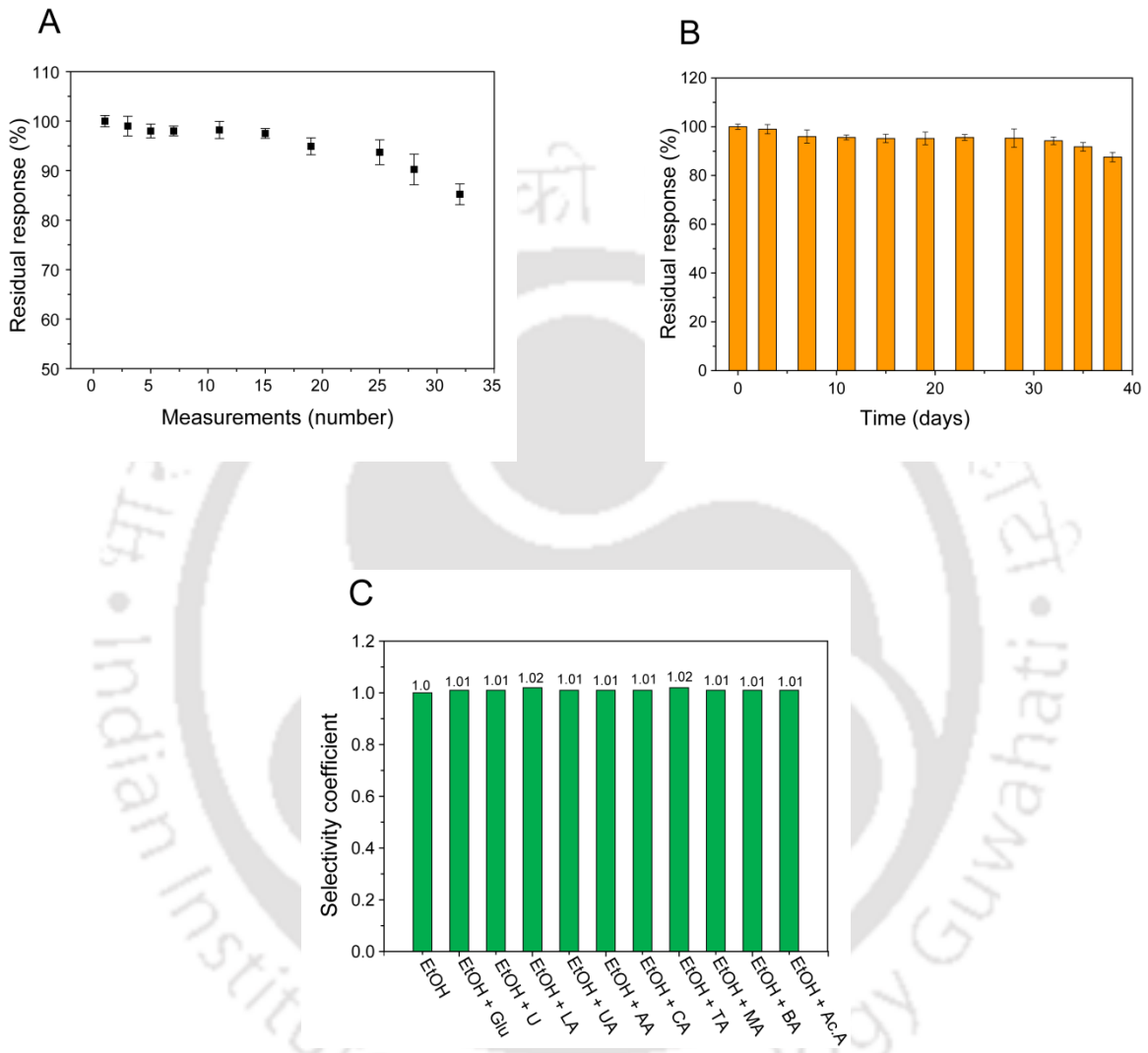

Figure 5.7 Stability studies of the GCE/Chit/PANI/AOx-AuNPs/Nf bioelectrode. **A**: Operational stability, **B**: Storage stability of the bioelectrode. Each datum point represents the average of the analysis of triplicate values (n =3), with the range indicated with error bars. **C**: Interference studies with GCE/Chit/PANI/AOx-AuNP/Nf bioelectrode: (EtOH: Ethanol, AA: ascorbic acid, Glu: glucose, UA: uric acid, U: Urea, LA: lactic acid, TA: tartaric acid, CA: citric acid, BA: butyric acid, MA: malic acid, Ac.A: acetic acid.

Conclusions and Scope for Future Work

Conclusions and scope for future work

Conclusions

The basic physico-chemical characteristics of AOx from *Pichia pastoris* necessary for its exploration for biosensor application were investigated and validated by comparing with the reported data. The secondary structural analysis of the AOx protein showed a stable conformation with highly ordered structure. Studies on AOx protein folding and unfolding established that MW mediated unfolding of the protein is a reversible phenomena and the reversibility is effectual at low MW exposure time (10 s) on the protein. The unfolding process enacted by the MW radiation occurs rapidly without passing through any intermediate transition state under the time scale units employed in the investigation. The reversible refolding techniques demonstrated through this investigation has clear advantages over the conventional chemical based approach owing to its direct nature that void the separation steps for the protein involved in chemical denaturant based approach. This MW based technique was utilized for stable entrapment of chemical activator ferrocene in the protein matrix of AOx for enhancing biocatalytic activity of the enzyme. The activated enzyme showed a two-fold increase in efficiency (k_{cat}/k_m) with no significant change of its secondary structure. The activator molecules were stably entrapped in the AOx protein matrix in a molar ratio of ~3:1 through electrostatic interaction with the Trp residues involved in the functional activity of the enzyme. The amplified biocatalytic activity of AOx achieved by stable entrapment of chemical activator ferrocene in the protein matrix was successfully exploited to develop an efficient biosensor for interference free detection of alcohol in real sample. The AOx with amplified activity was immobilized on a sol-gel chitosan layer assembled on HRP in a MWCNT matrix on the electrode surface. In this bi-enzyme sensor,

the H_2O_2 formed by the AOx catalyzed oxidation of alcohol was bioelectrocatalytically reduced by HRP through DET mechanism to generate the response. MWCNT provided high electroactive surface for facile electron exchange between the electrode and HRP. The silica-sol gel chitosan matrix provided biocompatible support for stability of the bi-enzyme complex on the electrode surface, desired porosity for easy diffusion of analyte and preconcentration of the analyte for electrochemical detection. Polyethylenimine was used to stabilize the FcAOx immobilized on the sol-gel chitosan film. The overall performance of the fabricated biosensor improved in terms of stability, linear detection range and sensitivity for detection of alcohol in liquid sample and exhibited good correlation with the standard analytical method. We however, sought for a simpler procedure for fabrication of the biosensor since the aforementioned method involves additional steps on preparing the activity amplified enzyme to be assembled on the electrode surface. Later, a stable AOx protein surface stabilized AuNPs synthesized by exploiting the native chemical drive of the protein molecules under alkaline condition was developed for the first time. In this nano-conjugate the intimately associated AuNPs found to enhance the kinetic activity of the AOx enzyme. The AOx-AuNPs conjugates encapsulated with PANI synthesised by exploiting a localized AOx catalysed oxidative reaction, implanted stably on the GCE by using chitosan and Nafion polymers. This nano composite bioelectrode based biosensor showed high operational and storage stability and wide linear current response against ethanol with very a low detection limit. The linear range is sufficient for quantitative analyses of alcohol in clinical, forensic and many other practical applications where sensitive detection of alcohol is important. The biosensor was also effectively used for determination of ethanol in commercial beverage samples. A comparative analysis on the performance of the biosensors constructed through this investigation with various prominent alcohol biosensors reported over the last 12 years was carried out as shown in table A.

Table A: Comparison on the performances of various AOx-based biosensors

Biosensor configuration	Sensing element	Immobilization method	Sensor Parameters	References
Pt/polyvinylferrocenium matrix	AOx	Entrapment	Linearity: 3 mM Detection limit: N.R Sensitivity: 9.1 µA mM^{-1} Stability: 94 % in 36 days	Gulce et al. 2002
Pt/Os-AP59/CP9	AOx HRP	Entrapment	Linearity: 2.0 mM Detection limit: N.R Sensitivity: 0.2 µA mM^{-1} Stability: 50 % in 14 days	Smutok et al. 2006
PVA-MWCNT	ADH	Physisorption	Linearity: 1.5 mM Detection limit: 13 µM Sensitivity: 0.196 µA mM^{-1} Stability: 12 % IN 30 min	Tsai et al. 2007
GNPs-MWCNT-MB-Nafion	ADH	Physisorptoin	Linearity: 0.2-2.5 mM Detection limit: 5.0 µM Sensitivity: 0.093 µA mM^{-1} Stability: 5.8 % in 30 days	Zhen et al. 2011
CFE/PNR	AOX	Cross linking	Linearity: 0-0.7 mM Detection limit: 29.7 µM Sensitivity: 0.70 µA mM^{-1} Stability: 12 % in 6 weeks	Barsan et al 2008
CFE/MWCNT	AOx	Cross linking	Linearity: 1.4 mM Detection limit: 86 µM Sensitivity: N.R Stability: 70 % in 3 weeks	Gouveia-Caridade et al. 2008
11-FUT/ Au	AOx HRP	Covalent binding	Linearity: 0.0–0.15 µM Detection limit: 10 µM Sensitivity: N.R Stability: No loss in 1 h	Hasunuma et al. 2004
ADH/PDAMS/PtNPs/Pt	ADH	Physisorptoin	Linearity: 0.9-7.0 mM Detection limit: 451.6 µM Sensitivity: 0.233 µA mM^{-1} Stability: 8 % in 3 weeks	Jimenez et al. 2014
MWCNT-CHIT	ADH	Physisorptoin	Linearity: N.R Detection limit:0.52 µM Sensitivity:164.6 µA mM-1 Stability: N.R	Lee and Tsai 2009
GCE/MWCNTs/HRP/sol-gel/Chit/FcAOx/PEI	**AOx HRP**	**Physisorptoin**	**Linearity: 0.005-3.0 mM** **Detection limit: 2.32 µM** **Sensitivity: 150 µA mM^{-1}** **Stability: 10 % in 5 weeks**	**Present work**
GCE/PANI/Chit/AOx-AuNPs/Nf	**AOx**	**Entrapment**	**Linearity: 0.01-4.7 mM** **Detection limit: 7 µM** **Sensitivity: 68.3 µA mM^{-1}** **Stability: 5 % loss in 5 weeks**	**Present work**

*Few values were normalized for making the units uniform for better comparision. The stability was reported as the decrease in biosensor response.

It is observed that though individual performance factors except the stability characteristics are not superior to the previously reported sensors the overall performance of the constructed biosensors is sensible for practical utility, thus validates the application potential of the bioelectrode fabrication concepts for developing a commercially viable biosensor device.

Scope for future work

Following points have been identified as major gap areas from the studies included in this thesis that warrant further investigations for augmenting the concept to develop alcohol biosensor for practical utility. The structure and map of FAD binding, substrate binding and overall catalytic sites of AOx protein (through x-ray crystallography and allied techniques) need to be elucidated. Based on these information the exact molecular mechanism of MW based partial unfolding of AOx protein and its stable interaction with the ferrocene molecules need to be explore to understand the molecular and redox participation of the electroactive ferrocene molecules in the catalytic activation of the AOx enzyme. These information likely to help in designing the protocol rationally for large scale preparation of AOx with amplified activity for commercial applications. Further, the detail molecular characterization of the AOx protein will also help in elucidating the exact molecular mechanism of the native chemical drive of the protein molecules for the *in-situ* synthesis of AOx protein stabilized AuNPs and activity amplification of the enzyme by the attached AuNps. The concepts which have been developed through this investigation for the fabrication of bioelectrodes need to be implemented in a commercially viable sensor platform such as, screen printed electrode in a microfluidic base for developing portable commercial ethanol biosensors for fast, cost effective and real-time monitoring of alcohol in clinical and other industrial applications.

Bibliography

List of Publications

Publications in referred journals

1. **Somasekhar R. Chinnadayyala**, Santhosh Mallesh, Pranab Goswami* (2012) Microwave based reversible unfolding and refolding of alcohol oxidase protein probed by fluorescence and circular dichroism spectroscopy, *J Biophy Chem* 3, 317.

2. **Somasekhar R. Chinnadayyala**, Ankana Kakoti, Santhosh Mallesh, Pranab Goswami* (2014) A novel amperometric alcohol biosensor developed in a 3rd generation bioelectrode platform using peroxidase coupled ferrocene activated alcohol oxidase as biorecognition system. *Biosens Bioelectron* 55, 120

3. **Somasekhar R. Chinnadayyala**, Santhosh Mallesh, Naveen K. Singh, Pranab Goswami* Alcohol oxidase protein mediated *in-situ* synthesized and stabilized gold nanoparticles for developing amperometric alcohol biosensor. (Communicated)

4. Pranab Goswami*****, **Somasekhar R. Chinnadayyala**, Mitun Chakraborty (equal 2nd author contribution), Adepu Kiran Kumar and Ankana Kakoti (2013) An overview on Alcohol Oxidases and their Potential Applications *Appl Microbiol Biotechnol* 97, 4259

5. Mallesh Santhosh, **Somasekhar R. Chinnadayyala**, Ankana Kakoti, Pranab Goswami*, (2014) Selective and sensitive detection of free bilirubin in blood serum using human serum albumin stabilized gold nanoclusters as fluorometric and colorimetric probe. *Biosens Bioelectron* 59, 370

6. Mitun Chakraborty, Manish Goel, **Somasekhar R. Chinnadayyala**, Ujjwal Ranjan Dahiya, Siddhartha Sankar Ghosh*, Pranab Goswami* (2014) Molecular characterization and expression of a novel alcohol oxidase from *Aspergillus terreus* MTCC6324, *PLoS One* 9(4): e95368. doi:10.1371/journal.pone.0095368

Abstracts Published in Conferences

1. **Somasekhar R. Chinnadayyala**, Santhosh Mallesh, Pranab Goswami*****, Bioengineering of alcohol oxidase by entrapping ferrocene in the protein matrix using microwave based reversible refolding technique. World Congress on Biotechnology, 2012, Hyderabad, India, 4-6 May 2009. Abstract no: P-50

2. **Somasekhar R. Chinnadayyala**, Santhosh Mallesh, Naveen K. Singh, Pranab Goswami*****, Alcohol oxidase protein mediated *in-situ* synthesized and stabilized gold nanoparticles for developing amperometric alcohol biosensor. New Advances and Horizons in Nanoscience and Nanotechnology, 2014, Guwahati, Assam, India, 20-21 December 2014. Abstract no: P-32

3. Mallesh Santhosh, **Somasekhar R. Chinnadayyala**, Ankana Kakoti, Pranab Goswami*, Human serum albumin stabilized gold nanoclusters as a novel fluorescent and colorimetric probe for the detection of bilirubin-IX. 24th Anniversary World Congress on Biosensors 2014, Melbourne, Victoria, Australia, 27-30 May 2014. Abstract no: P2-148